European Commission

JRC SCIENTIFIC AND POLICY REPORTS

Compatibility between Amateur Radio Services and Galileo in the 1260-1300 MHz Radio Frequency Band

Issue 1.1

José A. López-Salcedo, Matteo Paonni,
Michele Bavaro, Joaquim Fortuny-Guasch
European Commission, Joint Research Centre

2015

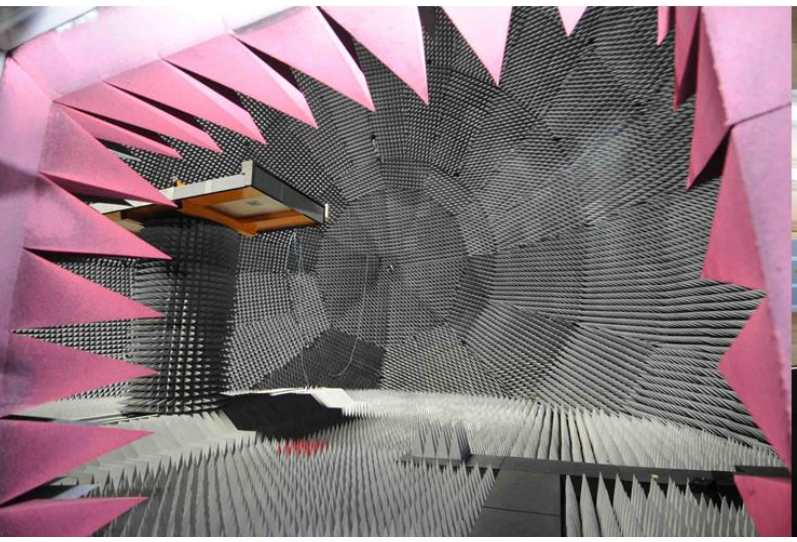

Joint Research Centre

European Commission
Joint Research Centre
Institute for the Protection and Security of the Citizen

Contact information
Joaquim Fortuny-Guasch
Address: Joint Research Centre, Via Enrico Fermi 2749, TP 723, 21027 Ispra (VA), Italy
E-mail: joaquim.fortuny@jrc.ec.europa.eu
Tel.: +39 0332 78 5104
Fax: +39 0332 78 5469

http://ipsc.jrc.ec.europa.eu/
http://www.jrc.ec.europa.eu/

JRC96769

Printed in Italy

TABLE OF CONTENTS

LIST OF FIGURES

ACRONYMS

ADC	Analog to Digital Converter
ARS	Amateur Radio Services
ATV	Amateur Television
BER	Bit Error Rate
BOC	Binary Offset Carrier
BPSK	Binary Phase Shift Keying
C/A	Coarse Acquisition
C/NAV	Commercial Navigation message
C/N0	Carrier power to Noise spectral density ratio
Ci/N0	Interference power to Noise spectral density ratio
CDMA	Code Division Multiple Access
CEML	Coherent Early-Minus-Late
CRB	Cramér Rao Bound
CS	Commercial Service
CW	Continuous Wave
D-ATV	Digital Amateur Television
DLL	Delay Locked Loop
DS-SS	Direct-Sequence Spread Spectrum
DVB-S	Digital Video Broadcasting Satellite
DVB-T	Digital Video Broadcasting Terrestrial
EIRP	Equivalent Isotropically Radiated Power
EME	Earth-Moon-Earth
EMSL	European Microwave Signature Laboratory
ESD	Energy Spectral Density
GCC	Galileo Control Center
GNSS	Global Navigation Satellite Systems
GPS	Global Positioning System
IARU	International Amateur Radio Union
ICD	Interface Control Document
IOV	In-Orbit Validation
ITU	International Telecommunications Union
kHz	kilo Hertz
Mcps	Mega chips per second
MGM	Machine-Generated Mode
Msps	Mega symbols per second
MHz	Mega Hertz
OFDM	Orthogonal Frequency Division Multiplexing
PLL	Phase Locked Loop
pRange	Pseudorange

PRBS	Pseudo Random Binary Sequence
PRN	Pseudorandom Noise
PSG	Programmable Signal Generator
PSD	Power Spectral Density
QAM	Quadrature Amplitude Modulation
QPSK	Quadrature Phase Shift Keying
RNSS	Radio Navigation Satellite Services
RUT	Receiver Under Test
SCPI	Standard Commands for Programmable Instruments
SIS	Signal In Space
SNR	Signal to Noise Ratio
SQRRC	Square Root Raised Cosine
SS	Spread Spectrum
SSC	Spectral Separation Coefficient
STD	Standard Deviation
SV	Space Vehicle
TTFF	Time To First Fix

1 INTRODUCTION

Galileo signals are transmitted in four different frequency bands, namely E5a, E5b, E6 and E1, which are contained within the portion of spectrum allocated to radionavigation satellite services (RNSS) by the International Telecommunications Union [1]. All Galileo frequency bands, except for E6, are also contained within the spectrum allocated to aeronautical radio navigation services (ARNS), which is specifically dedicated to safety-critical applications. This means that E5a, E5b and E1 are inherently protected from interference sources due to the stringent limitations that are imposed to other radiofrequency systems intending to operate within these bands.

While RNSS is still the primary service within E6, other systems are allowed to coexist in a secondary basis within this band, thus becoming a potential source of interference to Galileo E6 signals. In this context, there are two major concerns to be borne in mind. First, the extremely weak received power of RNSS signals, which is typically on the order of 10^{-16} W. This value is about one-billionth of a billionth (i.e. 10^{-18}) the power initially transmitted by the satellites. This leads RNSS signals completely vulnerable against interference signals from terrestrial services, whose power levels are several orders of magnitude larger [2]. Second, Galileo E6 signals will support the provision of added value services with improved and controlled performance, which could be seriously hindered by the disturbing presence of interference signals.

In view of the above considerations, ***the focus of this study is to assess the potential impact that interference signals may cause onto Galileo E6 signals. Particularly, those related to secondary stations operating in the E6 band,*** which are mainly concerned with amateur radio transmissions.

A wide range of different services and signaling formats may be found in the amateur radio domain, from narrowband to wideband signals, involving either voice, data or image transmissions. Among all possibilities, the present study concentrates on the case of amateur television (ATV). The reasons to do so are twofold. On the one hand, ATV is the dominant service within the central part of the Galileo E6 band. That is, the portion from 1272 to 1290 MHz, according to the frequency bandplan of the International Amateur Radio Union (IARU) [3]. On the other hand, ATV transmissions are quite popular in central European countries such as Germany, where several ATV stations can simultaneously be received in most locations of their territories. Consequently, there is a high probability for a Galileo E6 receiver to be interfered by the presence of one or several ATV signals coming from nearby stations.

This report is organized as follows: Section 2 presents some mathematical preliminaries regarding the signal model and the main tasks that are carried out within a GNSS receiver. Section 3 provides some analytical results to model the performance degradation of a GNSS receiver in terms of C/N0 degradation, pseudorange variance and bit error rate. Section 4 introduces the regulatory framework related to transmissions on the E6 band, and summarizes the main features of ATV signals considered in this study. Section 5 describes the experimental setup deployed at the JRC for the testing campaign, while Section 6 presents the experimental results for the different test cases. Finally, a summary of the main conclusions of this work is provided in Section 7.

2 PRELIMINARIES AND SIGNAL MODEL

2.1 CONTINUOUS-TIME MODEL FOR GNSS RECEIVED SIGNALS

We consider the propagation of GNSS signals through a single path additive Gaussian channel. The continuous-time signal at the input of the GNSS receiver can be modeled through the following complex baseband equivalent signal:

$$r_c(t) = \sum_{i=0}^{L-1} A_i s_{c,i}(t - \tau_{c,i}) e^{j2\pi F_{d,i} t} + w_c(t) \tag{1}$$

where L is the number of visible satellites, $s_{c,i}(t)$ is the signal from the i-th satellite and $w_c(t)$ is a zero-mean random Gaussian process that encompasses both the thermal noise and interference sources. The signal from each of the visible satellites is received with some complex amplitude A_i, time-delay $\tau_{c,i}$ and residual frequency error $F_{d,i}$, leading to the following signal model:

$$s_{c,i}(t) = \sum_{l=-\infty}^{\infty} b(l) \sum_{m=0}^{N_r-1} u(m) c_{c,i}(t - mT_{code} - lT_d) \tag{2}$$

with $b(l) = \{-1, +1\}$ the data modulating symbols transmitted at a rate $R_d = 1/T_d$ and $c_{c,i}(t)$ the pulse shaped spreading code for the i-th satellite, which has a time duration (i.e. code period) of T_{code} seconds. This code is also known as the primary code, and is repeated N_r times within the bit period as well as amplitude modulated by the so-called secondary code, $u(m)$. For instance, for GPS L1 C/A signals we have $u(m) = 1$, for all $m = 1, \dots, N_r$ but for GPS L5 or Galileo, they are randomly alternating between $\{-1, +1\}$. The signal model for the pulse shaped spreading code in (2) becomes,

$$c_{c,i}(t) = \sum_{q=0}^{N_c-1} x_i(q)\, g_c(t - qT_c) \tag{3}$$

with $x_i(q) = \{-1, +1\}$ the spreading code sequence for the i-th satellite, which is composed of N_c pseudorandom chips, each of them shaped with a pulse $g_c(t)$ with duration $T_c = 1/R_c$ seconds, with R_c the chip rate. For instance, for GPS L1 C/A and Galileo E1C we have $R_c = 1.023$ Mcps, whereas for Galileo E6B/C we have $R_c = 5.115$ Mcps.

The received signal in (1) is observed at the output of the radiofrequency front-end, once bandpass filtering and down-conversion have been applied. Consequently, the chip pulse $g_c(t)$ already encompasses the bandlimiting effects of the front-end bandpass filter. Let us denote the equivalent baseband frequency response of this filter by $H_f(\Omega)$, which has a two-sided bandwidth equal to B_f Hz, and ideally, it exhibits a brick wall shape.

Then, since $g_c(t)$ is a finite energy deterministic pulse, its energy spectral density (ESD) is given by:

$$S_{g_c}(\Omega) = S_{g_u}(\Omega) |H_f(\Omega)|^2 \tag{4}$$

where $S_{g_u}(\Omega) = |G_u(\Omega)|^2$ is the energy spectral density of the original (i.e. unfiltered) chip pulse $g_u(t)$ whose Fourier transform is $G_u(\Omega) \doteq \mathcal{F}\{g_u(t)\} = \int_{-\infty}^{\infty} g_u(t)e^{j\Omega t}dt$. Alternatively, $S_{g_u}(\Omega) = \mathcal{F}\{R_{g_u}(\tau)\}$ with $R_{g_u}(\tau)$ the autocorrelation of $g_u(t)$. As an example, this unfiltered chip pulse would be a rectangular pulse with duration T_c for GPS L1 C/A and Galileo E6B/C, whereas for Galileo E1C it would be the concatenation of two consecutive pulses of duration $T_c/2$ each, with reversed signs.

2.2 DISCRETE-TIME MODEL FOR GNSS RECEIVED SIGNALS

Current GNSS receivers are mostly based on digital architectures that operate with the discrete-time samples of the received signal [4]. To do so, the received signal is passed through a bandlimiting (i.e. antialiasing) filter and then through an analog-to-digital converter (ADC). At the output of the ADC we have the discrete-time and quantized version of the received signal in (1), which is represented by:

$$r(n) = \sum_{i=0}^{L-1} A_i \sum_{l=-\infty}^{\infty} b(l) \sum_{m=0}^{N_r-1} u(m) \sum_{q=0}^{N_c-1} x_i(q)g(n - qN_{sc} - mN_{scode} - lN_{sbit} - \tau_i)e^{j2\pi\nu_i n} + w(n) \quad (5)$$

where $r(n) \doteq r_c(nT_s)$, $g(n) \doteq g_c(nT_s)$ and $w(n) \doteq w_c(nT_s)$ are the discrete-time versions of the continuous-time signals in (1), with T_s the sampling time. Furthermore, the discrete-time synchronization parameters become $\tau_i \doteq \tau_{c,i}T_s$ and $\nu_i \doteq F_{d,i}T_s$, and any constant phase rotation is assumed to be contained within the complex amplitude A_i. The following parameters are also defined in the discrete-time domain: $N_{sc} \doteq T_c/T_s$ is the number of samples per chip, $N_{scode} \doteq T_{code}/T_s$ the number of samples per code period and $N_{sbit} \doteq T_{bit}/T_s$ the number of samples per bit period.

Following the conventional assumption in GNSS interference assessment, the discrete-time signal model in (5) assumes that the ADC is operating normally, which means that no saturation nor severe underutilization of quantization steps is incurred. Otherwise, the GNSS signal could be completely distorted and the receiver output observables would collapse, thus failing to provide any meaningful information. Some insights on the problem of abnormal ADC operation can be found in the existing literature, such as in [5], [6], [7] and the references therein.

For the sake of clarity, we will process the received signal samples in batches of one code period each (i.e. N_{scode} samples). To do so, we will assume that the GNSS receiver has already been running for a long enough period of time, so that the receiver is already in tracking mode. Consequently, it is reasonable to assume that:

A1) The residual code delay error τ is very small, typically, within a fraction of the chip duration. Therefore, we can assume that within each batch of one period samples, we observe a complete local replica of the satellite of interest, so that there is no contribution from the precedent nor the subsequent replicas.

A2) The receiver is already aligned to the secondary code, so that is able to perfectly remove $u(m)$ in (5), and thus we can get rid of it in the subsequent formulation.

A3) Similarly to A2), we assume that the receiver is bit-synchronized and that the observation interval for coherent integration purposes is smaller than the bit period. This allows us to assume that $b(l)$ is constant within the observation interval, and thus we can also get rid of it in the subsequent formulation.

Having in mind the assumptions above, let us consider the m-th code period of received signal, and let us stack the corresponding N_{scode} samples into the following vector:

$$\boldsymbol{r}(m) \doteq [r(mN_{scode}), r(mN_{scode}+1), \dots, r(mN_{scode}+N_{scode}-1)\,]^T \tag{6}$$

Assuming that we are interested in the i-th satellite, the inner structure of the received signal samples can be expressed in matrix formulation as follows:

$$\boldsymbol{r}(m) = A_i \boldsymbol{\Gamma}(m;\nu_i)\boldsymbol{c}_i(\tau_i) + \boldsymbol{w}(m) \tag{7}$$

where $\boldsymbol{\Gamma}(m;\nu_i)$ is a $(N_{scode} \times N_{scode})$ diagonal matrix encompassing the residual frequency error for the m-th code period, $\boldsymbol{c}_i(\tau_i)$ is a $(N_{scode} \times 1)$ vector with the samples of the pulse shaped spreading code for the satellite of interest, and finally, $\boldsymbol{w}(m)$ is a $(N_{scode} \times 1)$ vector with the contribution of thermal noise, the rest of satellites (which are below the noise floor) and interference sources. That is,

$$\boldsymbol{\Gamma}(m;\nu_i) = diag\left(\left[1, e^{j2\pi\nu_i}, e^{j2\pi\nu_i 2}, \dots, e^{j2\pi\nu_i(N_{scode}-1)}\right]e^{j2\pi\nu_i(m-1)N_{scode}}\right) \tag{8}$$

$$\boldsymbol{c}_i(\tau_i) = [c_i(-\tau_i), c_i(1-\tau_i), \dots, c(N_{scode}-\tau_i)]^T \tag{9}$$

$$\boldsymbol{w}(m) \doteq [w(mN_{scode}), w(mN_{scode}+1), \dots, w(mN_{scode}+N_{scode}-1)\,]^T \tag{10}$$

Furthermore, the pulse shaped spreading code can be further decomposed as follows:

$$\boldsymbol{c}_i(\tau_i) = \boldsymbol{G}(\tau_i)\boldsymbol{x}_i \tag{11}$$

where $\mathbf{G}(\tau_i)$ is a $(N_{scode} \times N_c)$ matrix whose columns are N_{sc} samples time-shifted versions of the filtered chip pulse $g(n)$ and $\boldsymbol{x}_i$ is a $(N_c \times 1)$ vector with the pseudorandom sequence of chips for the i-th satellite spreading code. That is,

$$\boldsymbol{G}(\tau_i) = [\boldsymbol{g}_0(\tau_i), \boldsymbol{g}_1(\tau_i), \dots, \boldsymbol{g}_{N_c-1}(\tau_i)] \tag{12}$$

$$\boldsymbol{g}_j(\tau_i) = [g(-jN_{sc}-\tau_i), g(1-jN_{sc}-\tau_i), \dots, g(N_{scode}-jN_{sc}-\tau_i)]^T \tag{13}$$

$$\boldsymbol{x}_i = [x_i(0), x_i(1), \dots, x_i(N_c-1)]^T. \tag{14}$$

We will concentrate on the i-th satellite, and for the sake of clarity, we will henceforth omit the subscript $(\,)_i$.

2.3 SIGNAL MODEL FOR THE GNSS CORRELATOR OUTPUT SAMPLES

Based on the received signal samples, the GNSS receiver performs the correlation with the local code replica and provides the resulting code correlation outputs to subsequent stages of the receiver. These output samples are then used to provide pseudorange and carrier measurements (i.e. using code and carrier tracking schemes) as well as some other useful metrics such as the estimated C/N0, which can be used for quality monitoring purposes. The underlying process can be formulated as an optimization

problem where the local code replica is aligned at code-level and carrier-level in such a way that the signal-to-noise ratio of the output samples is maximized. This is actually the same procedure followed by the well-known matched filter principle, and it can be mathematically formulated as follows:

$$\{\hat{\tau}(k), \hat{\nu}(k)\} = arg \max_{\tau,\nu} \left| R_{r,c}(\tau, \nu; k) \right| \tag{15}$$

where $R_{r,c}(\tau, \nu; k)$ is the coherent cross-correlation between the received signal and the local replica, which can equivalently be expressed in matrix notation (in virtue of assumptions A2 and A3) as:

$$R_{r,c}(\tau, \nu; k) \doteq \frac{1}{N_{coh}} \sum_{m=0}^{N_{coh}-1} \boldsymbol{x}^H \boldsymbol{G}^H(\tau) \boldsymbol{\Gamma}^H(m; \nu) \boldsymbol{r}(m + kN_{coh}) \tag{16}$$

with $(\,)^H$ denoting the hermitian operator (i.e. complex conjugate and transpose).

The expression above corresponds to the k-th coherent correlation output, which considers a coherent integration time of $T_{coh} = N_{coh} T_{code}$ seconds. The corresponding estimates of code delay and carrier frequency offset are denoted by $\hat{\tau}(k)$ and $\hat{\nu}(k)$ in (15). These estimates involve a multi-dimensional search according to (15), but typically, this search is carried out at the tracking stage by using two parallel architectures that operate separately at either the code or the carrier level. These are the delay-locked loop (DLL) and the phase locked loop (PLL). While the PLL requires just one output correlation sample (i.e. the so-called "prompt" sample, with (16) evaluated at $\tau = \hat{\tau}(k-1)$ and $\nu = \hat{\nu}(k-1)$), the DLL requires several output correlation samples, evaluated at different code delay values. Apart from the prompt sample, the conventional approach is to use two more correlation outputs by evaluating (16) at $\tau = \hat{\tau}(k-1) + \frac{N_\Delta}{2}$ and $\tau = \hat{\tau}(k-1) - \frac{N_\Delta}{2}$. The resulting correlation samples are referred to as the "early" and "late" samples, respectively. Thus, a total of (at least) three correlation output samples are typically used for code tracking.

Based on the above discussion, let us evaluate the coherent correlation in (16) for a generic set of $L = 2M + 1$ equispaced code delay values $\hat{\tau} + lN_\delta$ for $l = -M, ..0, ..M$, and let us stack the result into the following $(L \times 1)$ vector:

$$\boldsymbol{y}(k) = [y_{-M}(k), \dots, y_0(k), \dots, y_M(k)]^T \tag{17}$$

where each coherent correlation output sample is given by

$$y_l(k) = R_{r,c}(\hat{\tau} + lN_\delta, \hat{\nu}; k). \tag{18}$$

In the above formulation we have used $\hat{\tau}$ and $\hat{\nu}$ for brevity, since indeed, the tentative values used for correlation are actually $\hat{\tau}(k-1)$ and $\hat{\nu}(k-1)$. That is, the code and carrier estimates obtained from the previous evaluation of (15). For the sake of simplicity, we will consider that $N_\delta = 1$ sample. In matrix notation, the corresponding output correlation samples can be obtained as follows:

$$\boldsymbol{y}(k) = \frac{1}{N_{coh}} \sum_{m=0}^{N_{coh}-1} \boldsymbol{C}^H(\hat{\tau}) \boldsymbol{\Gamma}^H(m; \hat{\nu}) \boldsymbol{r}(m + kN_{coh}) \tag{19}$$

where the ($N_{scode} \times L$) multi-correlation matrix $\boldsymbol{C}(\hat{\tau})$ contains in each of its columns a N_δ-samples time-shifted version of the pulse shaped spreading code sequence, $\boldsymbol{c}(\hat{\tau}) = \boldsymbol{G}(\hat{\tau})\boldsymbol{x}$ in (11). That is,

$$\boldsymbol{C}(\hat{\tau}) = [\, \boldsymbol{c}(\hat{\tau} - M), \dots, \boldsymbol{c}(\hat{\tau}), \dots, \boldsymbol{c}(\hat{\tau} + M)]. \tag{20}$$

Using this formulation, the coherent correlation output samples in (17) can be decomposed into a deterministic signal contribution $\boldsymbol{s}(k)$ and an aggregated random noise contribution $\boldsymbol{n}(k)$ as follows:

$$\boldsymbol{y}(k) = \boldsymbol{s}(k) + \boldsymbol{n}(k) \tag{21}$$

where according to (7) and (19), the ($L \times 1$) signal and noise vectors are given by:

$$\boldsymbol{s}(k) = \frac{A}{N_{coh}} \sum_{m=0}^{N_{coh}-1} \boldsymbol{C}^H(\hat{\tau})\boldsymbol{\Gamma}^H(m; \hat{v}_\epsilon)\boldsymbol{G}(\tau)\boldsymbol{x} \tag{22}$$

$$\boldsymbol{n}(k) = \frac{1}{N_{coh}} \sum_{m=0}^{N_{coh}-1} \boldsymbol{C}^H(\hat{\tau})\boldsymbol{\Gamma}^H(m; \hat{v})\boldsymbol{w}(m + kN_{coh}) \tag{23}$$

with $\hat{v}_\epsilon \doteq v - \hat{v}$ the residual frequency offset after compensating the input signal with the tentative frequency $\hat{v}$.

2.3.1 SIGNAL CONTRIBUTION

Under assumptions A1 to A3 in Section 2.2, the GNSS signal can be considered to remain stationary within the coherent integration time, except for a time-varying carrier phase term due to the residual frequency offset. After some straightforward manipulations, and taking into account the orthogonality properties of the pseudorandom chip sequence, it can be found that the l-th entry of vector $\boldsymbol{s}(k)$ in (22) can be expressed for $l = -M, \dots, M$ as:

$$s_l(k) \doteq [\boldsymbol{s}(k)]_l = A\rho(\hat{v}_\epsilon)N_c R_g(\hat{\tau}_\epsilon + l) \tag{24}$$

where $\hat{\tau}_\epsilon \doteq \tau - \hat{\tau}$ is the residual code delay error between the received signal and the local replica with tentative code delay $\hat{\tau}$, then $R_g(\tau)$ is the autocorrelation of the filtered chip pulse, and $\rho(\hat{v}_\epsilon)$ is a sinc-shaped term that encompasses the losses incurred by coherently correlating in the presence of a residual frequency offset. That is,

$$|\rho(\hat{v}_\epsilon)| = \frac{1}{N_{coh}N_{scode}}\left|\frac{sin(\pi\hat{v}_\epsilon N_{coh}N_{scode})}{sin(\pi\hat{v}_\epsilon)}\right| \tag{25}$$

with $0 \leq |\rho(\hat{v}_\epsilon)| \leq 1$.

2.3.2 NOISE PLUS INTERFERENCE CONTRIBUTION

The linear processing carried out by the coherent integration in (23) can equivalently be expressed as:

$$\boldsymbol{n}(k) = \boldsymbol{C}^H(\hat{\tau})\boldsymbol{u}(k) \tag{26}$$

where the zero-mean noise vector $\boldsymbol{u}(k)$ is obtained through the following comb filtering:

$$\boldsymbol{u}(k) \doteq \frac{1}{N_{coh}} \sum_{m=0}^{N_{coh}-1} \boldsymbol{w}(m + kN_{coh}) \tag{27}$$

which coherently integrates equispaced samples at a distance N_{scode} and involves an observation window of $N_{coh}N_{scode}$ samples in total, for every value of the discrete-time index k. Such a filter can be expressed in scalar notation by the following impulse response and frequency response, respectively:

$$h_{coh}(n) = \frac{1}{N_{coh}} \sum_{m=0}^{N_{coh}-1} \delta(n - mN_{scode}) \tag{28}$$

$$\left|H_{coh}\left(e^{j\omega}\right)\right| = \frac{1}{N_{coh}}\left|\frac{sin(\omega N_{coh}N_{scode}/2)}{sin(\omega N_{scode}/2)}\right| \tag{29}$$

The frequency response of this filter is composed of periodic sinc shapes centered at frequencies $\omega = \frac{2\pi}{N_{scode}}p$ for $p = 0,1, \dots, N_{scode} - 1$. In continuous-time notation, this corresponds to frequencies multiples of the code rate $1/T_{code}$ (i.e. multiples of 1 kHz for GPS L1 C/A or Galileo E6B/C). Furthermore, the bandwidth of these periodic sinc-shapes is $\frac{2\pi}{N_{coh}N_{scode}}$ in discrete-time, or $\frac{1}{N_{coh}T_{code}}$ in continuous-

time. Therefore, the longer the coherent integration length, the narrower the teeth of the comb filter frequency response, and thus the larger the rejection against wideband interferences. An example on the frequency response of the coherent integration filter is represented in Figure 2-1 for three different configurations using 1, 2 and 10 ms coherent integration time.

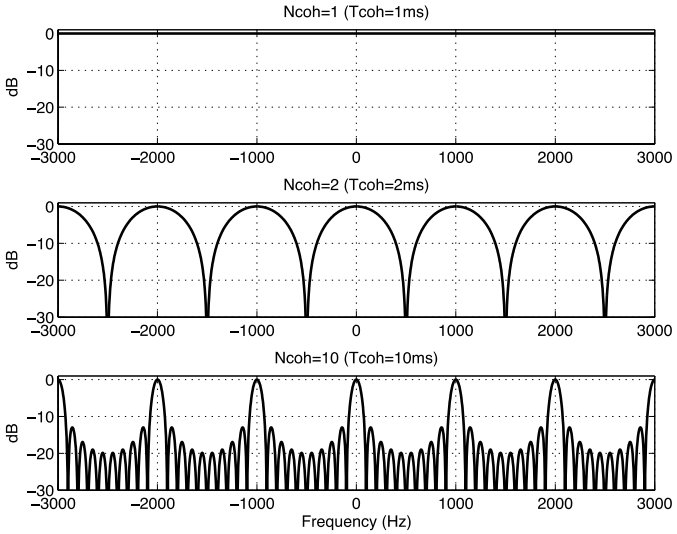

FIGURE 2-1 ZOOMED VIEW (FROM +/- 3KHZ) OF THE SQUARED FREQUENCY RESPONSE FOR THE COHERENT INTEGRATION FILTER ASSUMING A CODE PERIOD OF $T_{code} = 1$ ms. THREE CONFIGURATIONS ARE SHOWN FOR 1, 2 AND 10 ms COHERENT INTEGRATION TIME.

The effects of coherent integration are often disregarded in the existing literature on interference assessment, except for a few contributions such as the one in [8]. While for wideband interferences we do get some advantage, for narrowband interferences we may not. This is the case when narrowband interferences are aligned with any of these periodic sinc-shapes that are placed at multiples of the code rate. In that case, the interference can pass through and propagate to the correlator output. This periodic effect at multiples of the code rate has already been reported for instance in [10] or [11], but from a different perspective. In the sequel, though, we will consider the worst-case assumption, meaning that interference signals are placed at central frequencies multiples of the code rate.

Coming back to the noise plus interference term in (23), two main operations are carried out in there: first, the filtered noise at the comb filter output is correlated with the local code replica; second, the resulting signal is decimated by a factor of $N_{coh}N_{scode}$, which corresponds to the total span of the whole coherent integration length. Having in mind these operations, and since the entries within $\boldsymbol{n}(k)$ are identically distributed, we can express their power spectral density as follows:

$$S_n\left(e^{j\omega}\right) = \frac{1}{N_{coh}N_{scode}} \sum_{i=0}^{N_{coh}N_{scode}-1} \left(S_w\left(e^{j\omega\prime}\right)\left|H_{coh}\left(e^{j\omega\prime}\right)\right|^2 S_g\left(e^{j\omega\prime}\right)\right)_{|\omega'=\frac{\omega-2\pi i}{N_{coh}N_{scode}}} \tag{30}$$

where the replicas in the spectrum of $S_n\left(e^{j\omega}\right)$ are caused by the decimation by a factor of $N_{coh}N_{scode}$ at the coherent correlation output, and $S_w\left(e^{j\omega}\right)$ incorporates the contribution of the thermal noise and interference spectra at the front-end output. That is,

$$S_w\left(e^{j\omega}\right) = \left(N_0 + S_i\left(e^{j\omega}\right)\right)\left|H_f\left(e^{j\omega}\right)\right|^2 \tag{31}$$

where N_0 is the noise spectral density, $S_i(e^{j\omega})$ is the power spectral density of the interference signals and $H_f(e^{j\omega})$ is the discrete-time frequency response of the front-end filter. For simplicity, we consider an ideal brick wall filter such that $H_f(e^{j\omega}) = 1$ whenever $|\omega| < W_f/2$. Furthermore, and for reasons that will become evident later on, it is of interest to express both $S_g(e^{j\omega})$ and $S_i(e^{j\omega})$ in terms of their normalized unit power (within the front-end bandwidth) PSD. That is, $S_g(e^{j\omega}) = C\tilde{S}_g(e^{j\omega})$ and $S_i(e^{j\omega}) = C_i\tilde{S}_i(e^{j\omega})$, with C and C_i the signal and interference power, respectively.

3 INTERFERENCE EFFECTS ON GNSS RECEIVERS

Three main figures of merit will be considered herein in order to assess the performance degradation of GNSS receivers when operating in the presence of interference sources:

- **C/N0 degradation:** it is a commonly accepted metric for inferring the quality of the received signal in terms of carrier power to (effective) noise spectral density. It is often used as the most straightforward and accessible metric to assess the degradation incurred by interference sources on GNSS receivers [9], [10].
- **Pseudorange degradation:** it is typically measured through the variance of the code delay estimates at the code discriminator output [12], [13], [14]. While the access to this metric is not straightforward (e.g. due to the presence of additional effects, such as clock drift at the receiver), it provides a closer information to the actual accuracy of the estimated user's position.
- **Bit error rate:** for GNSS signals with specific data services (e.g. such as the commercial service in Galileo E6), the bit error rate is a key performance parameter from the end-to-end application point of view.

3.1 C/N0 DEGRADATION

C/N0 can be found as the signal-to-noise ratio (SNR) at the prompt correlator output per correlation time. Assuming a total coherent correlation time of $T_{coh} = N_{coh}T_{code}$ seconds, C/N0 can be obtained as:

$$\frac{C}{N_0} = \frac{1}{T_{coh}} \frac{\mu_P^2}{\sigma_n^2} \tag{32}$$

where μ_P^2 stands for the energy of the prompt correlator, and σ_n^2 the aggregated noise variance affecting the correlator output samples. According to the formulation in (17), the prompt correlator is the one corresponding to $l = 0$, so from (24) and (30) we have that

$$\mu_P^2 = \langle |s_0(k)|^2 \rangle = \left(A\rho(\hat{v}_\epsilon) N_c R_g(\hat{\tau}_\epsilon) \right)^2 \tag{33}$$

$$\sigma_P^2 = \frac{1}{2\pi} \int_{-\pi}^{\pi} S_n\left(e^{j\omega}\right) d\omega \tag{34}$$

For the latter term, we can take advantage of the superposition principle and the 2π-periodic structure of the discrete-time spectra. Since all replicas in (30) are identical expect for a frequency shift, the variance of the prompt correlator output turns out to be given by:

$$\sigma_n^2 = \frac{1}{2\pi} \int_{-\pi}^{\pi} S_w\left(e^{j\omega}\right) \left| H_{coh}\left(e^{j\omega}\right) \right|^2 S_g\left(e^{j\omega}\right) d\omega \tag{35}$$

$$= \frac{1}{2\pi} \int_{-W_f/2}^{W_f/2} \left(N_0 + S_i\left(e^{j\omega}\right) \right) \left| H_{coh}\left(e^{j\omega}\right) \right|^2 S_g\left(e^{j\omega}\right) d\omega. \tag{36}$$

Putting together both terms, and after some straightforward manipulations, the C/N0 at the coherent correlator output becomes:

$$\frac{C}{N_0} = \bar{\gamma}\left[1 + \frac{C_i}{N_0}\frac{1}{2\pi}\int_{-W_f/2}^{W_f/2} \tilde{S}_i\left(e^{j\omega}\right)\left|H_{coh}\left(e^{j\omega}\right)\right|^2 \tilde{S}_g\left(e^{j\omega}\right) d\omega\right]^{-1} \tag{37}$$

where $\bar{\gamma}$ is the baseline C/N0 when only thermal noise is present and C_i is the carrier power including the frequency offset mismatches due to the losses in $\rho(\hat{\nu}_\epsilon)$. The expression above can be simplified to

$$\boxed{\frac{C}{N_0} = \bar{\gamma}\left[1 + \frac{C_i}{N_0} SSC_{i,g}\right]^{-1}} \tag{38}$$

with $\mathrm{SSC}_{i,g}$ the so-called spectral separation coefficient (SSC) between the interference power spectrum and the coherent correlator spectrum:

$$SSC_{i,g} \doteq \frac{1}{2\pi}\int_{-W_f/2}^{W_f/2} \tilde{S}_i\left(e^{j\omega}\right)\left|H_{coh}\left(e^{j\omega}\right)\right|^2 \tilde{S}_g\left(e^{j\omega}\right) d\omega \tag{39}$$

It is interesting to note that contrary to other SSC definitions in the literature, such as the one in [13] where a similar result to (38) was derived, the expression above explicitly incorporates the filtering effects to due coherent correlation beyond the conventional one code period. However, unless otherwise indicated, a 1 ms coherent correlation time is considered in the theoretical plots to be shown within this section.

Finally, and according to (38), it is important to remark that the theoretical C/N0 degradation can be obtained from the C_i/N_0 and the corresponding $SSC_{i,g}$ as follows:

$$\frac{\Delta C}{N_0}(dB) = \bar{\gamma}(dBHz) - \frac{C}{N_0}(dBHz) = 10log_{10}\left(1 + \frac{C_i}{N_0} SSC_{i,g}\right) \tag{40}$$

which for a large enough $\frac{C_i}{N_0} SSC_{i,g}$ product, it can also be approximated by:

$$\frac{\Delta C}{N_0}(dB) \approx \frac{C_i}{N_0}(dBHz) + SSC_{i,g}(dB/Hz) \tag{41}$$

As can be seen, the SSC plays a paramount role in the assessment of C/N0 degradation in the presence of interference sources. Some further insights can be obtained by analyzing the different behavior of the SSC for different GNSS and interference signals. An example is shown in Figure 3-1 for Galileo E1, GPS L1 and Galileo E6, when subject to either a CW (left plot) or a DVB-S signal at 2 Msps (right plot).

Because of the larger mean square bandwidth of Galileo E6B/C signals, two effects are observed on the resulting SSC. On the one hand, the energy of Galileo E6B/C is spread over a larger range of frequencies,

and this makes Galileo E6B/C to exhibit a better immunity against narrowband interferences appearing in the central part of the spectrum (i.e. since less Galileo E6B/C power is present at that part of the spectrum). The corresponding SSC is about 7 dB lower than for narrower bandwidth GNSS signals, as observed on the left hand side of Figure 3-1. On the other hand, and because of such wider energy spread in the frequency domain, Galileo E6B/C is more sensitive to interference signals appearing outside the central lobe, and even at the edge of the band (i.e. at 20 to 30 MHz distance from the main lobe of the spectrum), as observed on both the left and right hand side of Figure 3-1 for a narrowband and wideband interference signals.

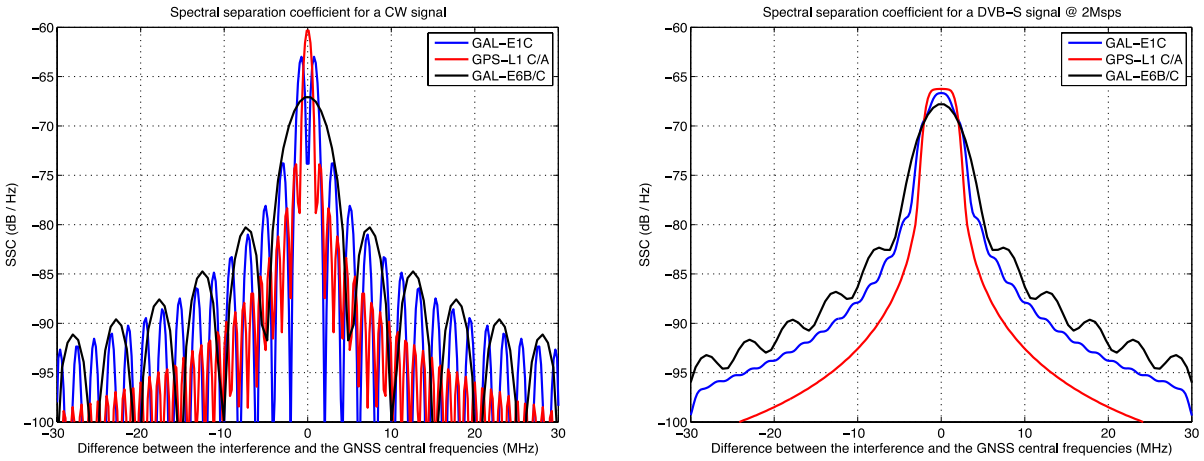

FIGURE 3-1 SSC FOR A CW INTERFERENCE SIGNAL (LEFT) OR A DVB-S INTERFERENCE SIGNAL (RIGHT) FOR DIFFERENT GNSS SIGNALS.

Focusing now on Galileo E6B/C, some illustrative examples are provided next on the SSC as a function of the receiver front-end bandwidth, for a set of representative interference signals that will be considered later on in this study. The results are shown in Figure 3-2 and Figure 3-3, corresponding to a CW, a DVB-S signal with either 2 or 5 MHz bandwidth, and a DVB-T signal with 5 MHz bandwidth.

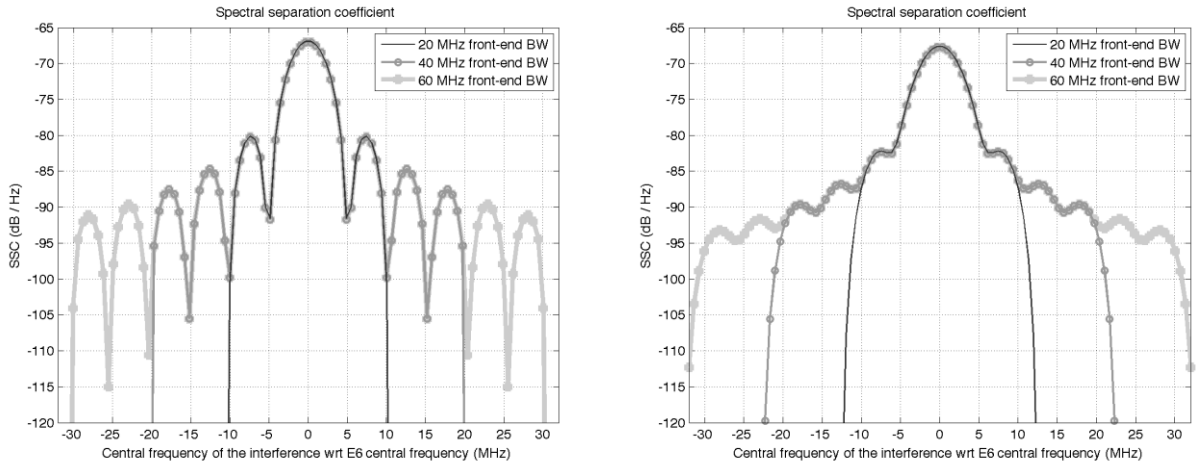

FIGURE 3-2 SSC BETWEEN GALILEO E6B/C AND A CONTINUOUS-WAVE SIGNAL (LEFT) OR A DVB-S SIGNAL WITH 2 MSPS (RIGHT).

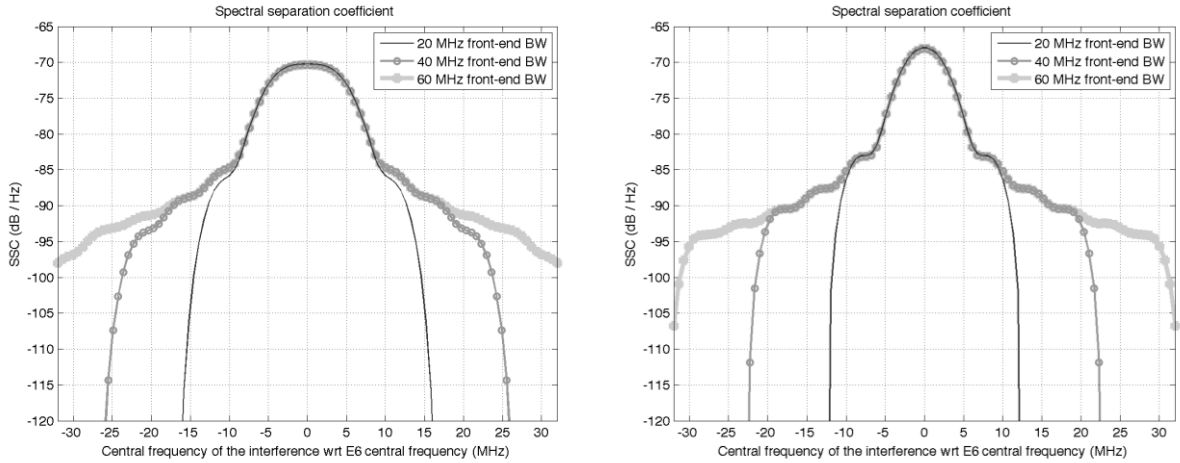

FIGURE 3-3 SSC BETWEEN GALILEO E6B/C AND A DVB-S SIGNAL WITH 5 MSPS (LEFT) OR A DVB-T SIGNAL WITH 5 MHZ (RIGHT).

Using the SSC described above, we can easily compute the C/N0 degradation using the expression in (40). Some results are presented next using the SSC values shown in Figure 3-2 and Figure 3-3, where it can be seen that the C/N0 degradation is quite high for a typical C_i/N_0 value around 100 dBHz, which would correspond to a source emitting on the E6 band with an EIRP of 1W at 3km distance from the receiver, or with an EIRP of 15 W at 10 km from the receiver.

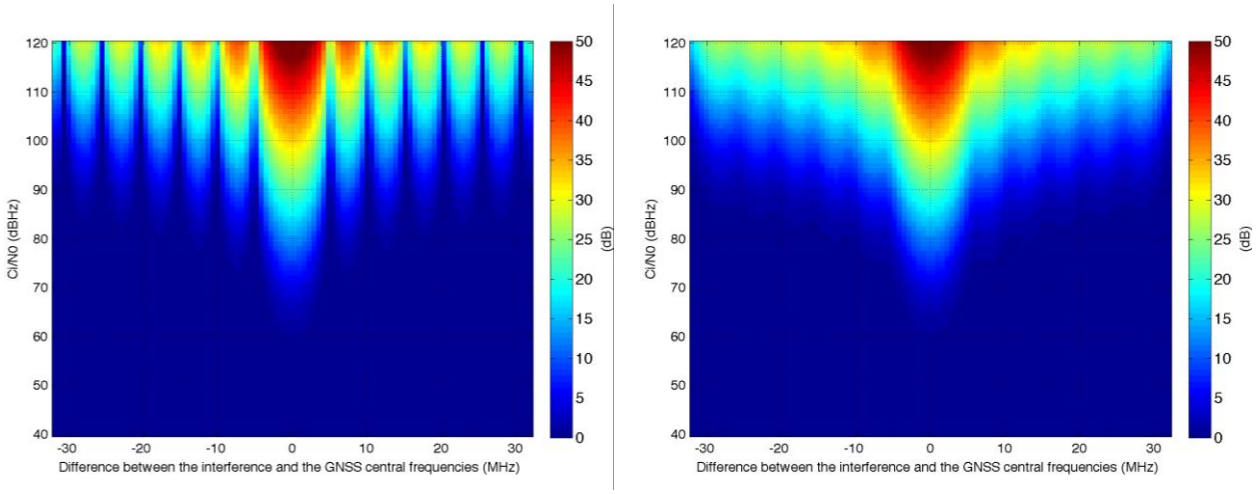

FIGURE 3-4 C/N0 DEGRADATION AS A FUNCTION OF THE RELATIVE CENTRAL FREQUENCY AND CI/N0 OF THE INTERFERENCE FOR A CW SIGNAL (LEFT) AND A DVB-S SIGNAL AT 2 MSPS (RIGHT).

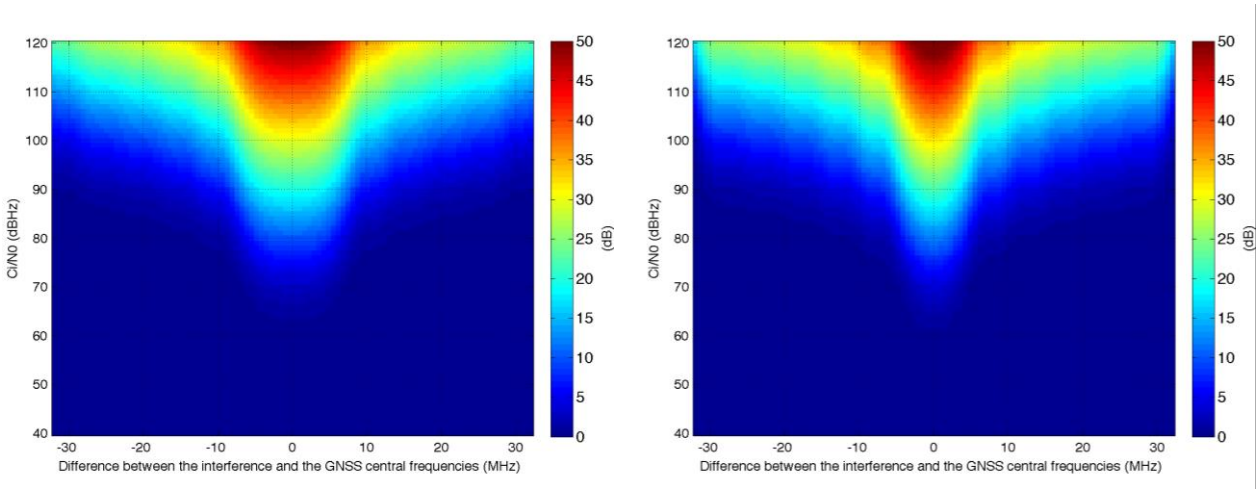

FIGURE 3-5 C/N0 DEGRADATION AS A FUNCTION OF THE RELATIVE CENTRAL FREQUENCY AND CI/N0 OF THE INTERFERENCE FOR A DVB-S SIGNAL WITH 5 MSPS (LEFT) AND A DVB-T SIGNAL WITH 5 MHZ (RIGHT).

For wideband interferences, the degradation could be reduced by increasing the coherent integration time at the code correlator from the standard 1ms considered herein. This, however, would depend on the specific application and working conditions of the receiver (e.g. user dynamics). For instance, in case a 10ms coherent integration time was possible, the effective C_i/N_0 of wideband interferences could be reduced by 10 dB due to the coherent integration filter, thus also reducing the corresponding C/N0 degradation by the same amount. In spite of that, the resulting C/N0 degradation would still be quite significant, around 20 dB, for the typical C_i/N_0 values appearing in amateur radio (i.e. around 100 dBHz, as described later on in Section 4.3).

3.2 PSEUDORANGE DEGRADATION

Pseudorange measurements are obtained from the code-delay estimates at the code discriminator output, and smoothed later on by the tracking loop filters. Several types of code discriminators can be found in practice, either coherent or non-coherent, but the coherent early-minus-late (CEML) is a simple and low-complexity implementation that fits well into our purposes of analytically modeling the pseudorange (i.e. code-delay) degradation. In practice, most of the results derived for the CEML can later on be extended to non-coherent discriminators by including some additional squaring losses [14].

The CEML discriminator is known to be an approximation of the maximum likelihood code delay estimator [15], thus providing asymptotically unbiased and efficient estimates as follows:

$$\hat{\tau}_{CEML}(k) = \frac{1}{K_d} Re[\epsilon_{CEML}(k)] \tag{42}$$

$$\epsilon_{CEML}(k) \doteq y_{-\frac{N_\Delta}{2}}(k) - y_{\frac{N_\Delta}{2}}(k) \tag{43}$$

where $y_{-\frac{N_\Delta}{2}}(k)$ and $y_{\frac{N_\Delta}{2}}(k)$ are the early and late correlator output samples and K_d is a normalizing constant that ensures the unitary input-output relationship of the discriminator. In particular,

$$K_d = \lim_{\Delta\tau \to \infty} \frac{E\left[\epsilon_{CEML}(k)_{|\tau_\epsilon = \Delta\tau}\right] - E\left[\epsilon_{CEML}(k)_{|\tau_\epsilon = 0}\right]}{\Delta\tau} \tag{44}$$

Taking into account the signal contribution in (24) and the even symmetry of the chip pulse shape autocorrelation function, it can be found that

$$K_d = 2A\rho(\hat{v}_\epsilon)N_c \frac{1}{2\pi} \int_{-W_f/2}^{W_f/2} \omega S_g\left(e^{j\omega}\right) sin\left(\frac{\omega N_\Delta}{2}\right) d\omega \tag{45}$$

Then, the variance of the code delay estimates in (42) is given by

$$\sigma^2_{\tau,CEML} = \frac{\sigma_n^2}{K_d^2}(1 - Re[R_n(N_\Delta)]) \tag{46}$$

where $\sigma_n^2 \doteq R_n(0)$ is the aggregated noise power and $R_n(N_\Delta)$ is the autocorrelation of the aggregated noise evaluated at the correlation lag N_Δ. This latter term can equivalently be computed in the frequency domain in virtue of the Wiener-Khinchin theorem as $R_n(\tau) = \frac{1}{2\pi}\int_{-\pi}^{\pi} S_n\left(e^{j\omega}\right) e^{j\omega\tau} d\omega$, for any generic correlation lag τ. By doing so, we have:

$$\sigma^2_{\tau,CEML} = \frac{1}{2\pi K_d^2} \int_{-W_f/2}^{W_f/2} S_n\left(e^{j\omega}\right)[1 - cos(\omega N_\Delta)] d\omega = \frac{1}{\pi K_d^2} \int_{-W_f/2}^{W_f/2} S_n\left(e^{j\omega}\right) sin^2\left(\frac{\omega N_\Delta}{2}\right) d\omega \tag{47}$$

Using this result, and substituting (45) into (47), the variance of the CEML discriminator becomes:

$$\sigma^2_{\tau,CEML} = \bar{\sigma}^2_{\tau,CEML}\left[1 + \frac{C_i \int_{-W_f/2}^{W_f/2} \tilde{S}_i\left(e^{j\omega}\right)\left|H_{coh}\left(e^{j\omega}\right)\right|^2 \tilde{S}_g\left(e^{j\omega}\right) sin^2\left(\frac{\omega N_\Delta}{2}\right) d\omega}{N_0 \int_{-W_f/2}^{W_f/2} |H_{coh}(e^{j\omega})|^2 \tilde{S}_g(e^{j\omega}) sin^2\left(\frac{\omega N_\Delta}{2}\right) d\omega}\right] \tag{48}$$

where $\bar{\sigma}^2_{\tau,\mathrm{CEML}}$ is the baseline CEML discriminator variance when only thermal noise is present. That is,

$$\bar{\sigma}^2_{\tau,CEML} \doteq \frac{\frac{1}{2\pi}\int_{-W_f/2}^{W_f/2}\left|H_{coh}\left(e^{j\omega}\right)\right|^2 S_g\left(e^{j\omega}\right) sin^2\left(\frac{\omega N_\Delta}{2}\right) d\omega}{\frac{2A^2}{N_0}\rho^2(\hat{v}_\epsilon) N_c \left(\frac{1}{2\pi}\int_{-W_f/2}^{W_f/2} \omega S_g(e^{j\omega}) sin\left(\frac{\omega N_\Delta}{2}\right) d\omega\right)^2} \tag{49}$$

For a closely spaced early-late correlator, in such a way that $|\omega N_\Delta| < 1$, we can approximate $\sin\left(\frac{\omega N_\Delta}{2}\right) \approx \frac{\omega N_\Delta}{2}$. Furthermore, due to the comb-like frequency response of the coherent correlation, we also have that $\left|H_{coh}\left(e^{j\omega}\right)\right|^2 S_g\left(e^{j\omega}\right) \approx \sum_{m=0}^{N_{scode}-1} S_g\left(e^{j2\pi m/N_{scode}}\right)$. With these considerations, the baseline variance of the unsmoothed CEML discriminator (i.e. leaving aside the smoothing of the code tracking loop filter) can be approximated by

$$\bar{\sigma}^2_{\tau,CEML} \approx \frac{1}{\frac{2A^2}{N_0}\rho^2(\hat{v}_\epsilon) N_c N_{coh} \frac{1}{2\pi}\int_{-W_f/2}^{W_f/2} \omega^2 S_g(e^{j\omega})\, d\omega} \tag{50}$$

$$= \frac{1}{2\frac{C'}{N_0} T_{coh} \overline{W_g^{\,2}}} \tag{51}$$

with $C' \doteq \frac{1}{T_{coh}} A^2 \rho^2(\hat{v}_\epsilon) N_c N_{coh} \frac{1}{2\pi}\int_{-\pi}^{\pi} S_g\left(e^{j\omega}\right) d\omega$ the carrier power including the losses due to frequency mismatches and $\overline{W_g^{\,2}}$ the mean square bandwidth of the chip pulse shape. That is,

$$\overline{W_g^{\,2}} \doteq \frac{1}{2\pi}\int_{-W_f/2}^{W_f/2} \omega^2 \tilde{S}_g\left(e^{j\omega}\right) d\omega \tag{52}$$

with $\tilde{S}_g\left(e^{j\omega}\right)$ such that $\frac{1}{2\pi}\int_{-W_f/2}^{W_f/2} \tilde{S}_g\left(e^{j\omega}\right) d\omega = 1$. It is interesting to note that (51) is nothing but the Cramér Rao bound (CRB) for time delay estimation in an additive white Gaussian noise channel (see Eq. (3.38) in [17]). This observation confirms that for a closely spaced early-late implementation, the performance of the CEML discriminator coincides with that of an optimal efficient time delay estimator.

With the above results, the physical limit on the CEML discriminator variance in the presence of interference sources can be expressed in a compact manner as:

$$\boxed{\sigma^2_{\tau,CEML} = \bar{\sigma}^2_{\tau,CEML}\left[1 + \frac{C_i}{N_0}\frac{\chi_{i,g}}{\overline{W^2}}\right]} \tag{53}$$

where $\chi_{i,g}$ can be thought as the mean square cross-bandwidth between the signal and the overall interference spectra (also known as "code tracking SSC"), and it is formally defined as follows:

$$\chi_{i,g} \doteq \frac{1}{2\pi}\int_{-\pi}^{\pi} \omega^2 \tilde{S}_i\left(e^{j\omega}\right)\left|H_{coh}\left(e^{j\omega}\right)\right|^2 \tilde{S}_g\left(e^{j\omega}\right) d\omega \tag{54}$$

It is interesting to note that $\chi_{i,g}$ is not a spectral separation coefficient since it includes a frequency-dependent quadratic kernel. This indicates that a different degradation is incurred by interference sources either in terms of code delay (i.e. pseudorange) accuracy or in terms of C/N0. The result in (53) was also derived in [13] using a continuous-time formulation, but where the effect of the coherent integration filter was not explicitly incorporated.

An example of the evolution of $\chi_{i,g}$ for different GNSS signals, and either a CW or a wideband interference, is shown in Figure 3-6. At large-scale, we can see that $\chi_{i,g}$ exhibits the same behavior when the interference is placed either over the central part of the GNSS spectrum or far away from it. This effect can be perceived more clearly for a wideband interference signal such as the one considered in the right hand side of Figure 3-6, where a nearly constant $\chi_{i,g}$ is observed. This suggests that in terms of pseudorange performance, a non-negligible degradation may be experienced even if the interference signal is placed far away the central lobe, within the receiver front-end bandwidth. This is in contrast to the conventional SSC involved in the C/N0 degradation, which is very sensitive to interference sources lying on the central lobe of the GNSS spectrum, but not that much when lying far away from it.

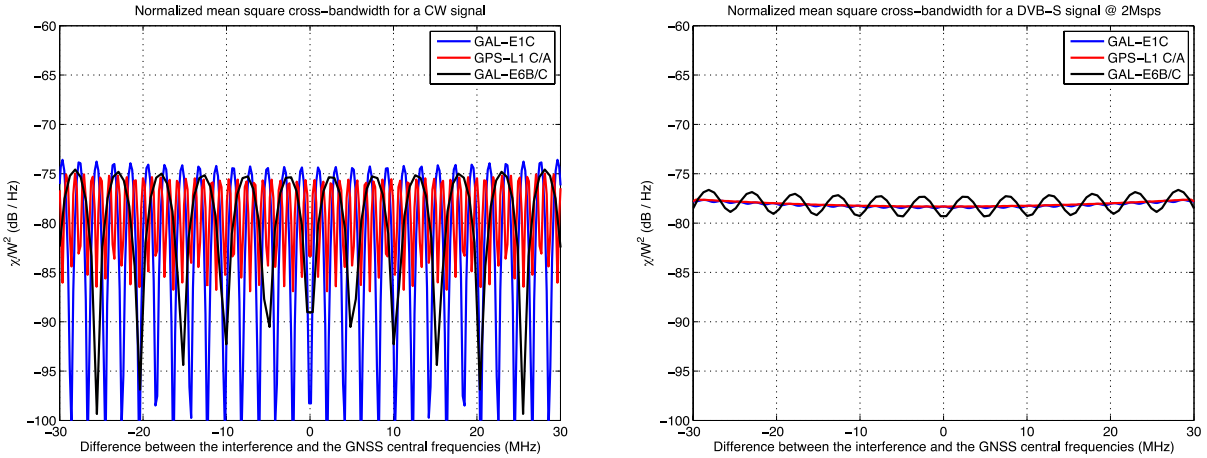

FIGURE 3-6 NORMALIZED MEAN SQUARE CROSS-BANDWIDTH IN (54) FOR A CW INTERFERENCE SIGNAL (LEFT) OR A DVB-S INTERFERENCE SIGNAL (RIGHT) FOR DIFFERENT GNSS SIGNALS

For the specific case of Galileo E6B/C, Figure 3-7 and Figure 3-8 show the evolution of $\chi_{i,g}$ for different receiver front-end bandwidths, when a set of representative interference sources is considered. The similar behavior of $\chi_{i,g}$ either at the center or at the edge of the spectrum is a relevant aspect that will be taken into account later on in the experimental assessment of the Galileo E6B/C performance degradation.

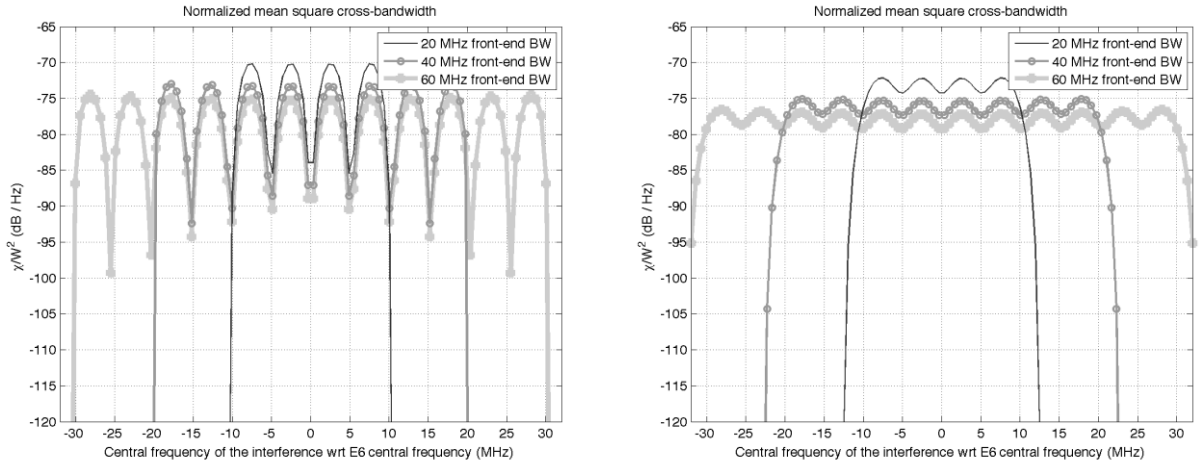

FIGURE 3-7 MEAN SQUARE CROSS-BANDWIDTH BETWEEN THE GALILEO E6B/C SPECTRUM AND TWO DIFFERENT INTERFERENCE SIGNALS: (LEFT) CONTINUOUS-WAVE; (RIGHT) DVB-S SIGNAL WITH 2 MSPS.

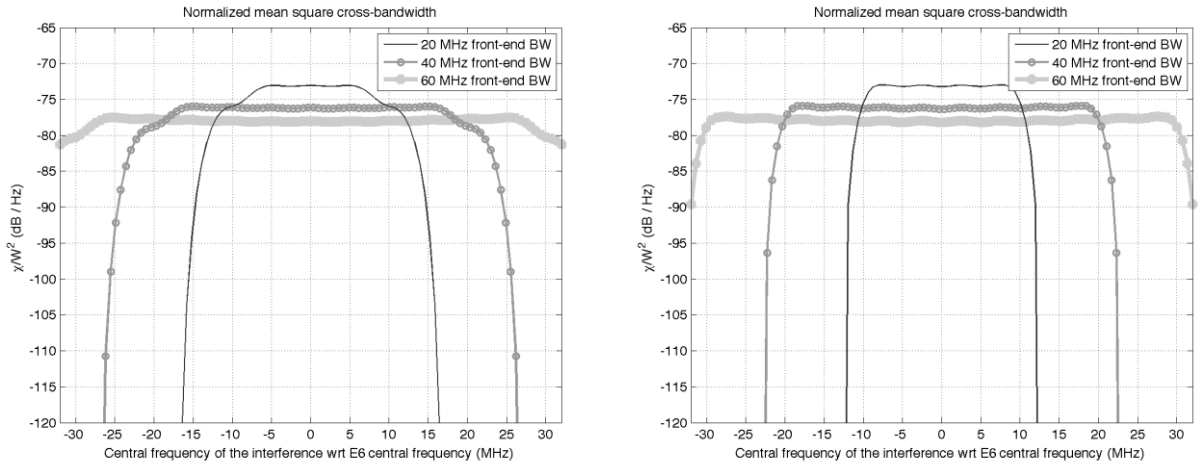

FIGURE 3-8 MEAN SQUARE CROSS-BANDWIDTH BETWEEN THE GALILEO E6B/C SPECTRUM AND TWO DIFFERENT INTERFERENCE SIGNALS: (LEFT) DVB-S SIGNAL WITH 5 MSPS; (RIGHT) DVB-T SIGNAL WITH 5 MHZ BANDWIDTH.

Using the SSC described above, we can easily compute the pseudorange degradation, defined as $10\log_{10}\left(\sigma^2_{\tau,CEML}/\bar{\sigma}^2_{\tau,CEML}\right)$ using the expression in (53). Some results are presented next using the SSC shown in Figure 3-2 and Figure 3-3, where the pseudorange degradation is found to be quite high for a typical C_i/N_0 value around 100 dBHz, which would correspond to a source emitting on the E6 band with an EIRP of 1W at 3km distance from the receiver, or with an EIRP of 15 W at 10 km from the receiver.

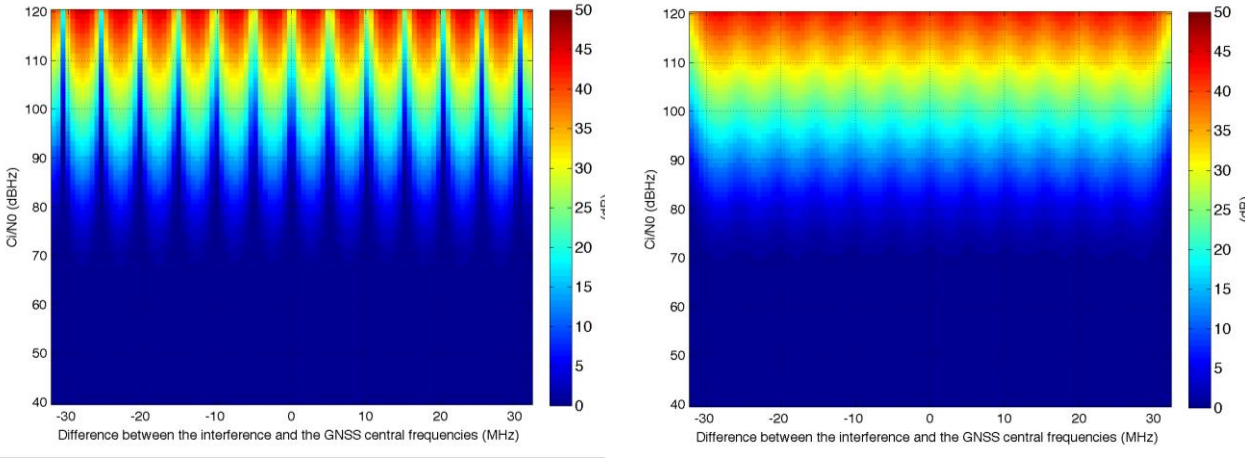

FIGURE 3-9 PSEUDORANGE DEGRADATION AS A FUNCTION OF THE RELATIVE CENTRAL FREQUENCY AND CI/N0 OF THE INTERFERENCE FOR A CW SIGNAL (LEFT) AND A DVB-S SIGNAL WITH 2 MSPS (RIGHT).

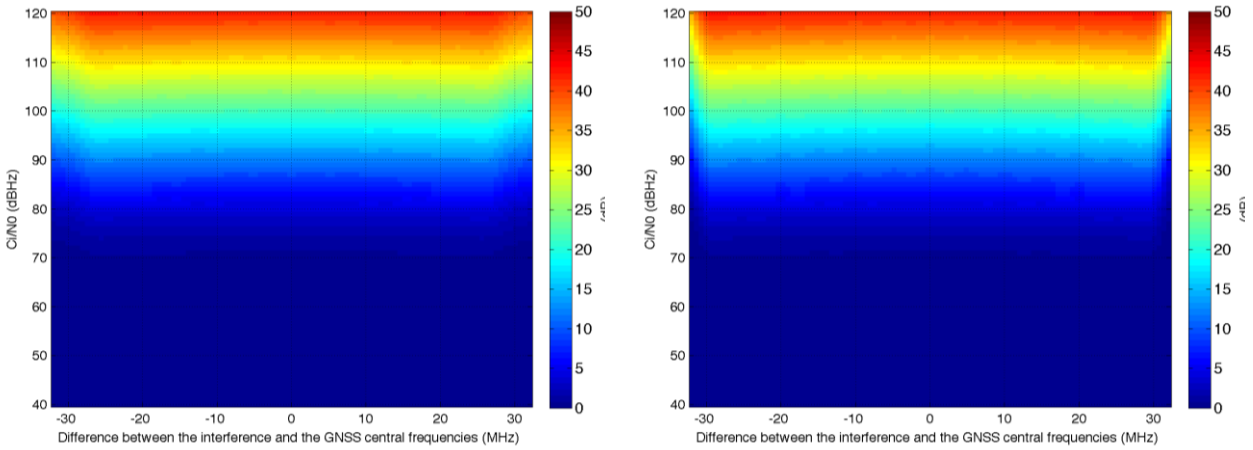

FIGURE 3-10 PSEUDORANGE DEGRADATION AS A FUNCTION OF THE RELATIVE CENTRAL FREQUENCY AND CI/N0 OF THE INTERFERENCE FOR A DVB-S SIGNAL WITH 5 MSPS (LEFT) AND A DVB-T SIGNAL WITH 5 MHZ (RIGHT).

For wideband interferences, and similarly to what happened for the C/N0, the pseudorange degradation could also be reduced by increasing the coherent integration time at the code correlator (when applicable, depending on the user working conditions and requirements) beyond the standard 1ms considered herein. In case a 10ms coherent integration time was possible, the effective C_i/N_0 of wideband interferences could be reduced by 10 dB, thus also reducing the corresponding pseudorange degradation by the nearly same amount. In spite of that, the resulting degradation of the pseudorange variance would still be quite significant, from 15 to 20 dB depending on the type of interference, assuming typical C_i/N_0 values around 100 dBHz.

3.3 BIT ERROR RATE (BER) DEGRADATION

Data demodulation plays a relevant role in GNSS receivers. On the one hand, it is needed for retrieving the ephemeris data of visible satellites (e.g. satellites orbits, clocks parameters, etc), which are required for determining the user's position based on the measured pseudoranges. On the other hand, additional data messages are sent by some specific GNSS signals with the aim of supporting commercial, integrity or governmental services. This is the case of Galileo E6B and the C/NAV message.

In this context, it is also of interest to assess the potential impact that interference signals may cause in terms of data demodulation performance. For the case of Galileo E6B, which is based on a BPSK modulation scheme, the probability of bit error rate (BER) is known to be given by:

$$P_e = Q\left(\sqrt{2\frac{C}{N_0}T_{bit}}\right) \tag{55}$$

where $T_{bit} = 1/R_{bit}$ is the information bit period, with $R_{bit} = 500$ bps for Galileo E6B, and the $Q(\cdot)$ function is defined as the right tail integral of a normalized Gaussian distribution, that is:

$$Q(x) \doteq \frac{1}{\sqrt{2\pi}}\int_x^\infty e^{-\lambda^2/2}d\lambda \tag{56}$$

Using the relationship in (55), the C/N0 degradation in (40) can be used to infer the BER degradation that may be experienced by Galileo E6 receivers. It is true however, that the relationship in (55) is not an exact one when nonlinear effects do appear, mainly because of the presence of high power interference sources. Even in that case, we can still use (55) to bound the actual (uncoded) BER. As reported in [7], the result in (55) becomes a lower bound when the empirical C/N0 (i.e. the one actually measured by the receiver) is used. Therefore, the result in (55) with the empirical C/N0 provides an optimistic indication on the potential degradation that may be incurred on GNSS data channels, such as the one conveyed in Galileo E6B. Moreover, this result can also be used to infer the degradation in terms of time-to-first-fix (TTFF), which is a key performance parameter at the user level [16].

An example of the BER as a function of C/N0 degradation is illustrated in Figure 3-11. As can be seen, quite a different BER is obtained for the same C/N0 degradation, depending on the initial nominal C/N0 (i.e. the interference-free C/N0).

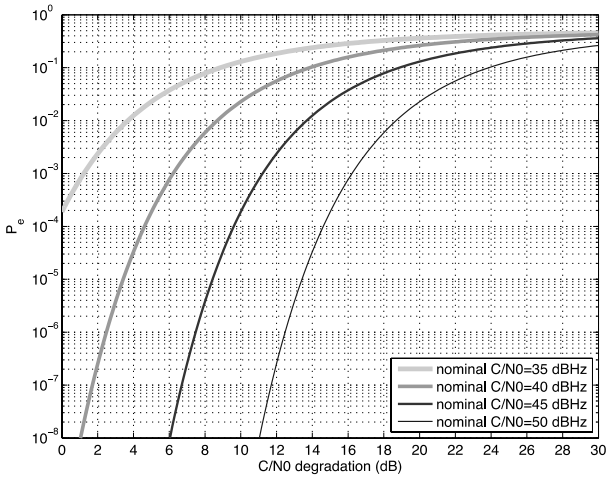

FIGURE 3-11 UNCODED BIT ERROR RATE OF GALILEO E6B AS A FUNCTION OF C/N0 DEGRADATION.

The results in Figure 3-11 do not depend on any specific interference but just on the C/N0 degradation being experienced by the GNSS receiver, as well as on the baseline (i.e. nominal) C/N0 at which it was initially operating. In that sense, any possible interference test case can easily be mapped onto the resulting BER performance just by using the resulting C/N0 degradation incurred at the receiver. In spite of that, it is of interest to assess the BER sensitivity to different types of interferences, and to different central frequencies. To do so, an example is shown in Figure 3-12 for a CW and DVB-S (4 Msps) interference. This figure represents the BER as a function of C_i/N_0 when the interference is placed at different equispaced central frequencies, f_i, within the E6 band. The Galileo receiver is assumed to be

nominally working at C/N0=45 dBHz. Thick lines represent the average BER for all central frequencies, and provide valuable information on the average BER that could be obtained within the E6 band in a realistic scenario. For a representative C_i/N_0 of 100 dBHz (which corresponds to a typical scenario with an interference using EIRP=15W at 10 km distance), the average (uncoded) BER lies within the range 0.01 to 0.1, which involves a severe degradation with respect to the nominal (almost error-free) case.

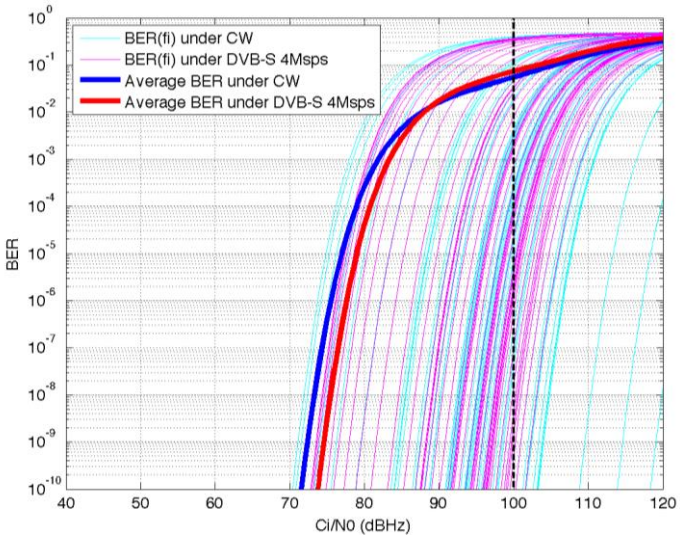

FIGURE 3-12 UNCODED BIT ERROR RATE AS A FUNCTION OF THE CENTRAL FREQUENCY OF THE INTERFERENCE.

4 OVERVIEW OF THE GALILEO E6 BAND

4.1 INTRODUCTION TO THE GALILEO E6 SIGNAL

According to the Galileo signal in space (SIS) interface control document (ICD), the Galileo E6 band is allocated to the portion of spectrum ranging from 1260 to 1300 MHz. It contains the so-called Galileo E6 signal, which is composed of two different components, namely E6B and E6C, which are modulated in-phase using two different spreading codes in a code division multiple access (CDMA) scheme. The underlying modulation does not follow the usual binary offset carrier (BOC) of other Galileo signals. Instead, it is based on a conventional binary phase-shift keying (BPSK) modulation with a rectangular pulse shape, similarly to GPS L1 C/A, but with a five times larger chip rate and code length. That is, $R_c = 5.115$ Mchips/s and spreading codes of $N_r = 5115$ chips, leading to a primary code duration of $T_{code} = 1$ ms.

The main difference between the E6B and E6C components lies in the presence or absence of data modulation. In particular, the E6B component does convey a data message corresponding to the so-called commercial navigation (C/NAV) data stream. This message is transmitted at a rate of 1000 symbols per second, and it can be used to broadcast information for professional or commercial applications. In contrast, the E6C component is a dataless or so-called "pilot" component, in the sense that the ranging code is transmitted without any superimposed data message. The E6C primary spreading code is just tiered with a secondary code with length $N_r = 100$ chips, which is based on a binary memory random code.

TABLE 1: MAIN PARAMETERS OF THE GALILEO E6 SIGNAL [1]

	E6B	**E6C**
Carrier frequency	1278.75 MHz	
Modulation scheme	BPSK(5)	
Chip rate	5.115 Mchips/s	
Primary code length	5115 chips	
Primary code duration	1 ms	
Secondary code length	N/A	100 chips
Data message	Yes	No
Data rate	1000 symbols/s 500 bits/s	N/A (Pilot component)
Minimum received power level on ground	-158 dBW	-158 dBW

One of the key features of Galileo E6 is the possibility of including authentication at both the spreading code and data level, thus enabling users to trust and rely on the signals broadcasted by the system. This feature is in line with one of the objectives of Galileo, which is the provision of a commercial service (CS) for the development of professional or commercial applications. That is, a service with controllable access, and capable of delivering improved performance and greater added value than those obtained by using open signals. In order to achieve these goals, it is of paramount importance to assess the potential degradation that may be experienced in the presence of potential interference sources already coexisting within the E6 band. A brief overview of the existing regulatory framework and the potential interference sources will be described next.

4.2 REGULATORY FRAMEWORK APPLICABLE TO GALILEO E6 SIGNALS

As previously described, the Galileo E6 signal is allocated within the frequency band ranging from 1260 to 1300 MHz, according to the Galileo SIS ICD [1]. This allocation is consistent with the recommendations of the International Telecommunications Union (ITU), which indicates that the frequency band from 1215 to 1300 MHz is primarily intended for radionavigation services (RNSS) [18]. As such, this band is already being used by other RNSS apart from Galileo, such as the Chinese Beidou and the Japanese QZSS systems.

While RNSS is the primary service within the frequency band from 1215 to 1300 MHz, international regulations do authorize the operation of amateur radio services (ARS) in a secondary basis. This means that, according to Article 5.28 of ITU regulations, ARS (as a secondary service) shall be deployed in such a way that they do not cause harmful interference to RNSS operating in the same band [19]. This is the case of amateur transmissions on the so-called 23 cm band, which ranges from 1240 to 1300 MHz, and that is actively used for amateur voice, data and image transmissions in many countries, and particularly, in Central Europe.

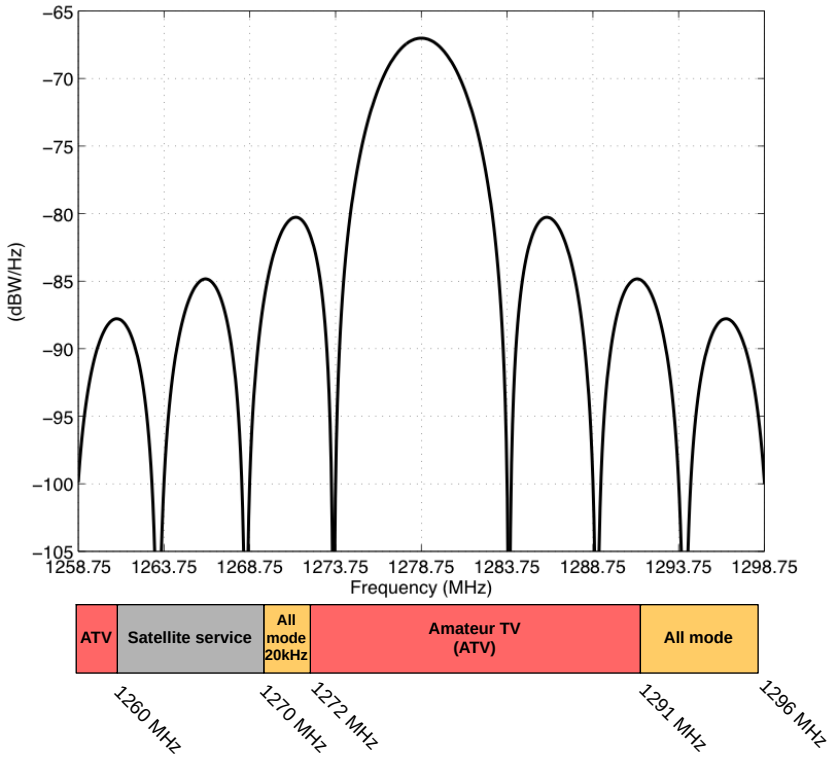

FIGURE 4-1 SCHEMATIC REPRESENTATION OF THE GALILEO E6B/C NORMALIZED PSD AND THE COEXISTING SERVICES WITHIN THE SAME BAND, ACCORDING TO THE IARU BANDPLAN ALLOCATION [3].

Among all the ARS in the 23 cm, amateur television (ATV) deserves some special attention. According to the International Amateur Radio Union (IARU), the portion of spectrum ranging from 1272 to 1291 MHz is intended for ATV, either analog or digital [3]. This portion falls completely within the central part of the Galileo E6 spectrum, as observed in Figure 4-1. That is, there where most of the Galileo E6 signal power is allocated[1]. As a result of such overlap, ATV is envisaged as a relevant potential threat to future

[1] One exception to this rule is found in the UK, where ATV stations are typically allocated outside the E6 band (e.g. from 1242 to 1249 MHz, or from 1300 to 1325 MHz) [20].

Galileo services to be delivered on the E6 band. There have been recent incidents that support this statement, such as the disruption of service experienced at the Galileo Control Center (GCC) in Oberpfaffenhofen, Germany, on March 2014. The German regulator, the Bundesnetzargentur (BnetzA), determined that the event had been caused by a nearby ATV station (at 18 km distance from the GCC) emitting at the central frequency of Galileo E6. After verifications, the ATV station was instructed to be shut down.

In spite of the evidence above, there does not exist a detailed and realistic assessment on what the actual degradation of ARS, and in particular, ATV, might be on the performance of Galileo E6 receivers. The present study is intended to fill this gap by providing empirical evidences obtained with high-end Galileo E6 receivers and a set of representative ATV interfering signals, as described next.

4.3 AMATEUR TELEVISION ON THE GALILEO E6 BAND

ATV transmissions within the E6 band are quite popular in central European countries, such as Germany, where there is a wide and active network of ATV repeaters. ATV transmissions are mostly used for personal use, with amateur users sharing and broadcasting their own edited video contents for communicating with each other. Certain events or local activities are often covered by amateur operators, who broadcast live video to the surrounding neighbourhoods in a similar manner as a local television channel would do.

Because of the experimental nature of many amateur transmissions, ATV within the E6 can be very heterogeneous. Many amateur operators carry out experimental tests with their equipment in search of the best transmission scheme fitting their own needs. As a result, a myriad of different ATV schemes do coexist in practice, from analog to digital and from narrowband to wideband. Regarding the transmitted power levels, they can also be quite heterogeneous. While the typical equivalent isotropically radiated power (EIRP) ranges from 0.1 W to 15 W, some amateur stations are currently operating with 100, 200 or even 750 W.

In order to shed some light on the most representative ATV schemes, and on the concern of ATV emissions on Galileo E6 performance, conversations were initiated between the JRC and a delegation of IARU members from UK, Germany and Italy amateur societies in the Fall of 2014. The goal of these conversations was to agree on a test plan to assess the potential degradation effects caused by ATV on Galileo E6 receivers, and to focus on a representative subset of ATV signaling formats. While analog TV is known to be widespread deployed, many ATV stations are already migrating to digital modulation schemes due to their better efficiency and noise immunity. In that sense, the trend is that digital signaling will gradually become the default ATV scheme in the coming years, and therefore, will be the focus of the present study.

Regarding digital ATV (D-ATV), modulation formats following the guidelines of the Digital Video Broadcast (DVB) group are becoming the preferred option for most D-ATV users. In particular, the satellite and terrestrial DVB recommendations, namely the DVB-S and DVB-T standards, respectively.

4.3.1 DVB-S SIGNALS

DVB-S was originally designed for digital video broadcasting through satellite links [21]. Its physical layer is based on quadrature phase shifty keying (QPSK) modulation, where a square root raised cosine (SQRRC) pulse shape is adopted with roll-off factor 0.35. In order to ensure adequate transitions between consecutive symbols, the input bits are randomized using a pseudo random binary sequence (PRBS) generator. This ensures that the transitions between output consecutive symbols do also

preserve a pseudo random behavior, and therefore, undesired spectral peaks are avoided. In virtue of the assumption of pseudo random symbols, the output spectrum of DVB-S is dominated by the PSD of the SQRCC pulse (see Section 4.5 in [21]) as observed in the lower plot of Figure 4-2.

4.3.2 DVB-T SIGNALS

DVB-T was originally designed for digital video broadcasting through terrestrial links [22]. As such, it was specifically conceived to cope with multipath propagation, since this is one of the main deleterious impairments in wireless terrestrial communications. To do so, DVB-T adopts a multicarrier signal scheme based on orthogonal frequency division multiplexing (OFDM), which is based on the parallel transmission of several low data rate subcarriers with a rectangular pulse shape. The advantage of OFDM signaling primarily comes from its inherent multipath protection and the low complexity channel equalization [23], when compared to conventional single carrier modulation schemes.

The resulting spectrum, again under the assumption of randomized bits, is given by the superposition of the sinc-shaped spectra of each subcarrier, leading to kind of brick-wall spectrum, as observed in the lower plot of Figure 4-3. The total data rate of the transmitted signal depends on the selected constellation, which can be either QPSK, 16-QAM or 64-QAM for all subcarriers. Nevertheless, the DVB-T standard specifies four possible transmission bandwidths: 5, 6, 7 and 8 MHz depending on the number of subcarriers and their frequency separation. Two predefined operation modes are defined, namely the 2k and 8k modes, which correspond to a total of 2048 and 8192 raw subcarriers (1705 and 6817 useful subcarriers), respectively.

The smallest number of subcarriers (i.e. the 2k mode) is recommended for single transmitter operation and for small networks with limited transmitter distances [22], as it is the case of D-ATV. It is for this reason that the 2k mode is actually the preferred operation mode in most D-ATV equipment.

4.3.3 NARROWBAND MISCELLANEOUS SIGNALS

While the focus of this study is primarily on D-ATV, we will give some special consideration to the case of narrowband interference signals, which do also populate the E6 band. These signals correspond to a wide range of different services and applications, from repeater beacons for channel sounding, to telegraphy, machine generated mode (MGM) transmissions, or Earth-Moon-Earth communications (EME), just to mention a few. In many cases, the transmitted signal may have a very narrow bandwidth of less than 1 kHz (as in telegraphy or MGM), or even is based on a pure continuous wave (CW) signal.

Apart from that, very narrowband or CW signals are also of interest for assessing the performance of GNSS receivers. Most GNSS signals, as it is the case with Galileo E6B/C, are based on CDMA through direct-sequence spread spectrum (DS-SS) technology. At the receiver side, the code despreading provides some inherent interference protection against interference sources, since the latter are spread and diluted in frequency at the code correlator output [15]. The protection against narrowband interferences is provided by the spreading gain, which can be found as the ratio between the chip rate and the data rate. For GPS L1 C/A it is about 43dB while for Galileo E6B (assuming a data rate of 500 bits/s) it is a bit less, about 40 dB.

In that sense, it is of interest to assess the effectiveness of such inherent protection in order to determine the potential performance degradation that may be experienced by Galileo E6 receivers in practice. For that reason, we have also considered the case of CW signals in the tests carried out within the scope of this study.

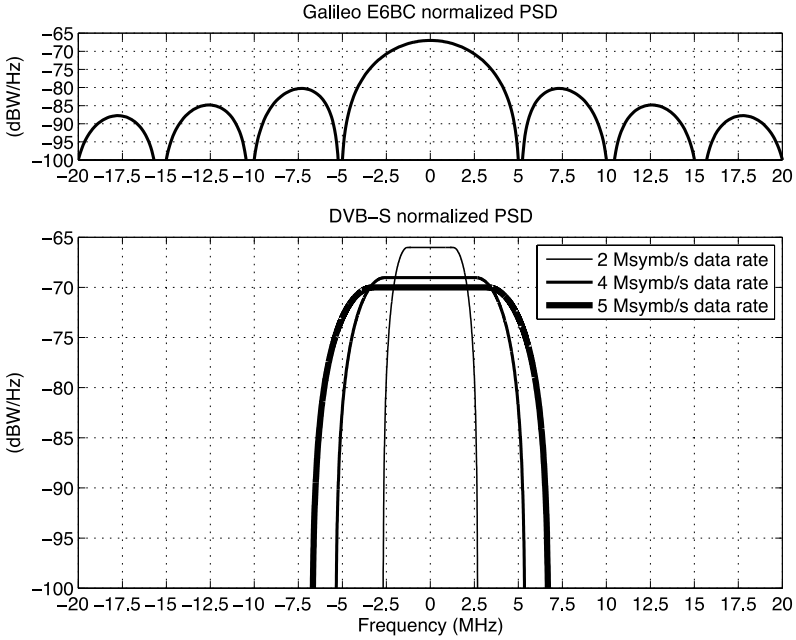

FIGURE 4-2 COMPARISON BETWEEN THE NORMALIZED PSD OF GALILEO E6BC (UP) AND THE NORMALIZED PSD OF DVB-S (DOWN) FOR DIFFERENT DVB-S DATA RATES.

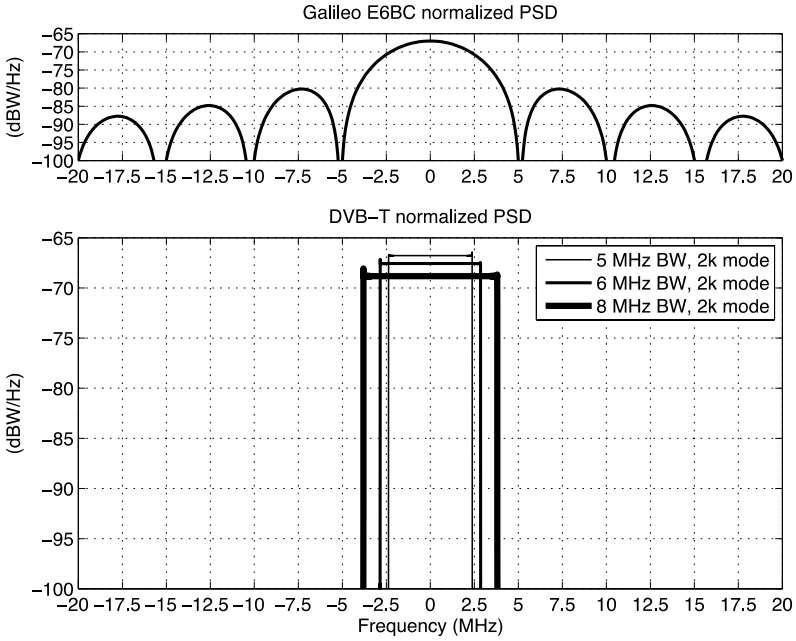

FIGURE 4-3 COMPARISON BETWEEN THE NORMALIZED PSD OF GALILEO E6BC (UP) AND THE NORMALIZED PSD OF DVB-T (DOWN) FOR DIFFERENT TRANSMISSION BANDWIDTHS AND THE 2K MODE.

5 EXPERIMENTAL SETUP AT THE JRC

In order to reproduce a realistic scenario, a set of high-end Galileo E6 receivers where exposed to live signals coming from both Galileo satellites and interference sources. The tests were carried out within the anechoic chamber of the European Microwave Signature Laboratory (EMSL), at the JRC premises in Ispra, Italy. This facility provides a unique environment for performing over-the-air measurements in a controlled, automated and repeatable manner. A schematic representation of the EMSL anechoic chamber is illustrated in Figure 5-1, which has a spherical shape with a radius of 10 meters and the floor is at 5 meters below the center of the sphere. For this study, GNSS signals were broadcasted from an antenna placed on the upper part of the chamber, while interference signals were transmitted from a side antenna, at the same horizontal plane where the receivers were located (see right hand side of Figure 5-2).

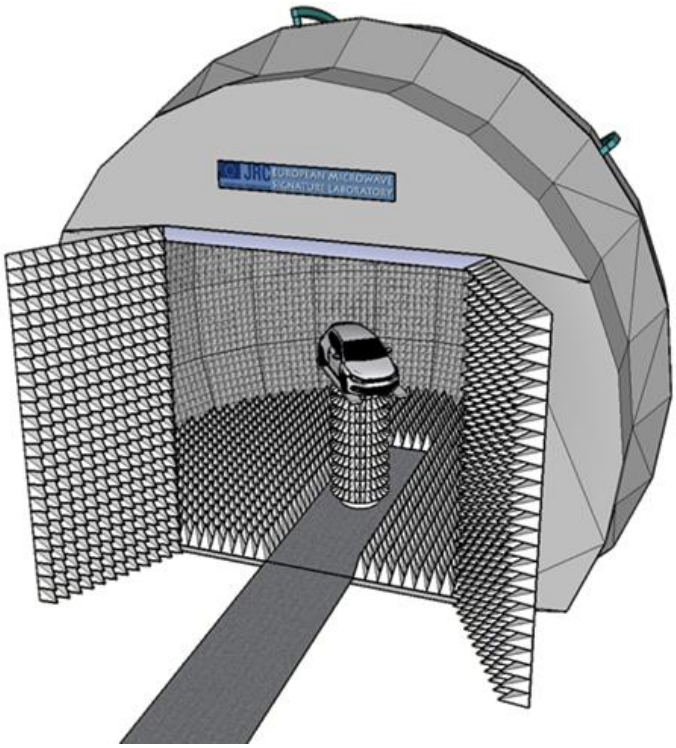

FIGURE 5-1 ILLUSTRATION OF THE EMSL ANECHOIC CHAMBER WHERE THE MEASUREMENTS OF THIS STUDY WERE CARRIED OUT.

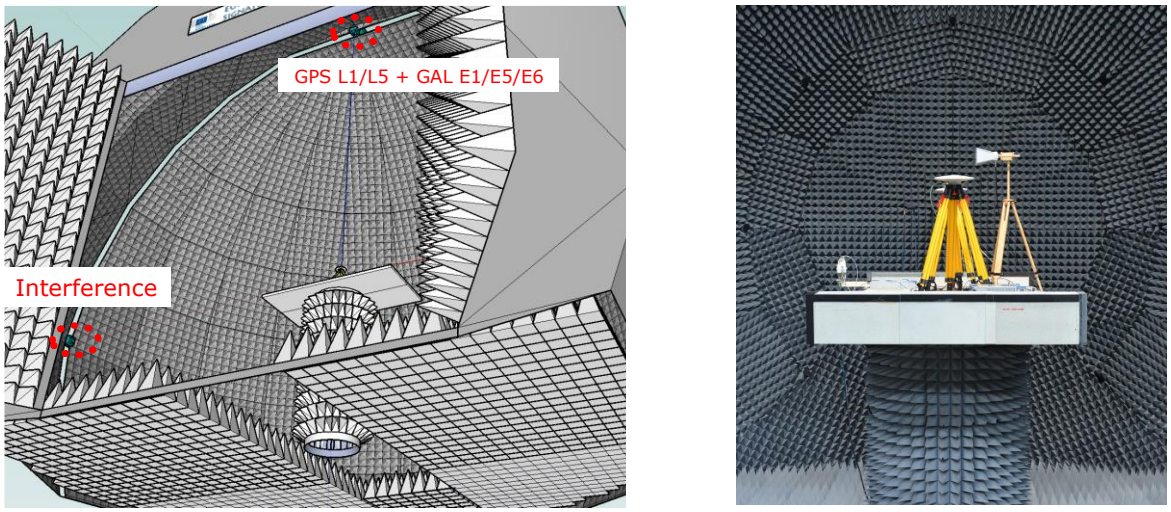

FIGURE 5-2 (LEFT) PLACEMENT OF THE TRANSMIT ANTENNAS FOR BROADCASTING GNSS AND INTERFERENCE SIGNALS WITHIN THE EMSL. (RIGHT) DETAIL OF THE PLATFORM AT THE CENTER OF THE CHAMBER, WHERE THE RECEIVERS UNDER TEST ARE PLACED.

A schematic representation of the whole experimental setup is presented in Figure 5-3, where the transmission and reception chains are highlighted inside two green shaded areas. These two setups are described in more detail in Section 5.1 and Section 5.2, respectively.

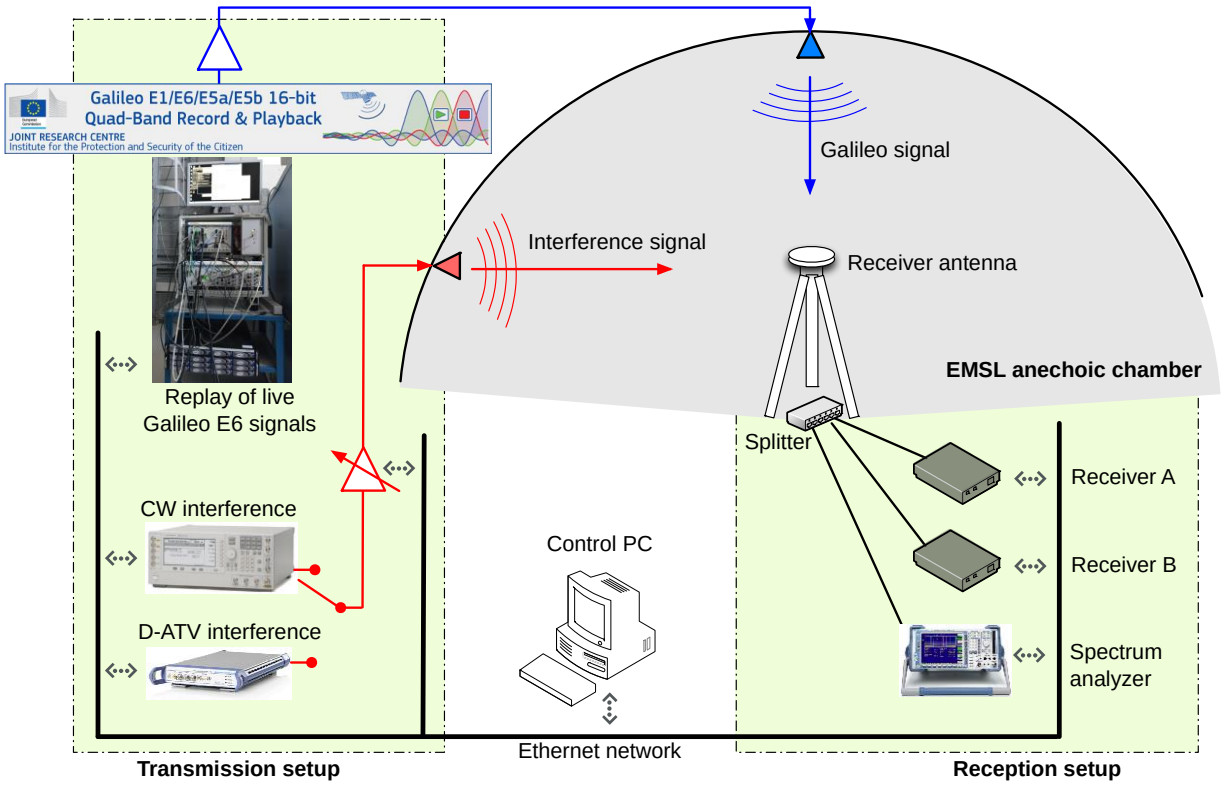

FIGURE 5-3 SCHEMATIC REPRESENTATION OF THE EXPERIMENTAL SETUP.

5.1 TRANSMISSION SETUP

Two different types of signals are broadcasted within the EMSL, namely Galileo E6 signals and D-ATV like interference signals, each of them with its own transmission setup. Regarding the Galileo signal, it is broadcasted using a transmit antenna placed on the ceiling of the anechoic chamber, and vertically aligned with the platform where the receivers are placed. This Galileo signal was recorded on May 16, 2014, at 21:10h GPS time at the JRC site, using an active antenna placed on the roof of the EMSL building and a National Instruments PXI front-end and data grabber. All four Galileo IOV satellites were visible at that time, even though for the analyses to be presented next, only the three satellites with PRN 11, 12 and 19 were considered. Once stored, the same set of recorded Galileo samples was replayed and broadcasted for each of the experiments to be carried out, thus making sure that all experiments were performed in the same working conditions.

Regarding interference signals, the ones corresponding to D-ATV were generated using a Rhode Schwarz SFC compact modulator, which is capable of generating a wide range of different TV test signals, including DVB-S and DVB-T. The DVB parameters and the central frequency of the modulated signal were automatically adjusted for each of the tests. To do so, the device was interfaced by means of SCPI commands sent from a dedicated control software over the EMSL Ethernet network. In order to have a large enough dynamic range, a 30 dB amplifier was connected to the R&S SFC output, followed by a 90 dB Ethernet-based programmable attenuator. The attenuator, which can be adjusted in steps of 0.25 dB,

was used to adjust the output power of the generated D-ATV signals according to the specific power profile considered in the tests.

For CW interference signals, the Agilent E8267D PSG vector signal generator was used instead. In that case, the dynamic range was already enough and no additional equipment was required to adjust the output power levels. As with the S&R SFC, the device was automatically configured by means of SCPI commands sent through the EMSL network.

Once the interference signal (either D-ATV or CW) was properly generated and conditioned, it was fed to one of the sled transmit antennas within the EMSL anechoic chamber. Even though the sled could be moved along the rail system, it remained fixed during the experiments, and it pointed to the end-fire of the Galileo E6 receive antennas. This placement is consistent with the fact that most ATV interference signals are expected to come from the surroundings of the user, and thus, with low elevation angles. Interestingly, this provides an additional protection against interferences due to losses of the receive antenna radiation pattern at low elevation angles. Figure 5-4 shows the measured radiation pattern of the Galileo E6 antenna used in this study, where it can be seen that up to 14 dB attenuation are experienced between the vertical and horizontal axis.

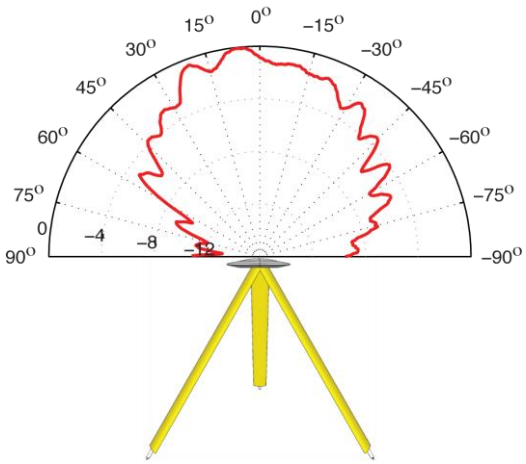

FIGURE 5-4 MEASURED RADIATION PATTERN OF THE GALILEO E6 RECEIVE ANTENNA USED IN THIS STUDY.

Therefore, we could understand the results of this study to be "optimistic", in the sense that the elevation angle considered herein is the one providing the largest interference attenuation. In practice, interference signals coming from any other higher elevation angle will be less attenuated by the receive antenna, and thus will be causing an even larger performance degradation to the user receiver.

5.2 RECEPTION SETUP

A set of two different high-end Galileo E6 receivers was used in this study. The receivers were provided to the JRC by different receiver manufacturers under a non-disclosure agreement (NDA), and they were all tested simultaneously under the same working conditions. To do so, a splitter was used to distribute the signal at the antenna output to the different receivers under test. A spectrum analyzer was also connected to the splitter in order to monitor the spectral occupancy of the signals being received (particularly, the interference ones) as well as their power levels. This information was used later on to compute the effective interference power coming into each of the receivers, as well as the noise spectral density at the antenna output.

The receivers were remotely controlled by the control PC, and their output observables were logged into separate data files, and later on converted into Rinex 3.0 files. The information contained in these Rinex files was the input source for the analyses that were conducted in this study. Mainly, we focused on the carrier to noise spectral density (C/N_0) and the variance of the pseudorange estimates provided by each receiver.

Post-processing of the pseudorange observables

Regarding the pseudorange variance, some considerations must be made. First of all, pseudoranges $\rho_i(k)$ from the i-th satellite can be modeled as a slow time-varying component $\bar{\rho}_i(k)$ (i.e. due to the satellite movement relative to the receiver under test) plus some random disturbance $\xi_i(k)$. That is,

$$\rho_i(k) = \bar{\rho}_i(k) + \xi_i(k) \tag{57}$$

In order to be able to compute the pseudorange variance, which is actually caused by the random disturbance $\xi(k)$, we need to get rid of the slowly time-varying component $\bar{\rho}_i(k)$. To do so, we stack a set of L_m consecutive pseudoranges (corresponding to 100 seconds) into vector form, $\boldsymbol{\rho}_i \doteq [\rho_i(0), \rho_i(1), \dots, \rho_i(L_m - 1)]^T$, and find their least square fit with a fifth order polynomial with coefficients $\boldsymbol{\alpha}_i \doteq [\alpha_{i,0}, \alpha_{i,1}, \alpha_{i,2}, \alpha_{i,3}, \alpha_{i,4}]^T$, which can be found as:

$$\widehat{\boldsymbol{\alpha}}_i = arg\min_{\boldsymbol{\alpha}_i} \|\boldsymbol{\rho}_i - \boldsymbol{B}\boldsymbol{\alpha}_i\|^2 \tag{58}$$

where $\boldsymbol{B} \doteq [\boldsymbol{t}^0, \boldsymbol{t}^1, \boldsymbol{t}^2, \boldsymbol{t}^3, \boldsymbol{t}^4]$ is a $(L_m \times 5)$ Vandermonde matrix with $\boldsymbol{t} \doteq [0,1, \dots, k, \dots, L_m - 1]^T$ the discrete-time indexation vector. The vector of pseudorange residuals $\boldsymbol{\xi}_i \doteq [\xi_i(0), \xi_i(1), \dots, \xi_i(L_m - 1)]^T$ can then be estimated as

$$\hat{\boldsymbol{\xi}}_i = \boldsymbol{P}_{\boldsymbol{B}}^{\perp}\boldsymbol{\rho}_i \tag{59}$$

with $\boldsymbol{P}_{\boldsymbol{B}}^{\perp} = \boldsymbol{I} - \boldsymbol{B}(\boldsymbol{B}^T\boldsymbol{B})^{-1}\boldsymbol{B}^T$ the orthogonal projection matrix onto the subspace spanned by $\boldsymbol{B}$, and $\boldsymbol{I}$ the identity matrix. We will often refer to these residuals simply as the "pseudorange error".

5.3 TEST PLAN

In line with the discussion in Section 4.3 a test plan was defined encompassing three different types of interference signals: continuous-wave (CW), DVB-S and DVB-T. For each of these signals, a power swept and a frequency swept were carried out in order to assess the potential degradation as a function of both the interference power and frequency location along the E6 spectrum.

5.3.1 POWER SWEEP

The interference power starts at a negligible level for the Galileo receivers, and then it gradually increases in steps of 0.5 dB following a predefined power ramp, as represented in Figure 5-5. This ensures that the receivers under test are restarted properly at the beginning of each test, they successfully acquire the visible satellites, and then once in tracking mode, the interference is gradually introduced.

The maximum interference power level impinging on the Galileo receiver antenna was -60 dBm for CW, and -50 dBm for DVB-S and DVB-T. Therefore, D-ATV signals were tested with 10 dB more power than

CW signals. However, since the interference sources were emitted at 0º elevation (i.e. in the same horizontal plane where the receivers are placed), the attenuation introduced by the antenna radiation pattern was significant, on the order of 14 dB, as observed in Figure 5-4[2]. Both the interference power impinging on the receiver antenna, and the effective one (i.e. including the radiation pattern) are represented in Figure 5-5. The maximum effective interference power was then on the order of -74 dBm for CW and -64 dBm for DVB-S and DVB-T. The resulting maximum interference power to noise spectral density (C_i/N_0) was around 100 and 110 dBHz, respectively, asssuming the conventional noise floor of $N_0 = -204$ dBW/Hz. These C_i/N_0 values will appear later on when discussing the test results, since they are the ones actually linking the empirical results with the analytical ones derived in Section 3.

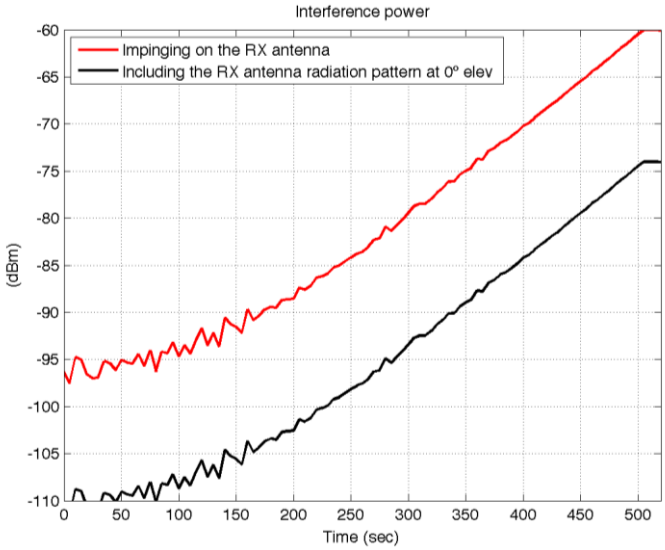

FIGURE 5-5 INTERFERENCE POWER IMPINGING ON THE GALILEO E6 RECEIVER ANTENNA FOR THE TEST WITH CW INTERFERENCE SIGNALS.

It is interesting to compute the physical distance that corresponds to the interference received power levels. This provides us an indication on how far/close would be located the interference source from the Galileo E6 receiver. The results are shown in Figure 5-6 for the received power levels impinging on the receiver antenna (left) and for the received power levels including the attenuation due to the radiation pattern (right). The latter are the ones that actually enter into the Galileo E6 receiver, and thus, will be the responsible for the degradations to the analyzed later on.

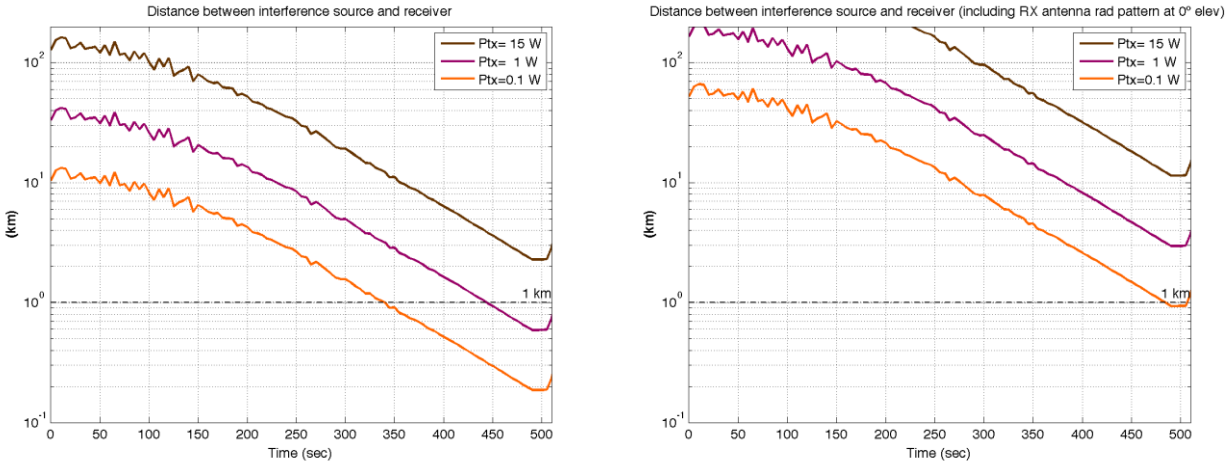

FIGURE 5-6 DISTANCE BETWEEN THE INTERFERENCE SOURCE AND THE GALILEO E6 RECEIVER. (LEFT) USING THE RECEIVED INTERFERENCE

[2] The 0º elevation angle corresponds to the 90º angle with respect to the vertical axis in Figure 5-4.

POWER IMPINGING ON THE RECEIVER ANTENNA. (RIGHT) INCLUDING THE ATTENUATION INTRODUCED BY THE RECEIVER ANTENNA RADIATION PATTERN AT 0º ELEVATION.

5.3.2 FREQUENCY SWEEP

The frequency range within the E6 band was discretized into a set of 19 frequency bins, which correspond to the maxima and minima of the Galileo E6B/C spectral lobes, as shown in Figure 5-7. At each of these frequency bins, the power sweep mentioned above was applied to the interference signal, thus providing a bi-dimensional representation (i.e. power and frequency) of the potential degradation experienced by the receivers. This, however, leads to a large set of possible test cases when considering all combinations of power levels and central frequencies. It is for this reason that, for the sake of clarity, we focus the present report on just a small subset of three representative frequency bins. These are:

- The main lobe of the Galileo E6B/C spectrum (i.e. frequency bin "f10" in Figure 5-7).
- The first null of the Galileo E6B/C spectrum (i.e. frequency bin "f12" in Figure 5-7).
- The upper edge of the E6 band (i.e. frequency bin "f17" in Figure 5-7, which lies inside the front-end bandwidth of the receivers under test).

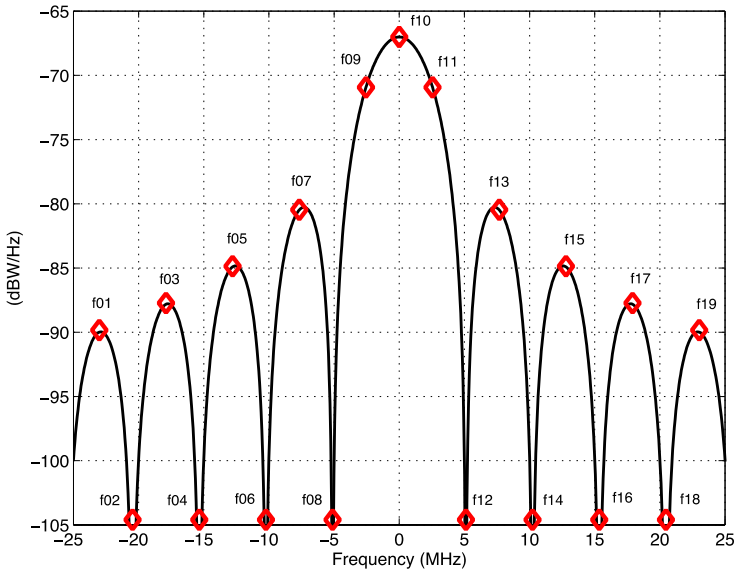

FIGURE 5-7 DISCRETIZED SET OF FREQUENCY BINS FROM THE GALILEO E6B/C SPECTRUM THAT WERE CONSIDERED IN THE TESTS.

5.3.3 SUMMARY OF TEST CASES

As a result of the interference signals considered herein, and the set of representative frequency bins mentioned above, the following test cases are defined and presented in Section 6:

- **Test 1. Continuous wave (CW) signal**
  - Test 1.1. Center of the Galileo E6B/C spectrum.
  - Test 1.2. First null of the Galileo E6B/C spectrum.
  - Test 1.3. Edge of the E6 band.
- **Test 2. DVB-S signal**
  - Test 2.1. Center of the Galileo E6B/C spectrum.
  - Test 2.2. First null of the Galileo E6B/C spectrum.
  - Test 2.3. Edge of the E6 band.
- **Test 3. DVB-T signal**
  - Test 3.1. Center of the Galileo E6B/C spectrum.
  - Test 3.2. First null of the Galileo E6B/C spectrum.

- Test 3.3. Edge of the E6 band.

6 TEST RESULTS

6.1 BASELINE PERFORMANCE

The two receivers under test were first analyzed in the absence of any interference signal so that a set of nominal (i.e. baseline) data could be obtained. These data were used later on as a reference benchmark to compare with, once interference signals were present. In that way we were able to determine the actual degradation that was incurred by the interference signals with respect to the nominal case. The results corresponding to the baseline C/N_0 and baseline pseudorange errors are shown in Figure 6-1 and Figure 6-2, respectively. Both receivers under test exhibit a quite similar performance, with C/N_0 values on the order of 50 dBHz for the three visible IOV satellites.

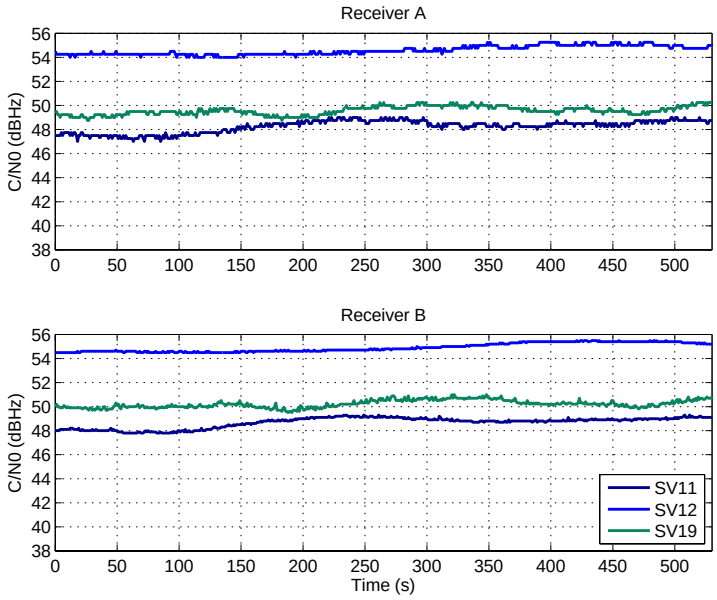

FIGURE 6-1 BASELINE C/N0 MEASURED BY THE SET OF GALILEO E6 RECEIVERS UNDER TEST

The pseudorange errors (once removed the time-varying component) are shown in Figure 6-2. As can be seen, the 3σ values of these errors remain stable around 0.5 meters for both receivers. This performance is in line with the theoretical one, as derived from the Cramér-Rao bound using the tentative parameters of the receiver configuration being used.

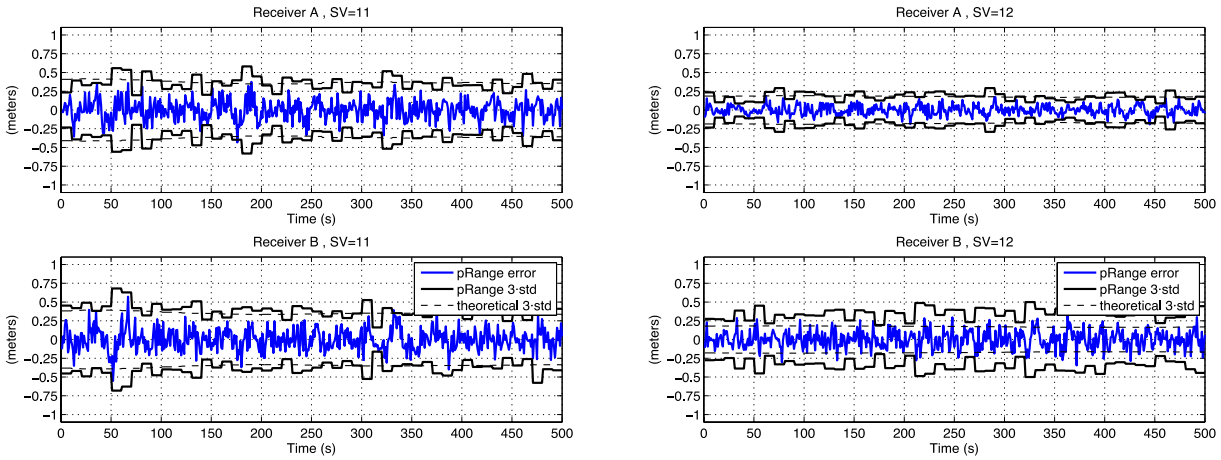

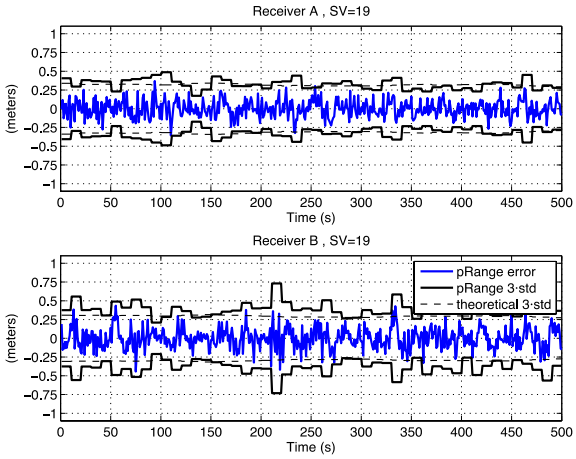

FIGURE 6-2 BASELINE PERFORMANCE OF THE PSEUDORANGE ERRORS FOR THE THREE GALILEO SATELLITES UNDER ANALYSIS.

Among the two above metrics, the C/N_0 is the most widely adopted one within the GNSS community when it comes to assess the receiver performance degradation in the presence of interference sources. In part, this is due to the simplicity in dealing with C/N_0 measurements, which are readily provided by most GNSS receivers and do not require any additional nor precise pre- or post-processing. This is in contrast to pseudorange variance, which requires some post-processing for removing the time-varying effect caused by the satellite trajectories, and some propagation impairments that may be disturbing the precise pseudorange measurement. Furthermore, the C/N_0 metric has the advantage of sharing some links with the bit error rate (BER) of the receiver (as already discussed in Section 3.3), since the C/N_0 is related to the variability of the prompt correlator outputs, there where the bit decisions are actually carried out.

In the sequel, and to avoid an excessive plethora of results, most of the emphasis will be placed on C/N_0 degradation. In some specific cases of interest, the pseudorange degradation will also be reported in order to highlight the sensitivity of the receiver to interference sources far away from the central lobe of the GNSS signal spectrum, as inferred from (53)-(54), as well from Figure 3-7 and Figure 3-8. Regarding BER performance, the C/N_0 losses reported herein can easily be mapped to the resulting (uncoded) BER by using the curves in Figure 3-11.

6.2 TEST CASE 1. CONTINUOUS WAVE (CW) INTERFERENCE

6.2.1 OVERVIEW

In the presence of a CW interference, the C/N_0 degradation is summarized in the time-frequency plot of Figure 6-3. The frequency sweep covers the whole E6 band and the power sweep (measured at the receiver antenna) is indicated in the corresponding lower subplot. For both receiver A and receiver B, the C/N_0 degradation in the presence of a narrowband interference may go up to 30 dB. For receiver A, this can be observed for received powers of about -75 dBm. For typical EIRP levels of ATV, which range from 0.1 to 15 W, these received powers would correspond to propagation distances on the order of just a few kilometres, as observed in the degradation versus distance plots in Figure 6-5.

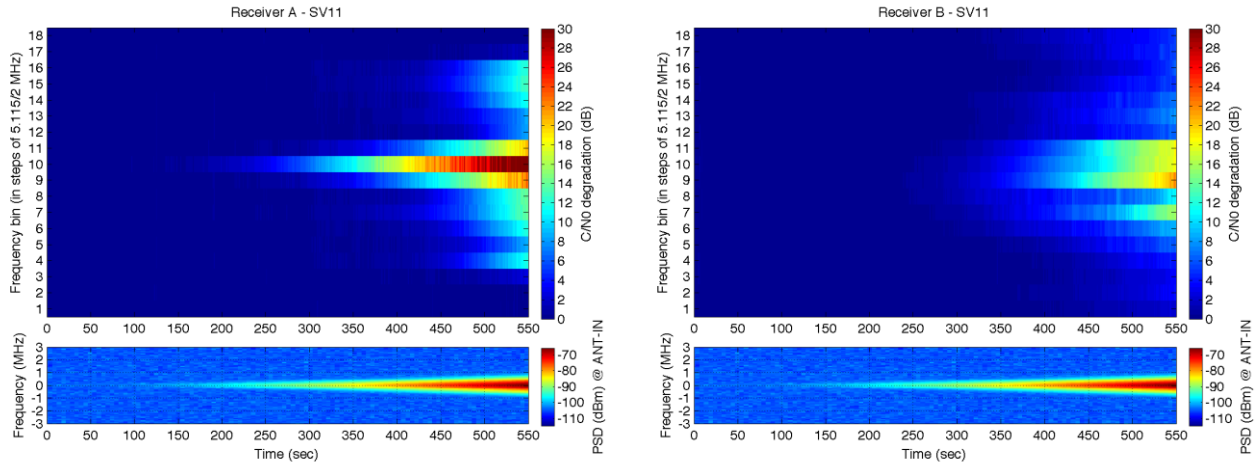

FIGURE 6-3 (CW) TIME-FREQUENCY REPRESENTATION OF THE C/N0 DEGRADATION EXPERIENCED BY THE TWO GALILEO E6 RECEIVERS.

In the sequel, we will take a closer look at the C/N_0 degradation for the three key frequency bins of interest: the center of E6 where the main lobe of the Galileo E6B/C spectrum is located; the first null of this spectrum; and the upper edge of E6, but within the front-end bandwidth of the receivers under test.

6.2.2 IMPACT AT THE CENTER OF THE E6 BAND

The C/N_0 degradation when placing the CW at the center of the E6 band (i.e. at 1278.75 MHz) is shown below in Figure 6-4 for the three visible Galileo IOV satellites considered in this study.

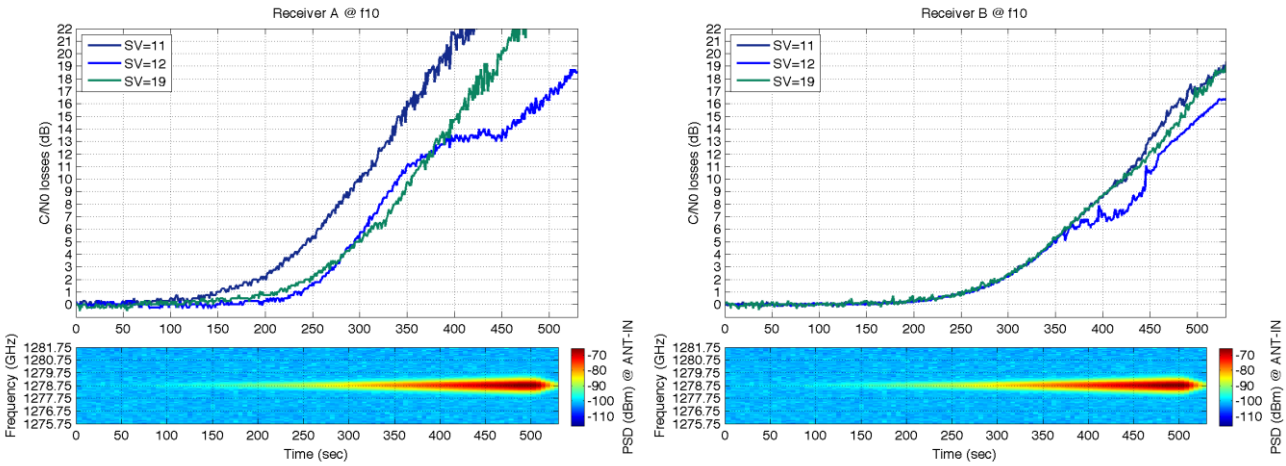

FIGURE 6-4 (CW@CENTER) C/N0 LOSSES OF THE TWO GALILEO E6 RECEIVERS UNDER TEST FOR THE DIFFERENT SATELLITES IN VIEW.

For receiver A (see left plot in Figure 6-4), the different C/N_0 degradation is likely to be caused by the different Doppler frequencies of each satellite, as well as the use of a long coherent integration time at the receiver side. The latter causes the frequency response of the coherent integration filter to become quite selective, and therefore, more sensitive to the rejection of narrowband interferences lying outside of the 1kHz aliased replicas of the coherent integration frequency response (see Figure 2-1). This is the case of satellite with PRN 12, whose Doppler frequency was approaching -400 Hz by the end of the observation interval. After compensating the received signal by this frequency offset, the CW interference is moved by the same amount and then subject to the stop band of the coherent integration filter. This makes the interference effects for satellite with PRN 12 to be smaller than for the rest of satellites (whose Doppler frequencies turn out to be close to 1 kHz), since some additional attenuation is already applied to the CW interference. In contrast, receiver B exhibits almost the same C/N_0 degradation for all satellites in view. This suggests that the correlation process is carried out in a different manner with respect to receiver A, probably using a shorter coherent integration time, and thus leading to a wider coherent filter that attenuates the CW interference in a similar manner for all satellites.

Finally, results in Figure 6-5 provide the mapping between the C/N_0 losses and the physical distance of the interfering ATV stations. To do so, three representative transmit powers have been considered for the ATV stations, namely 0.1 W, 1 W and 15 W. Nevertheless, it is interesting to point out that much larger transmit powers may also be found in practice, since some ATV stations do operate with transmit powers beyond 100 W.

The mapping has been computed using the interference power that actually impinges onto the receiver antenna during the power sweep, and assuming free-space propagation losses. For each of the resulting distances (which in the end, they are nothing but a received power level) we plot the corresponding C/N_0 degradation in dB that was observed at the receiver. The result is thus, a representation of the C/N_0 degradation that we would observe as a function of the distance between interference and user receiver. As can be seen in Figure 6-5, 10 dB of C/N_0 degradation can easily be suffered at 30 km (receiver A) or 10 km (receiver B) from an ATV station using a moderate transmit power of 15W.

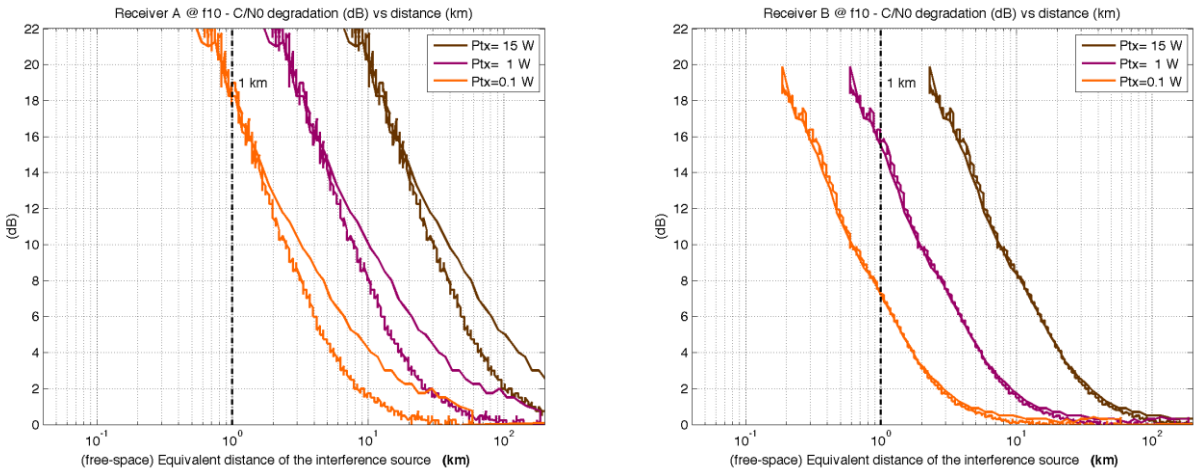

FIGURE 6-5 (CW@CENTER) C/N0 DEGRADATION AS A FUNCTION OF DISTANCE BETWEEN ATV TRANSMITTER AND THE GNSS RECEIVER.

6.2.3 IMPACT AT THE FIRST NULL OF GALILEO E6B/C SPECTRUM

In the previous section we showed how the maximum C/N_0 degradation went beyond 30 dB when the CW interference was placed over the main lobe of the Galileo spectrum (see left hand side of Figure 6-3). By moving the interference to the first null of the spectrum, the degradation is largely reduced as observed in Figure 6-6. Nevertheless, it still remains quite significant, with values on the order of 10 dB degradation for receiver A and up to 8 dB for receiver B, even for distances from ATV station to Galileo receiver between 1 and 10 km, as observed in Figure 6-7. Such a degradation makes difficult to use the nulls of the Galileo E6B/C spectrum for allocating narrowband ATV emissions, since a significant degradation is actually observed.

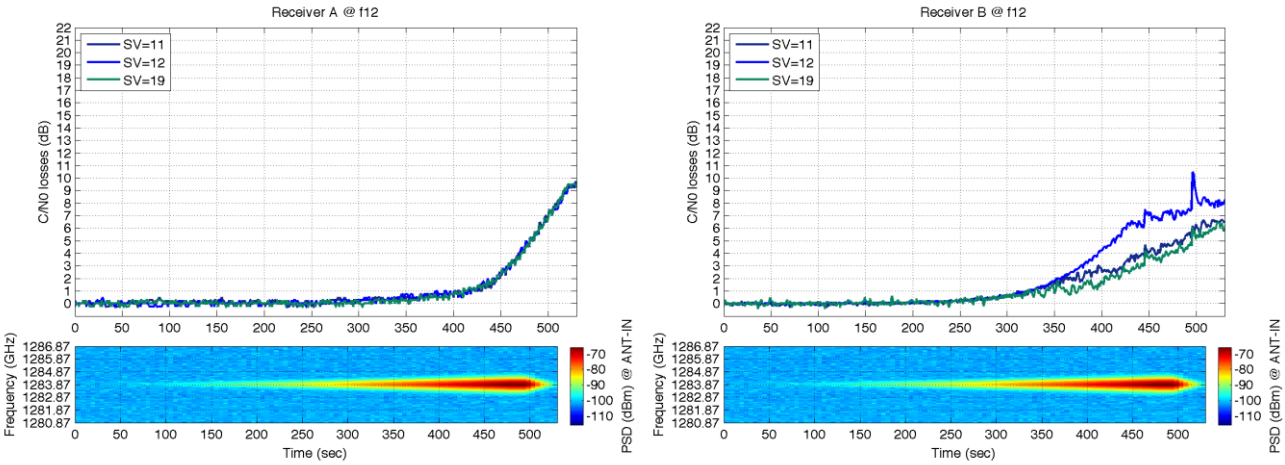

FIGURE 6-6 (CW@NULL1) C/N0 LOSSES OF THE TWO GALILEO E6 RECEIVERS UNDER TEST FOR THE DIFFERENT SATELLITES IN VIEW.

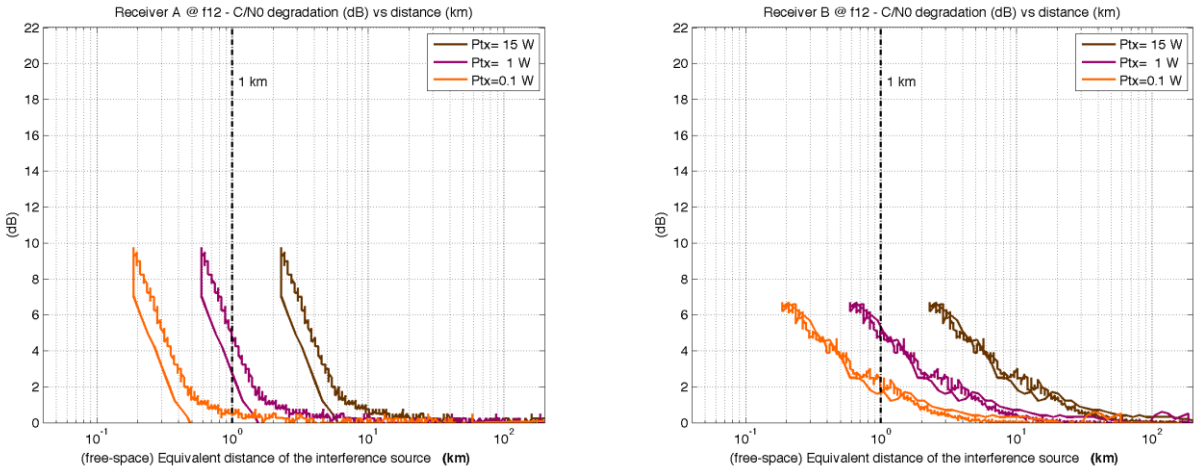

FIGURE 6-7 (CW@NULL1) C/N0 DEGRADATION AS A FUNCTION OF DISTANCE BETWEEN ATV TRANSMITTER AND THE GNSS RECEIVER.

6.2.4 IMPACT AT THE EDGE OF THE E6 BAND

The third central frequency to be analyzed is that when the interference is placed at the edge of the E6 band. As in the previous cases, the C/N_0 losses are reported in Figure 6-8 and Figure 6-9 as a function the increasing interference power and the distance from source to receiver, respectively. In general, and despite the very low received interference power, a non-negligible degradation is still observed, which for the case of receiver B is on the order of 6 to 8 dB.

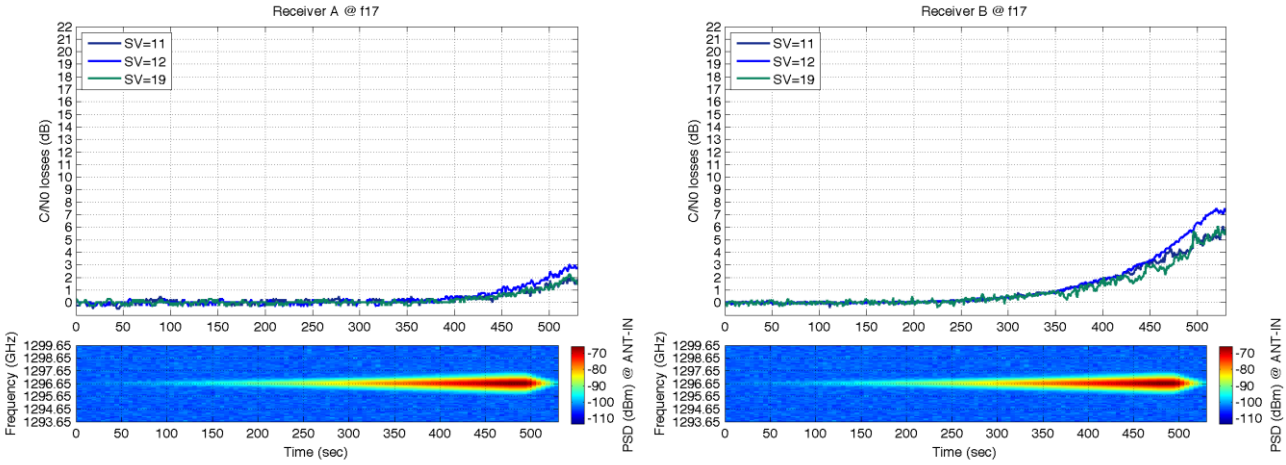

FIGURE 6-8 (CW@EDGE) C/N0 DEGRADATION FOR THE DIFFERENT SATELLITES IN VIEW.

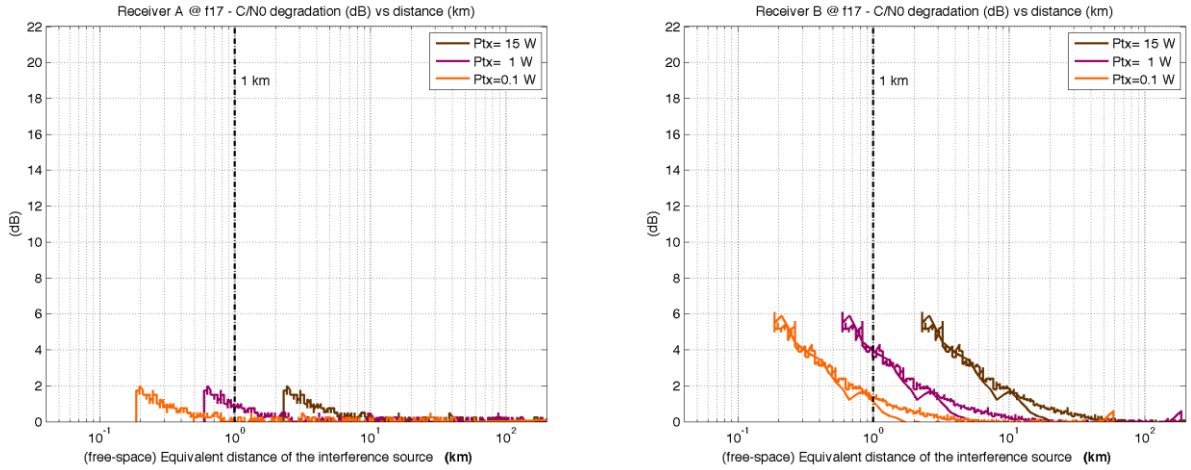

FIGURE 6-9 (CW@EDGE) C/N0 DEGRADATION AS A FUNCTION OF DISTANCE BETWEEN ATV TRANSMITTER AND GNSS RECEIVER.

Additionally, we include for this scenario the equivalent C/N_0 that would correspond to the pseudoranges actually reported by the receiver. To do so, we compute the variance of the pseudorange residuals and we find the corresponding C/N_0 that would lead to this variance, according to the Cramér-Rao bound for the receiver at hand. This is an intuitive way of understanding the pseudorange degradation in terms of "equivalent" C/N_0 degradation. As can be seen in Figure 6-10 for receiver A, the pseudoranges are experiencing a larger degradation than the one apparently corresponding to the C/N_0 being measured. The difference is on the order of about 4 dB at the end of the data record, there where the interference power ramp reaches its maximum value. This observation suggests that for the edge of the band (but still within the front-end bandwidth), the actual performance degradation experienced by the pseudoranges may be larger than the one inferred from the measured C/N_0 being reported by the receiver. In summary, allocation of narrowband ATV signals at the edge of the E6 band is also likely to incur in a non-negligible degradation to high-end Galileo E6 receivers.

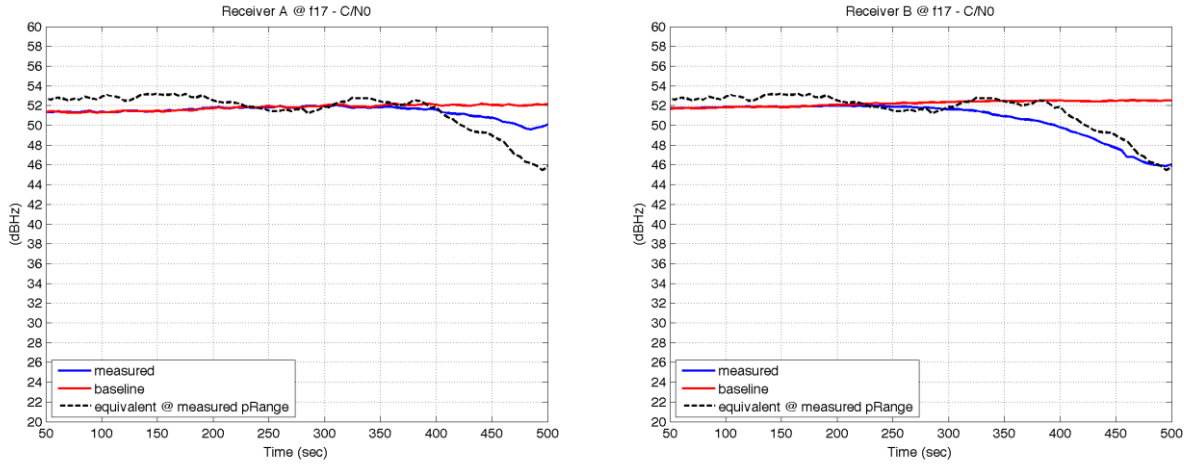

FIGURE 6-10 (CW@EDGE) EQUIVALENT C/N0 CORRESPONDING TO THE BASELINE PSEUDORANGES AND TO THE MEASURED ONES IN THE PRESENCE OF INTERFERENCE.

6.2.5 C/N0 DEGRADATION ALONG THE E6 BAND

A summary of the maximum C/N_0 degradation at all the central frequencies under test is represented in Figure 6-11 for both receiver A and B. The results are compared with the expected theoretical ones (see dashed lines) using a tentative estimate of the main hardware parameters of each receiver, since the true and detailed specifications were kept confidential in this study. In general terms, a reasonable match is observed between empirical and theoretical results, particularly for the frequency bins where the peaks of the spectrum are located. Receiver B apparently has a slightly better immunity against CW interferences, with empirical C/N_0 degradations quite below the expected ones, mainly at the central lobe and at the right hand side of the spectrum.

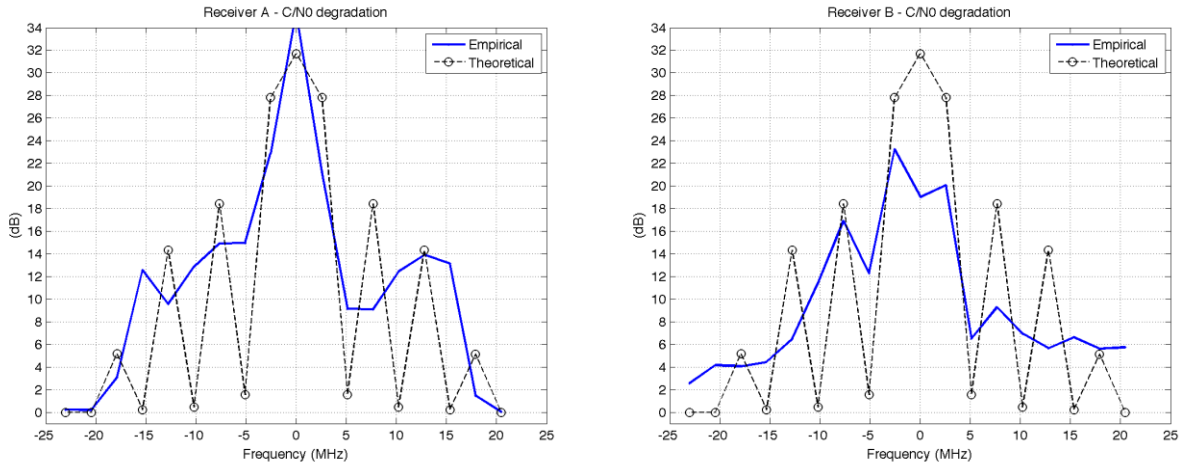

FIGURE 6-11 (CW) C/N0 DEGRADATION AS A FUNCTION OF FREQUENCY FOR THE MAXIMUM INTERFERENCE LEVEL CONSIDERED IN THE TESTS (Ci/N0=100 dBHz).

6.3 TEST CASE 2. DVB-S INTERFERENCE

Tests for DVB-S interference signals were carried out for three representative bandwidths of D-ATV emissions, namely 2, 4 and 5 MHz. The results are presented next in Sections 6.3.1, 6.3.2 and 6.3.3, respectively. It is important to bear in mind that, as previously discussed, the maximum interference power for D-ATV signals (i.e. DVB-S and DVB-T) was 10 dB higher than for the narrowband case (i.e. CW).

6.3.1 2 MSPS SYMBOL RATE

6.3.1.1 OVERVIEW

The time-frequency representation of the overall C/N_0 degradation is summarized in Figure 6-12. At first glance we can see a maximum performance degradation of about 22-24 dB for receiver A, and below 20 dB for receiver B when the maximum interference level is applied (i.e. $C_i/N_0 = 110$ dBHz). This is about 10 dB less degradation than for the CW signal analyzed in Section 6.2, even though the maximum interference power is now 10dB higher than for the CW. In contrast to the CW case, we can see a leakage of C/N_0 degradation across the frequency domain, which is due to the wideband nature of DVB-S signals. Significant losses on the order of 10 to 14 dB are now uniformly seen over a wider frequency range than for the previous CW case.

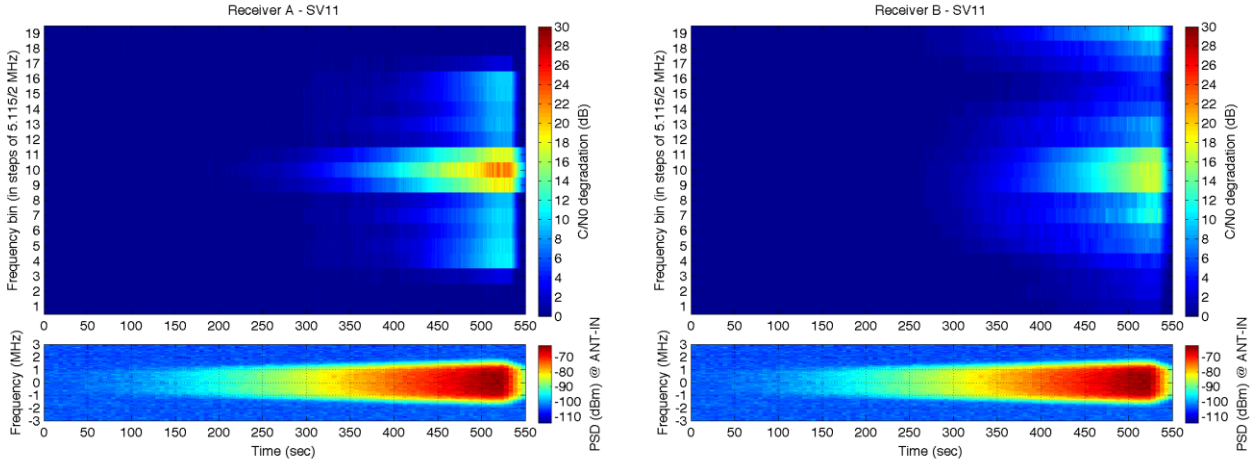

FIGURE 6-12 (DVBS-2M) TIME-FREQUENCY REPRESENTATION OF THE C/N0 DEGRADATION EXPERIENCED BY THE TWO GALILEO E6 RECEIVERS

6.3.1.2 IMPACT AT THE CENTER OF THE E6 BAND

Figure 6-13 takes a closer look at the C/N_0 degradation along the main spectral lobe of Galileo E6 where 20-22 dB are observed. These values are on the order of 10 dB less than the ones experienced for the CW signal, even though the maximum interference power is now 10 dB higher than the one used for CW. This gives us a relative difference on the order of 20 dB less degradation for DVB-S signals compared to CW, which is likely to be caused by the filtering effects of using an effective 100ms coherent integration filter at the receiver. Despite of that, we are still observing a significantly high C/N_0 degradation for DVB-S signals, as shown in the summary of Figure 6-12, even when relatively moderate interference power levels are used. Please note that a $C_i/N_0 = 110$ dBHz would correspond to a D-ATV station with 1W of EIRP at 1km distance from the receiver, or with 15 W at 4 km distance.

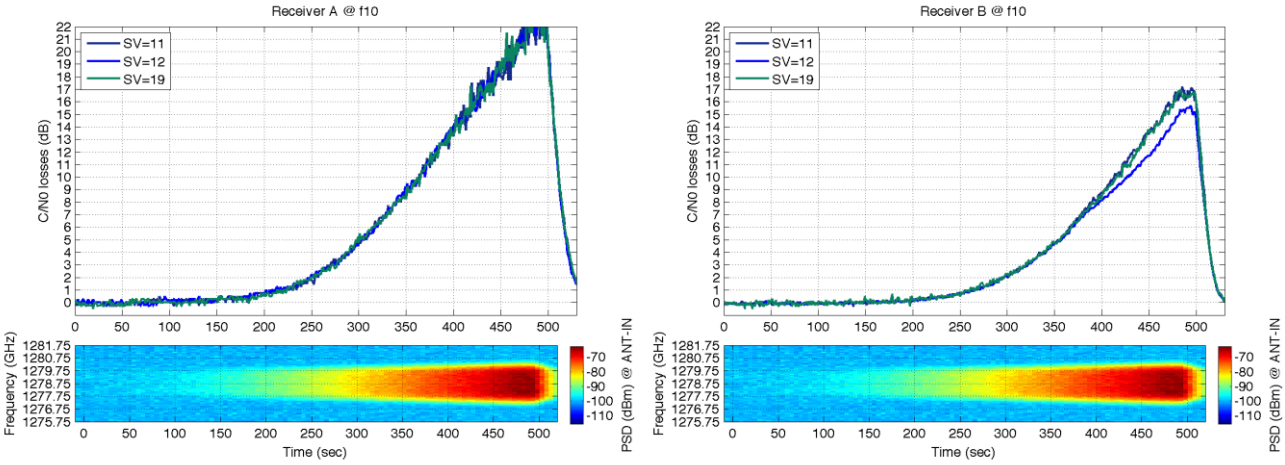

FIGURE 6-13 (DVBS-2M@CENTER) C/N0 DEGRADATION FOR THE DIFFERENT SATELLITES IN VIEW.

The distances at which a D-ATV station would have to be placed in order to cause the losses reported in Figure 6-13 are represented in Figure 6-14. Because of the 20 dB difference between the maximum C/N_0 degradation on DVB-S and CW (for the current receiver configuration), the distances for DVB-S have been reduced roughly by a factor of 10. This is due to the linear relationship between C/N_0 degradation and interference power, but the quadratic relationship between received power and distance (i.e. assuming free-space propagation losses).

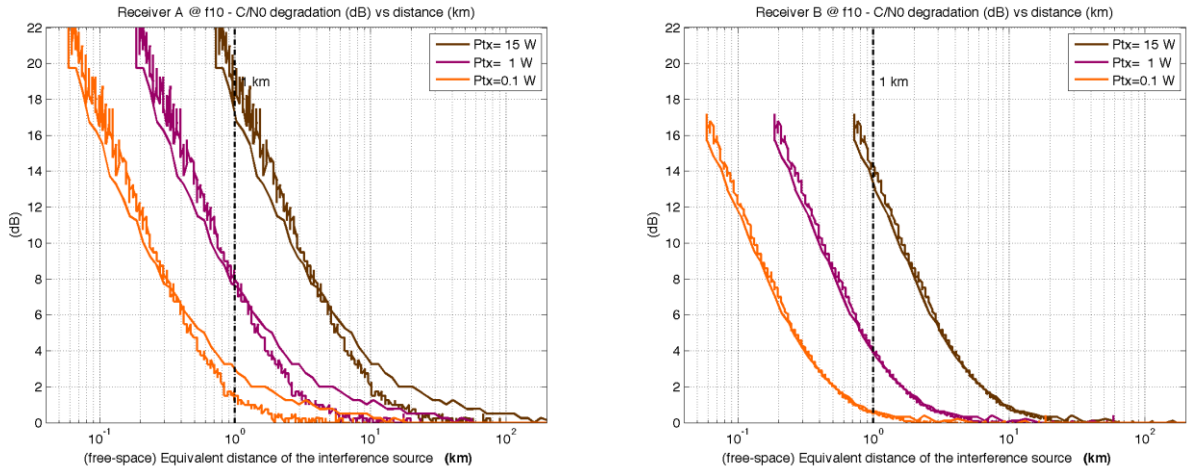

FIGURE 6-14 (DVBS-2M@CENTER) C/N0 DEGRADATION AS A FUNCTION OF DISTANCE BETWEEN ATV TRANSMITTER AND GNSS RECEIVER.

6.3.1.3 IMPACT AT THE FIRST NULL OF GALILEO E6B/C SPECTRUM

When placing the DVB-S signal over the first null of the Galileo spectrum, the C/N_0 degradation reported in Figure 6-15 is obtained. As can be seen, the degradation is on the same order of magnitude than the one obtained for the CW signal in Section 6.2 even though 10 dB more power were now used. In relative terms, we could thus say that there is a 10 dB more degradation for a CW than for a DVB-S interference, when they both are placed at the first null of the spectrum. This is in contrast to the 20 dB more degradation that were observed when both interferences were placed at the central part of the spectrum, since in that case, the CW signal at the correlator output was not attenuated by the null on the spectrum of the Galileo code replica. The DVB-S signal, on the other hand, remains rather insensitive to these effects due to its wider bandwidth. Even when placed over a null of the Galileo spectrum, a

significant amount of power is actually spread outside of the null, as compared to the case of a CW signal.

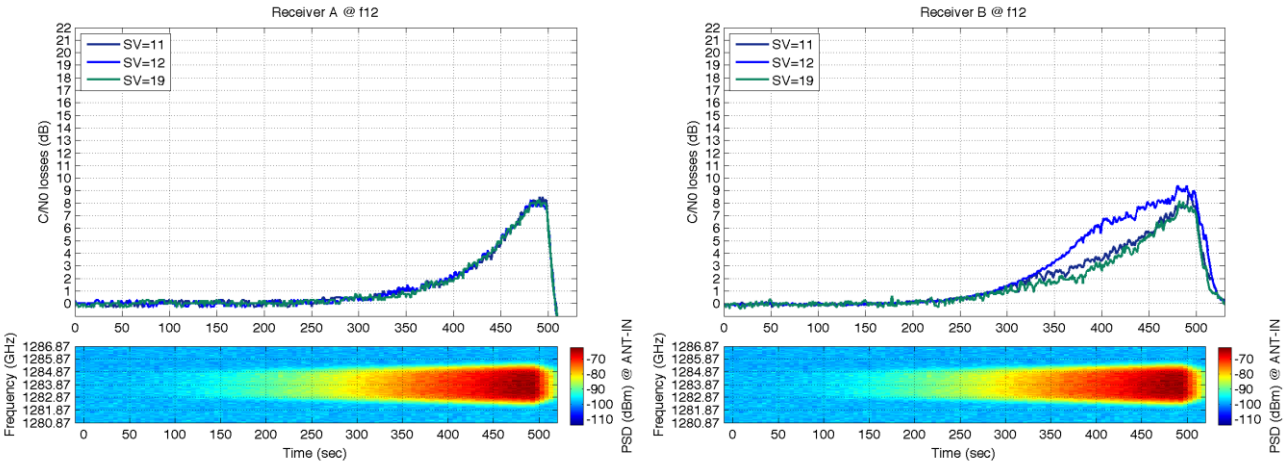

FIGURE 6-15 (DVBS-2M@NULL1) C/N0 DEGRADATION FOR THE DIFFERENT SATELLITES IN VIEW.

The distance at which a D-ATV station should be placed in order to cause the degradation reported above is shown next in Figure 6-16. Because of the 10 dB difference between DVB-S and CW at the first null of the Galileo spectrum, the resulting distances in Figure 6-16 are shifted by a factor of 5 dB in the horizontal axis (i.e. a factor of about 3, in linear scale) when compared to the ones reported in Figure 6-7 for the CW.

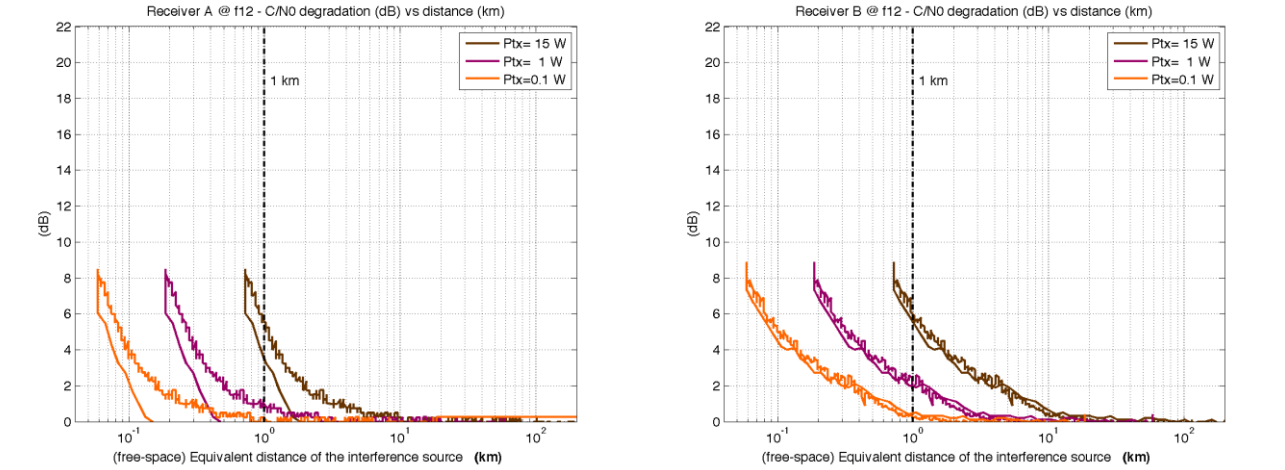

FIGURE 6-16 (DVBS-2M@NULL1) C/N0 DEGRADATION AS A FUNCTION OF THE DISTANCE BETWEEN ATV TRANSMITTER AND GNSS RECEIVER.

6.3.1.4 IMPACT AT THE EDGE OF THE E6 BAND

When placing the DVB-S signal at the edge of the E6 band, similar results to the ones for CW are obtained. Bearing in mind the 10 dB more maximum power of DVB-S compared to CW, the conclusions are the same as for the previous case at the first null of the spectrum. That is, the overall relative difference between DVB-S and CW is about 10 dB, and this leads to the distances between ATV and receiver to exhibit the same horizontal shift of 5 dB already reported in the previous section, when comparing DVB-S and CW in Figure 6-9.

Moreover, it is interesting to highlight the similar performance degradation that is observed either at the first null or at the edge of the band. In both cases, the C/N_0 performance degradation is significant,

with values that can reach up to 8 dB degradation, depending on the receiver. This indicates that neither placing the interference on a null of the Galileo spectrum, nor working far away from the main lobe (e.g. at the edge of the band, but still within the front-end bandwidth) can prevent the receiver to suffer from a significant degradation when a D-ATV signal is present.

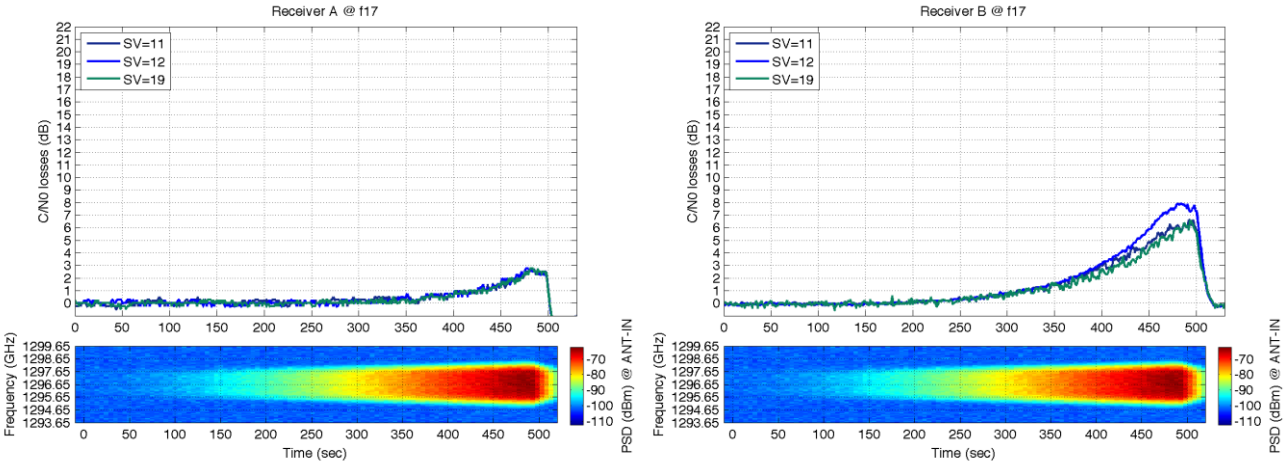

FIGURE 6-17 (DVBS-2M@EDGE) C/N0 DEGRADATION FOR THE DIFFERENT SATELLITES IN VIEW.

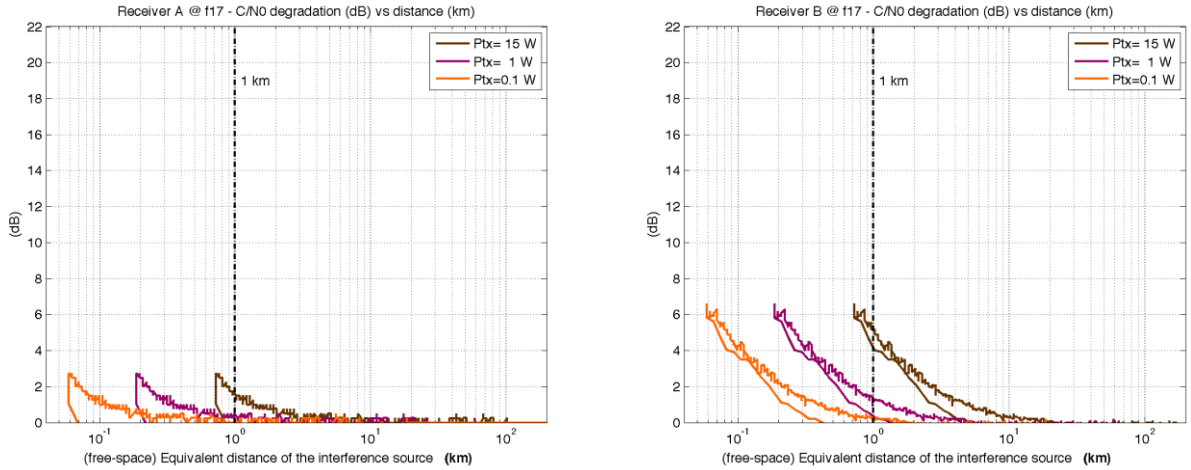

FIGURE 6-18 (DVBS-2M@EDGE) C/N0 DEGRADATION AS A FUNCTION OF THE DISTANCE BETWEEN ATV TRANSMITTER AND GNSS RECEIVER.

In terms of pseudorange performance, Figure 6-19 represents the equivalent C/N_0 that would correspond to the pseudoranges being provided by the receiver. This equivalent C/N_0 is compared to the C/N_0 actually reported by the receiver. As can be seen in Figure 6-19 for receiver A, the pseudorange equivalent C/N_0 when the maximum interference power is applied (i.e. from time 400 to 500) is about 2–3 dB worse than the C/N_0 actually reported by the receiver. This indicates that even when the interference is placed far beyond the main lobe of the spectrum, a non-negligible and (larger than expected) performance degradation may be experienced.

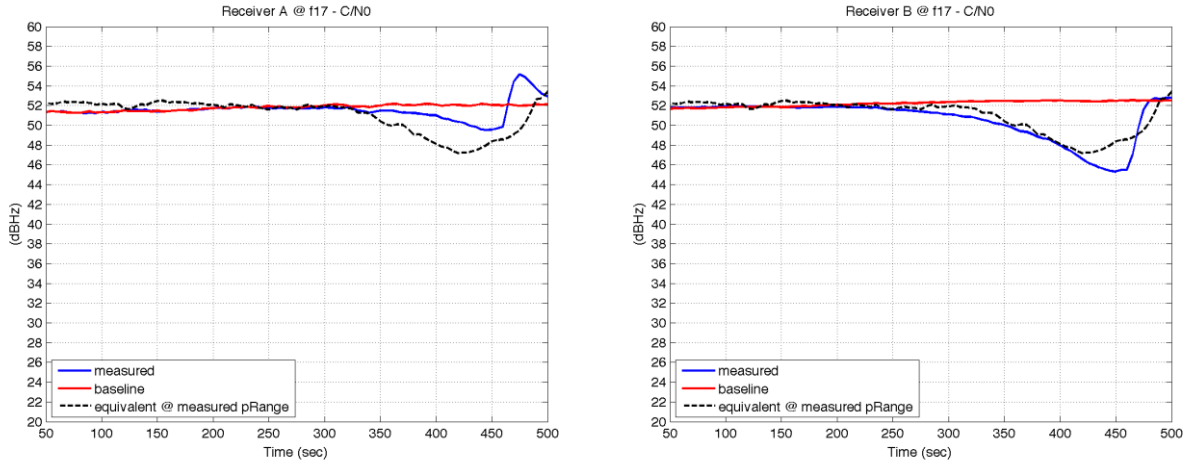

FIGURE 6-19 (DVBS-2M@EDGE) EQUIVALENT C/N0 CORRESPONDING TO THE BASELINE PSEUDORANGES AND TO THE MEASURED ONES IN THE PRESENCE OF INTERFERENCE.

6.3.1.5 C/N0 DEGRADATION ALONG THE E6 BAND

Regarding the C/N_0 degradation along the E6 band, results are presented in Figure 6-20 for both the empirical and the expected theoretical results. Except for some frequency bins, in general there is a fair match between both results. It is interesting to observe the rather uniform behavior of receiver A for the C/N_0 degradation outside the main lobe of the Galileo spectrum (i.e. outside +/- 5.115 MHz), as well as the effect of the receiver front-end bandwidth. For the case of receiver B the behavior is a bit more heterogeneous, with a degradation smaller than the one expected at the central lobe, but larger than the one expected for the right hand side edge of the spectrum.

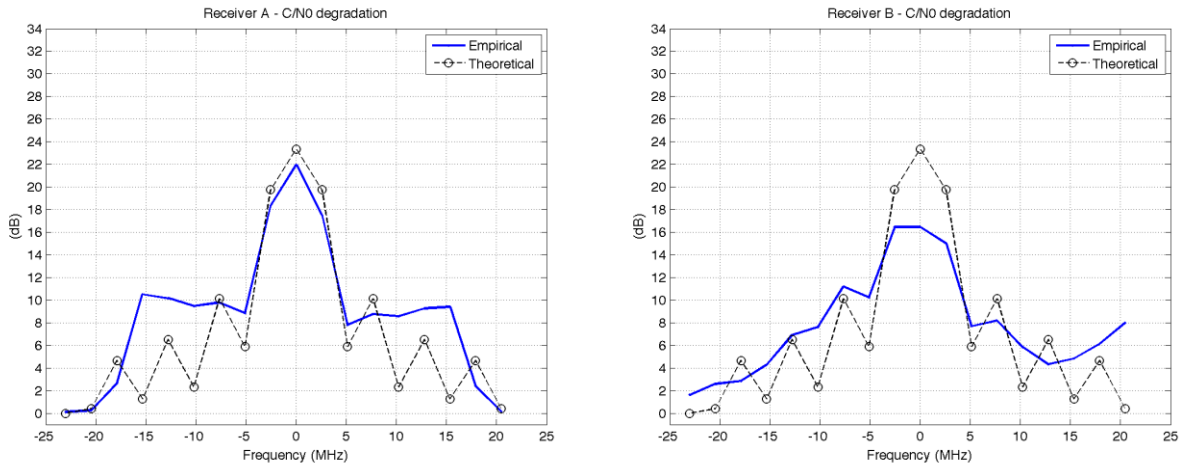

FIGURE 6-20 (DVBS-2M) C/N0 DEGRADATION AS A FUNCTION OF FREQUENCY FOR THE MAXIMUM INTERFERENCE LEVEL CONSIDERED IN THE TESTS (Ci/N0=110 dBHz).

As a summary for the 2 Msps DVB-S signal, 10 dB C/N_0 degradation are experienced for receiver A within its whole front-end bandwidth, except at the central frequency where more than 20 dB are observed. For receiver B, average losses are on the order of 6 to 8 dB, with a peak of 16 dB at the central frequency.

6.3.2 4 MSPS SYMBOL RATE

6.3.2.1 OVERVIEW

The time-frequency representation of the overall C/N_0 degradation is summarized in Figure 6-21. Results are very similar to the ones reported in the previous section for a 2 Msps DVB-S signal. This corresponds to about 22-24 dB degradation in terms of C/N_0 for receiver A, and about 15-17 dB for receiver B when the maximum interference level is applied (i.e. $C_i/N_0 = 110$ dBHz).

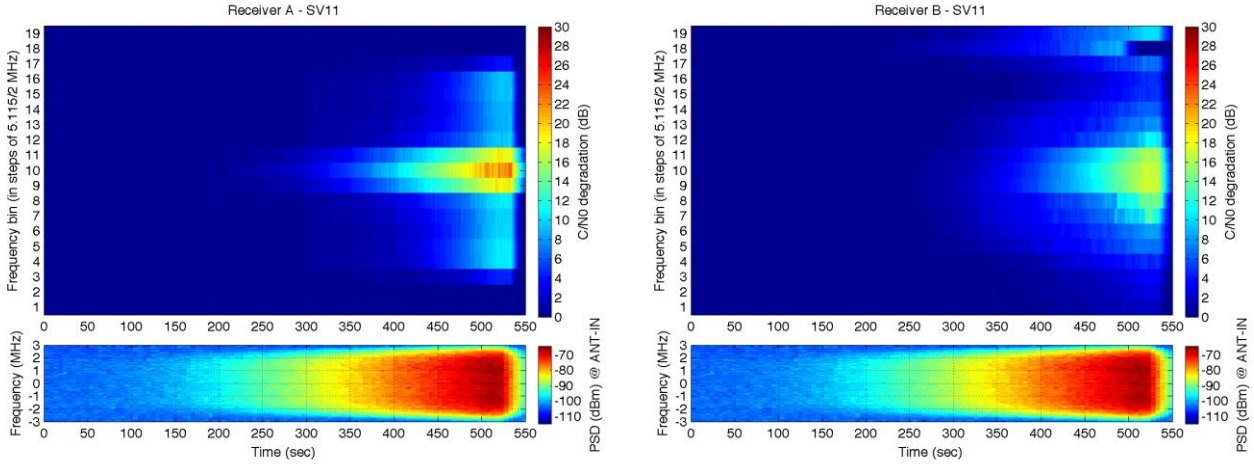

FIGURE 6-21 (DVBS-4M) TIME-FREQUENCY REPRESENTATION OF THE C/N0 DEGRADATION EXPERIENCED BY THE TWO GALILEO E6 RECEIVERS

6.3.2.2 IMPACT AT THE CENTER OF THE E6 BAND

The results for a 4 Msps DVB-S interference at the center of the E6 band are almost coincident with the ones already presented in Figure 6-13 and Figure 6-14 for the 2 Msps signal.

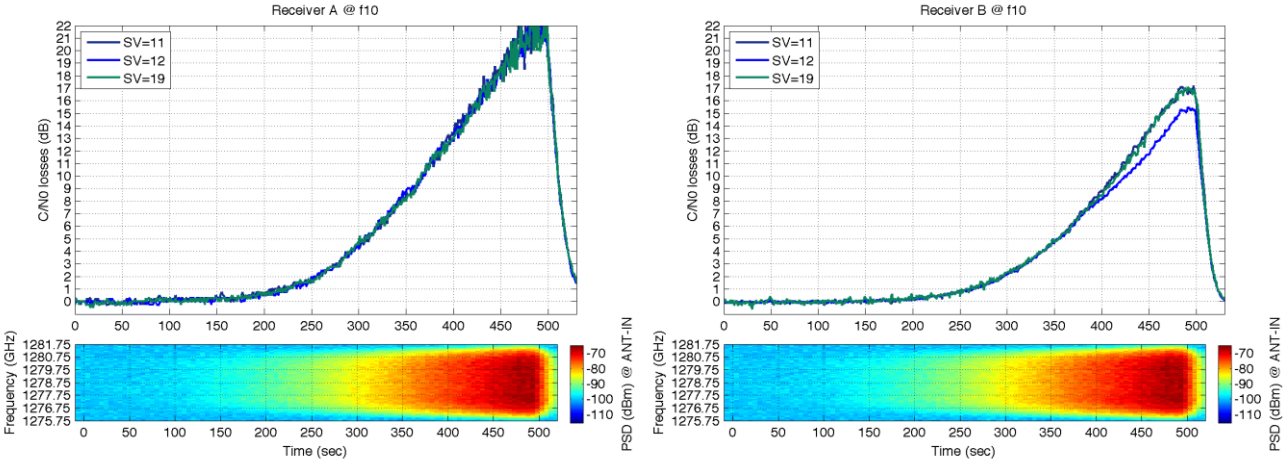

FIGURE 6-22 (DVBS-4M@CENTER) C/N0 DEGRADATION FOR THE DIFFERENT SATELLITES IN VIEW.

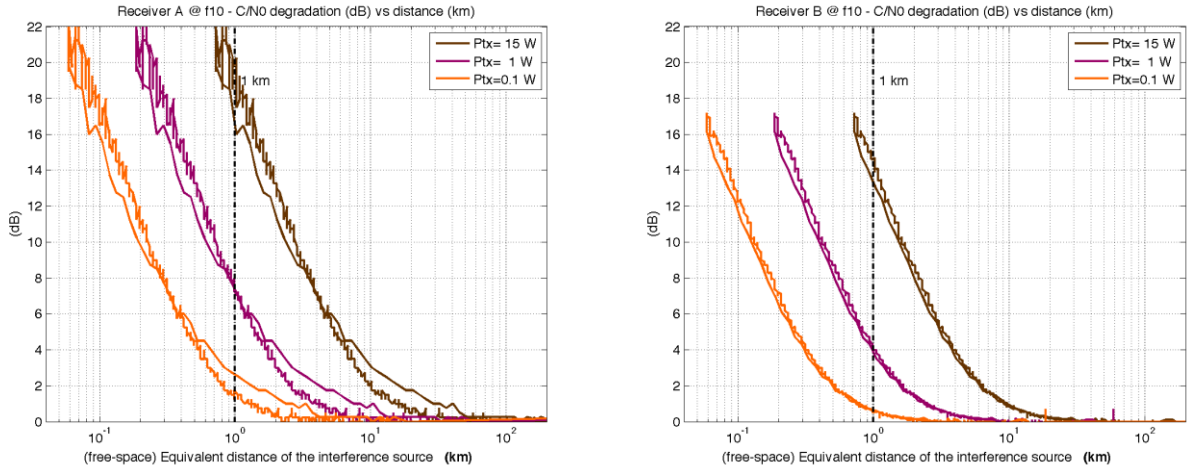

FIGURE 6-23 (DVBS-4M@CENTER) C/N0 DEGRADATION AS A FUNCTION OF DISTANCE BETWEEN ATV TRANSMITTER AND GNSS RECEIVER.

6.3.2.3 IMPACT AT THE FIRST NULL OF GALILEO E6B/C SPECTRUM

In this case we observe a slightly higher degradation for the 4 Msps DVB-S signal, with C/N_0 losses reaching up to 10 dB for receiver A and about 11-12 dB for receiver B. These values are about 2 dB higher than the ones observed in Figure 6-15 and Figure 6-16 for a 2 Msps DVB-S signal.

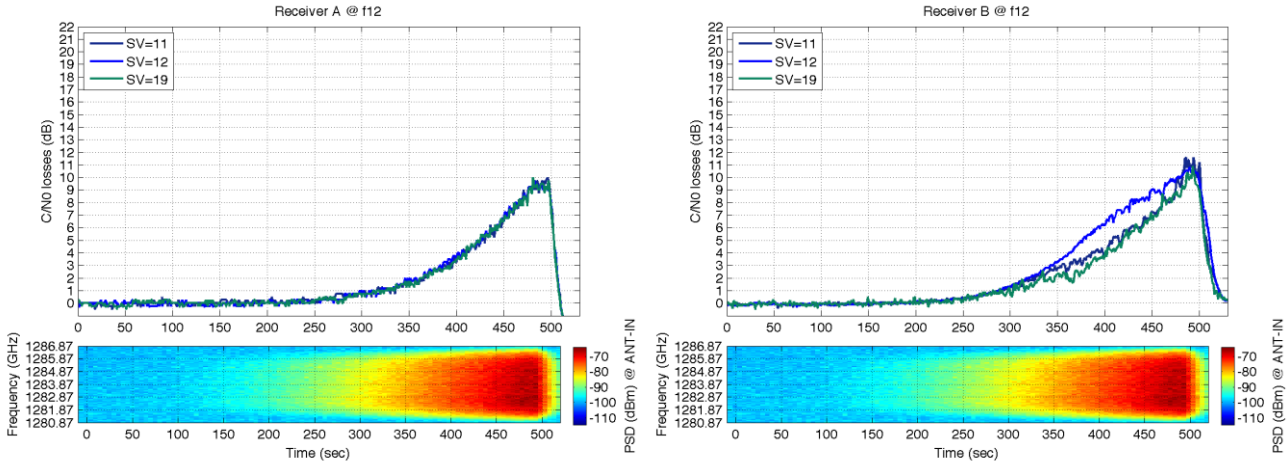

FIGURE 6-24 (DVBS-4M@NULL1) C/N0 DEGRADATION FOR THE DIFFERENT SATELLITES IN VIEW.

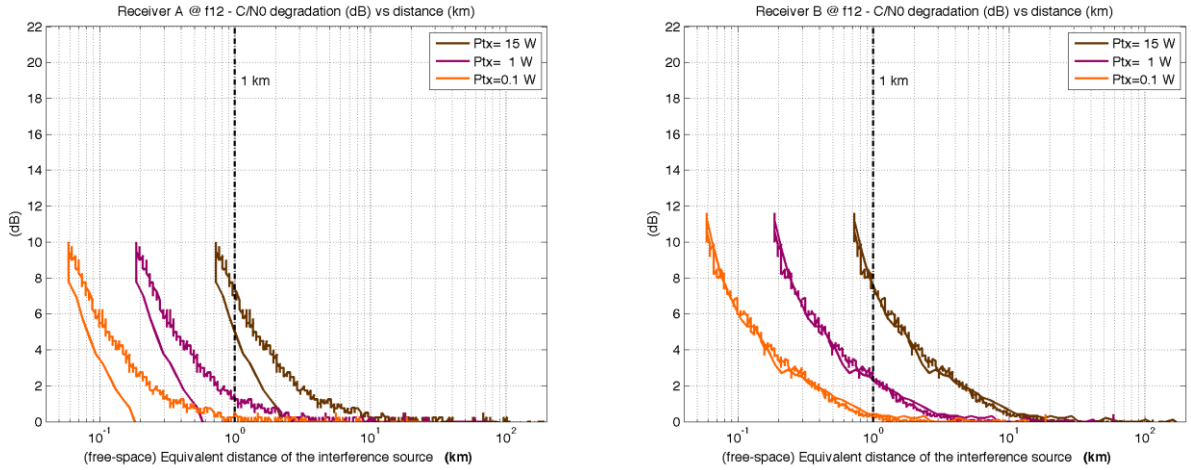

FIGURE 6-25 (DVBS-4M@NULL1) C/N0 DEGRADATION AS A FUNCTION OF DISTANCE BETWEEN ATV TRANSMITTER AND GNSS RECEIVER.

6.3.2.4 IMPACT AT THE EDGE OF THE E6 BAND

In this case, 1 to 2 dB more degradation is observed with respect to the same case using a 2 Msps DVB-S signal.

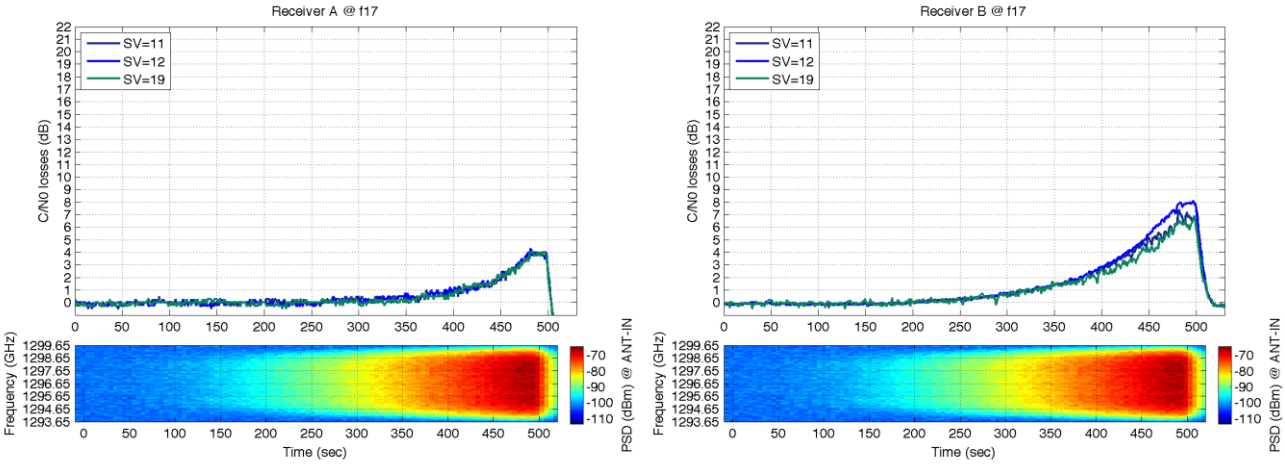

FIGURE 6-26 (DVBS-4M@EDGE) C/N0 DEGRADATION FOR THE DIFFERENT SATELLITES IN VIEW.

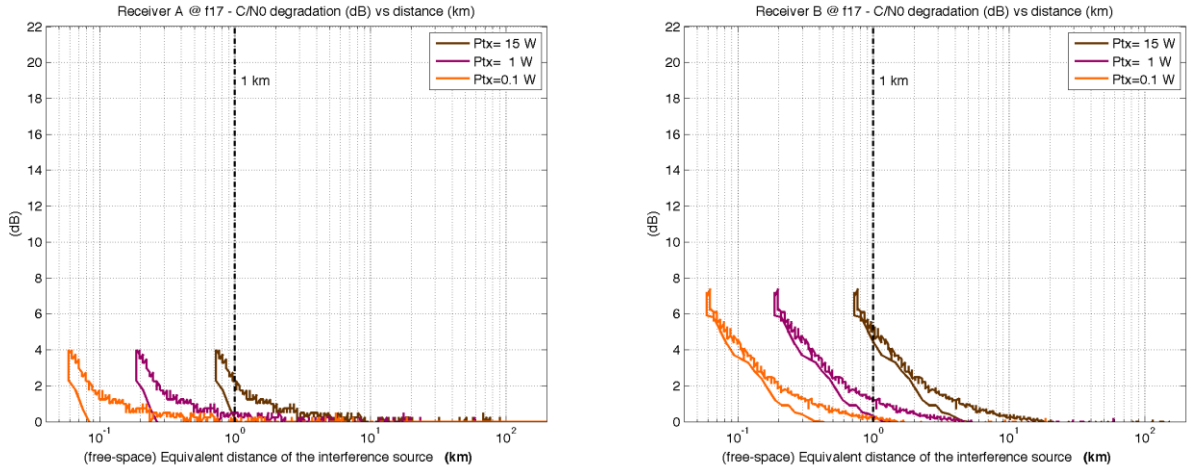

FIGURE 6-27 (DVBS-4M@EDGE) C/N0 DEGRADATION AS A FUNCTION OF DISTANCE BETWEEN ATV TRANSMITTER AND GNSS RECEIVER.

For the pseudorange performance, receiver A is also exhibiting a slightly worse performance (around 2 dB) than the one expected for the C/N_0 being reported by the receiver.

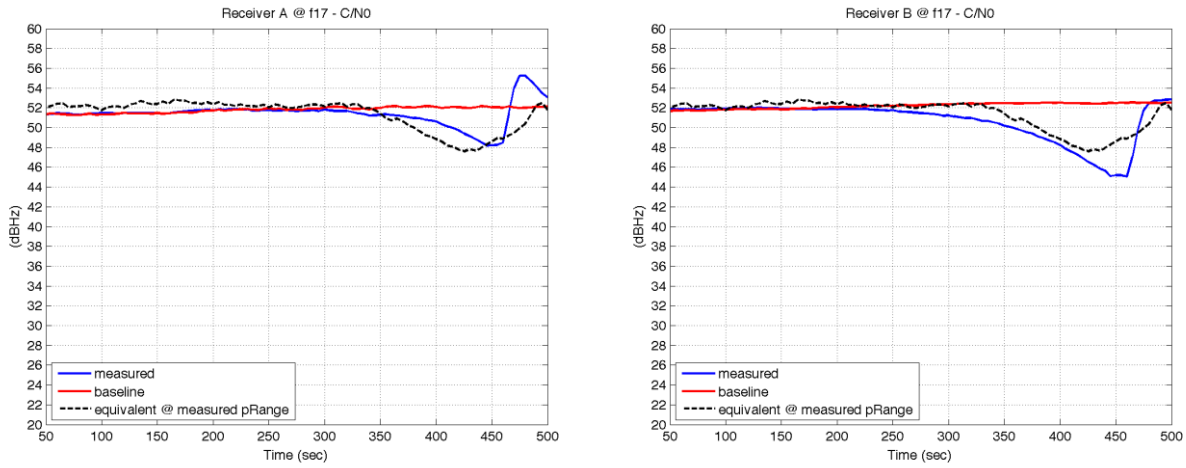

FIGURE 6-28 (DVBS-4M@EDGE) EQUIVALENT C/N0 CORRESPONDING TO THE BASELINE PSEUDORANGES AND TO THE MEASURED ONES IN THE PRESENCE OF INTERFERENCE.

6.3.2.5 C/N0 DEGRADATION ALONG THE E6 BAND

The summary of the maximum observed C/N_0 degradation (for the interference powers considered herein, leading to $C_i/N_0 = 110$ dBHz) is shown in Figure 6-29. For the case of receiver B, a slightly smoother shape is observed with respect to the 2 Msps case in Figure 6-20, as a result of the wider bandwidth and the resulting smoother spectral separation coefficient.

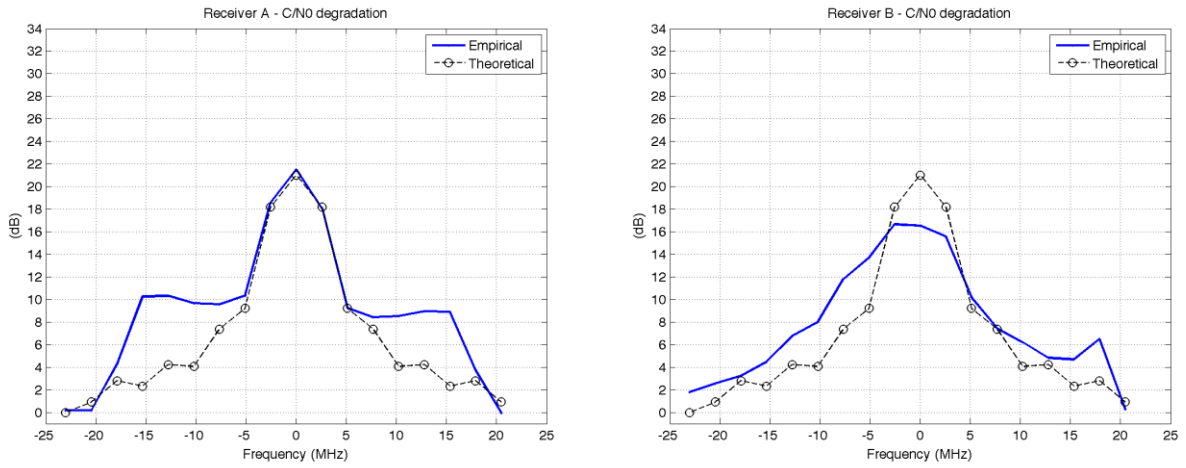

FIGURE 6-29 (DVBS-4M) C/N0 DEGRADATION AS A FUNCTION OF FREQUENCY FOR THE MAXIMUM INTERFERENCE LEVEL CONSIDERED IN THE TESTS (Ci/N0=110 dBHz).

6.3.3 5 MSPS SYMBOL RATE

6.3.3.1 OVERVIEW

Because of the similarities with the previous cases, the 5 Msps case has been tested for a reduced set of just four frequency bins, including the central lobe, the first null, the first secondary lobe of the Galileo E6 signal, and the edge of the E6 band. Results are summarized in the time-frequency representation shown in Figure 6-30.

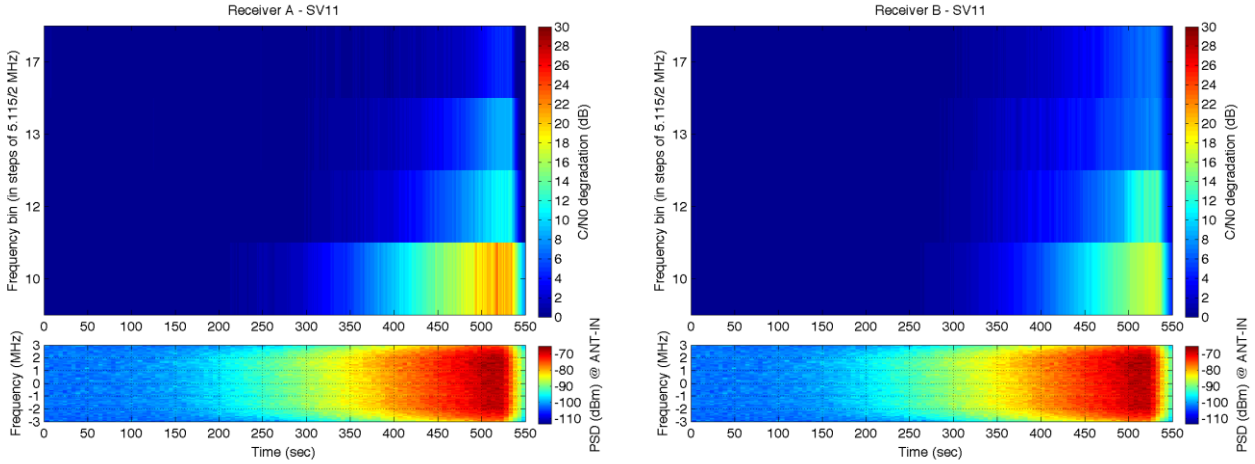

FIGURE 6-30 (DVBS-5M) TIME-FREQUENCY REPRESENTATION OF THE C/N0 DEGRADATION EXPERIENCED BY THE TWO GALILEO E6 RECEIVERS.

6.3.3.2 IMPACT AT THE CENTER OF THE E6 BAND

The results for a 5 Msps DVB-S interference at the center of the E6 band are very similar to the ones already presented for the 4 Msps signal in Figure 6-22 and Figure 6-23, with a maximum C/N_0 degradation on the order of 20 dB for receiver A and 15 dB for receiver B.

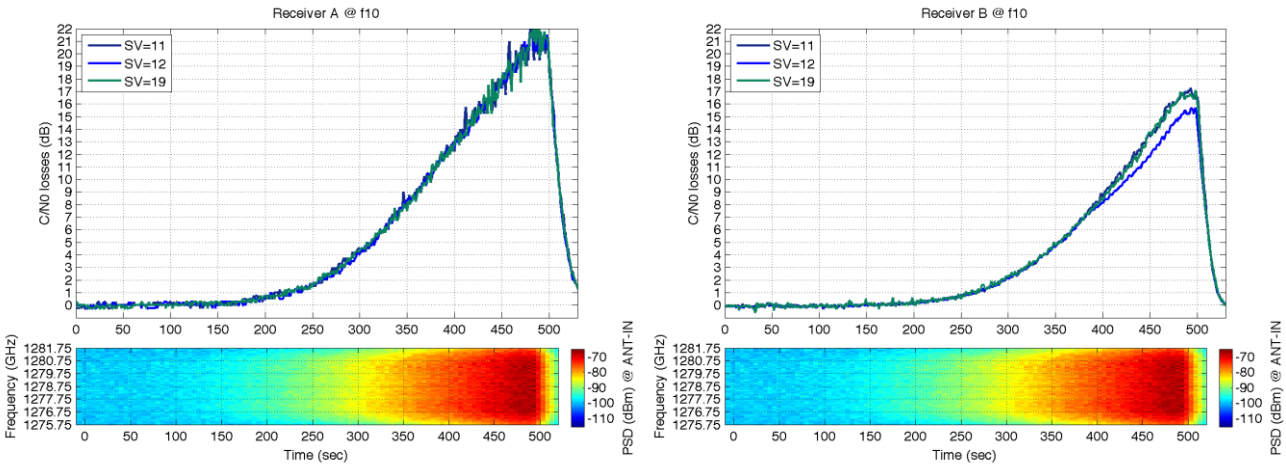

FIGURE 6-31 (DVBS-5M@CENTER) C/N0 DEGRADATION FOR THE DIFFERENT SATELLITES IN VIEW.

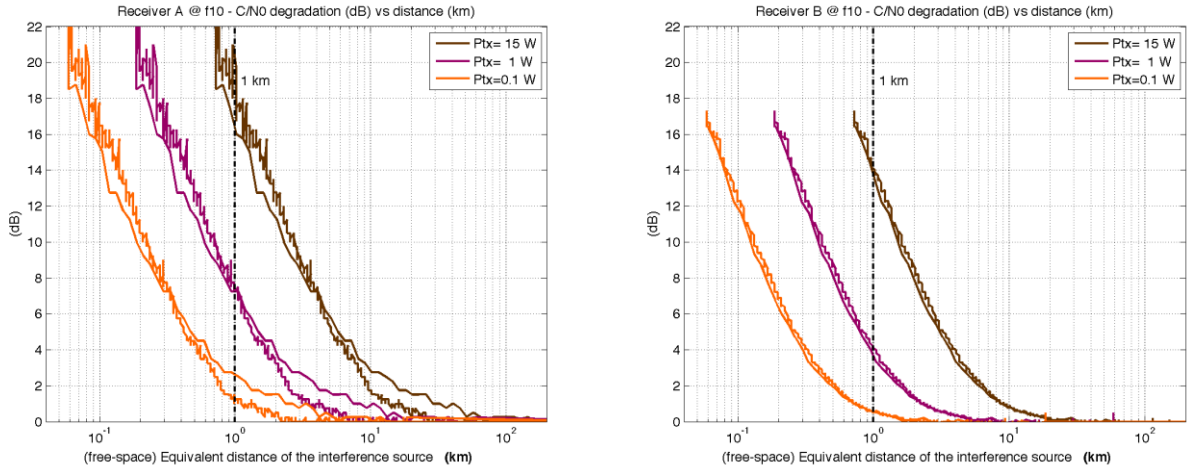

FIGURE 6-32 (DVBS-5M@CENTER) C/N0 DEGRADATION AS A FUNCTION OF DISTANCE BETWEEN ATV TRANSMITTER AND GNSS RECEIVER.

6.3.3.3 IMPACT AT THE FIRST NULL OF GALILEO E6B/C SPECTRUM

Here we find a slightly higher degradation than the one already observed for DVB-S signals with smaller symbol rate. While for 2 Msps we had around 8 dB degradation, and for 4 Msps we had around 10 dB, for 5 Msps we have now 12 dB for receiver A and around 14 dB for receiver B. This confirms that even though the interference is placed over a null of the Galileo spectrum, the larger the interference bandwidth, the larger the spectral overlap outside of this null, and therefore the larger the resulting C/N_0 degradation.

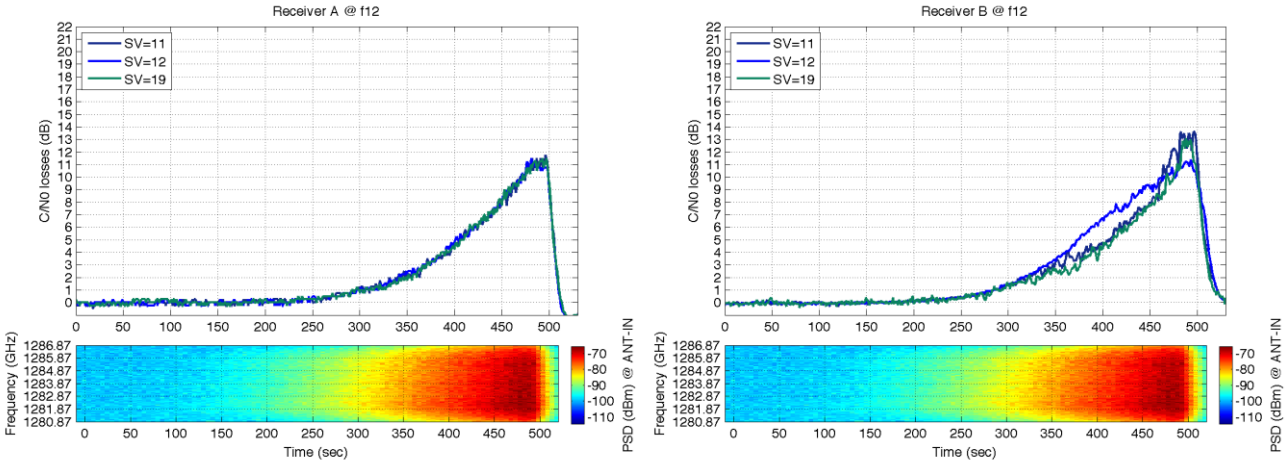

FIGURE 6-33 (DVBS-5M@NULL1) C/N0 DEGRADATION FOR THE DIFFERENT SATELLITES IN VIEW.

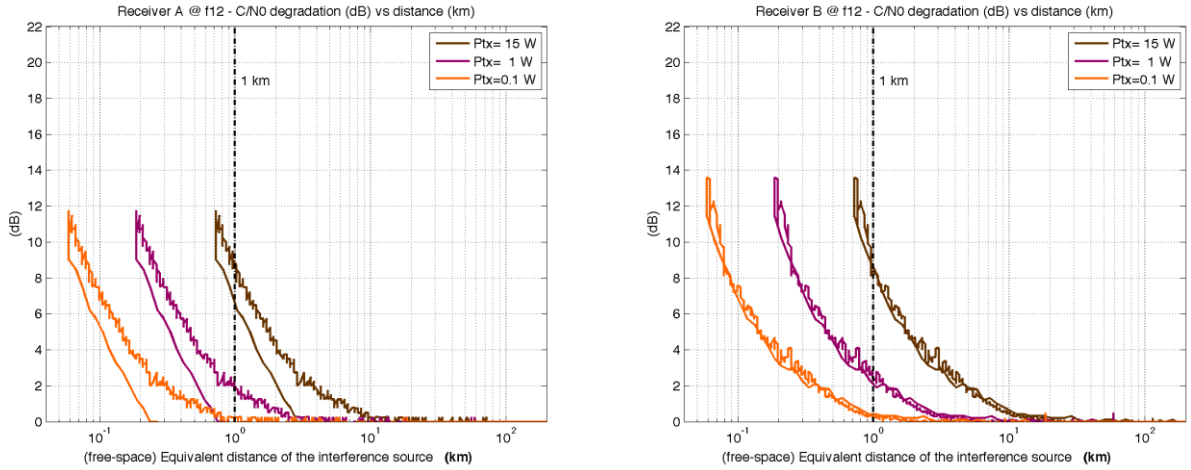

FIGURE 6-34 (DVBS-5M@NULL1) C/N0 DEGRADATION AS A FUNCTION OF DISTANCE BETWEEN ATV TRANSMITTER AND GNSS RECEIVER.

6.3.3.4 IMPACT AT THE EDGE OF THE E6 BAND

At the edge of the band we observe a slightly higher degradation, about 1 to 2 dB more, than the one for the previous symbol rate of 4 Msps in Figure 6-26.

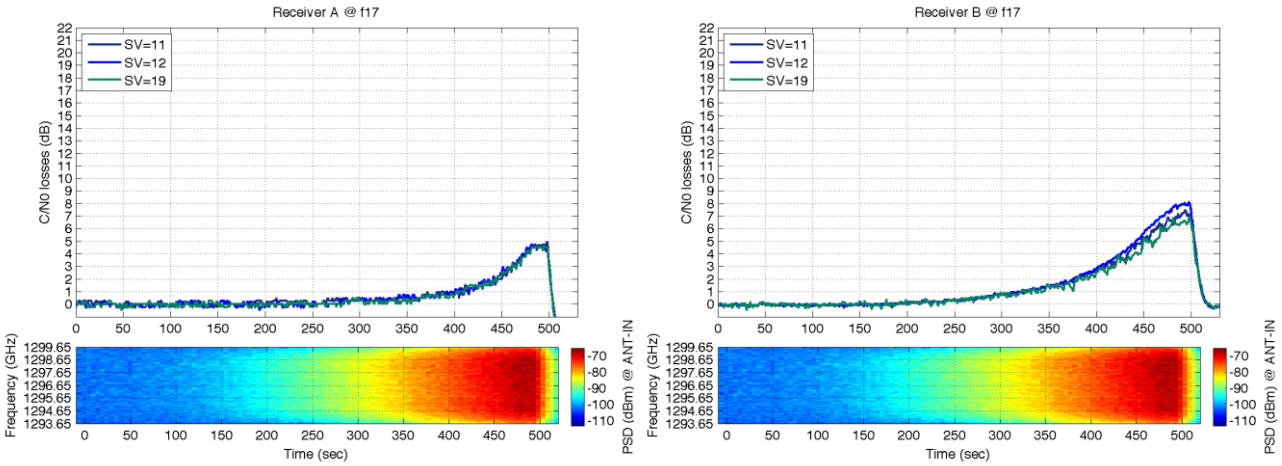

FIGURE 6-35 (DVBS-5M@EDGE) C/N0 DEGRADATION FOR THE DIFFERENT SATELLITES IN VIEW.

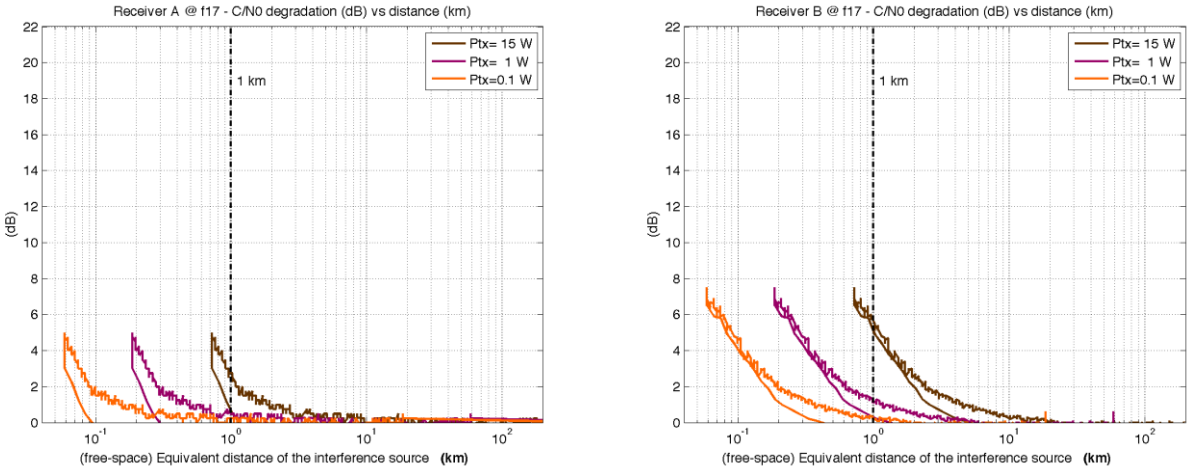

FIGURE 6-36 (DVBS-5M@EDGE) C/N0 DEGRADATION AS A FUNCTION OF THE DISTANCE BETWEEN ATV TRANSMITTER AND GNSS RECEIVER.

For the pseudorange performance, receiver A is exhibiting a slightly worse performance (around 1-2 dB) than the one expected for the C/N_0 being reported by the receiver, while for receiver B this effect cannot be perceived.

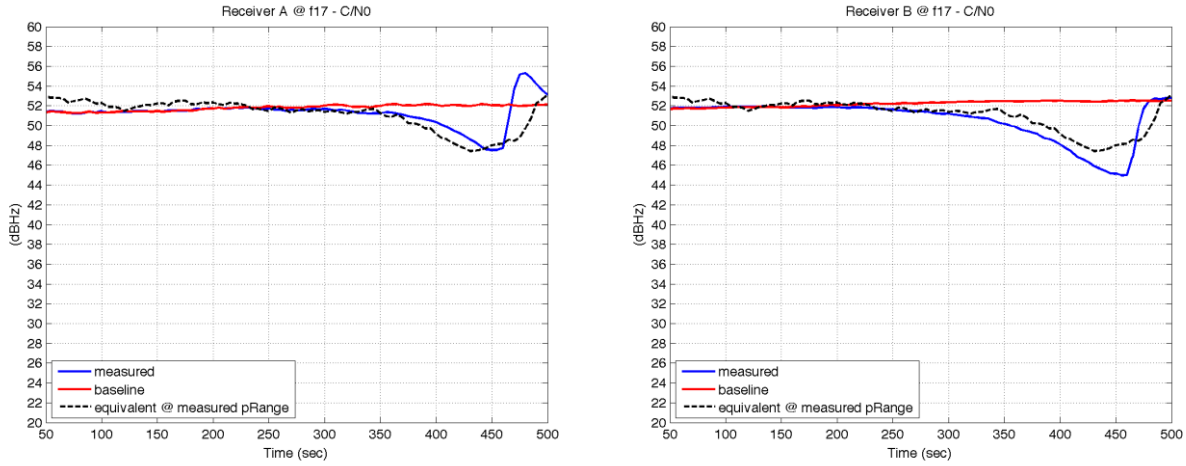

FIGURE 6-37 (DVBS-5M@EDGE) EQUIVALENT C/N0 CORRESPONDING TO THE BASELINE PSEUDORANGES AND TO THE MEASURED ONES IN THE PRESENCE OF INTERFERENCE.

6.3.3.5 C/N0 DEGRADATION ALONG THE E6 BAND

The summary of the maximum observed C/N_0 losses (for the interference powers considered herein, leading to $C_i/N_0 = 110$ dBHz) is shown in Figure 6-38. Due to the larger bandwidth of the interference, a smoother transition is observed in the C/N_0 degradation as a function of frequency, as compared to the behavior observed in the right tails of Figure 6-20 and Figure 6-29 for DVB-S signals with 2 and 4 Msps, respectively.

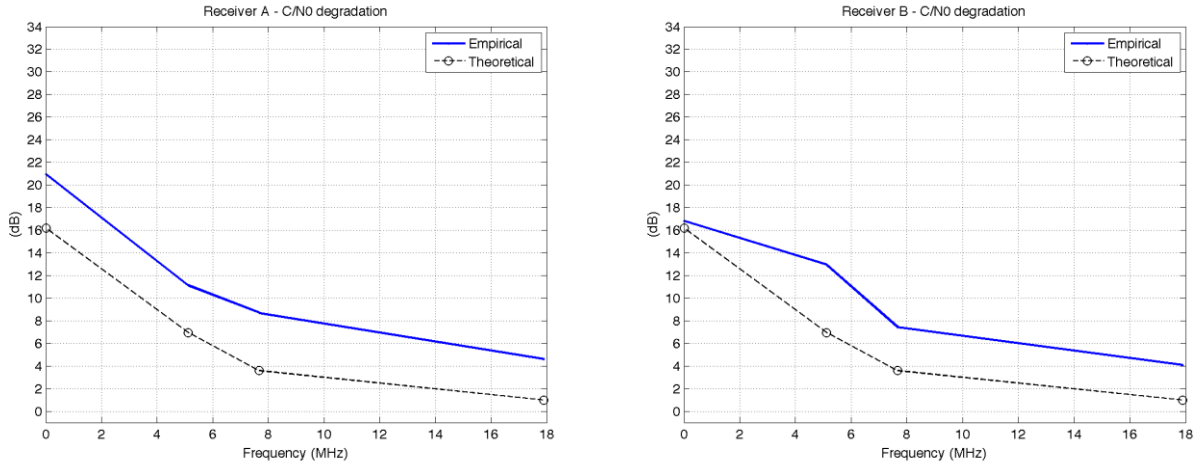

FIGURE 6-38 (DVBS-5M) C/N0 DEGRADATION AS A FUNCTION OF FREQUENCY FOR THE MAXIMUM INTERFERENCE LEVEL CONSIDERED IN THE TESTS (Ci/N0=110 dBHz).

6.4 TEST CASE 3. DVB-T INTERFERENCE

6.4.1 5 MHZ BANDWIDTH

6.4.1.1 OVERVIEW

As for the DVB-S signal at 5 Msps, the case of DVB-T with 5 MHz bandwidth has been tested for a reduced set of four frequency bins, including the central lobe, the first null, the first secondary lobe of the Galileo E6 signal, and the edge of the E6 band. The results are summarized in the time-frequency representation shown in Figure 6-39.

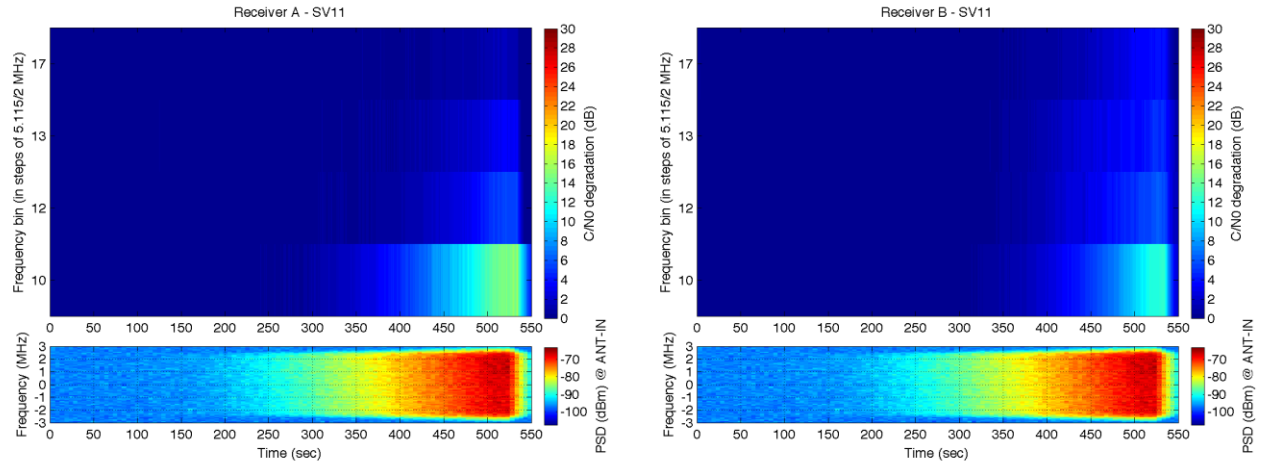

FIGURE 6-39 (DVBT-5M) TIME-FREQUENCY REPRESENTATION OF THE C/N0 DEGRADATION EXPERIENCED BY THE TWO GALILEO E6 RECEIVERS.

6.4.1.2 IMPACT AT THE CENTER OF THE E6 BAND

Compared to the C/N_0 degradation for DVB-S signals, the one observed for DVB-T is about 5 dB less. In spite of that, the maximum C/N_0 degradation is still quite high, on the order of 15 dB for receiver A and 12 dB for receiver B, when subject to an interference with $C_i/N_0 = 110$ dBHz.

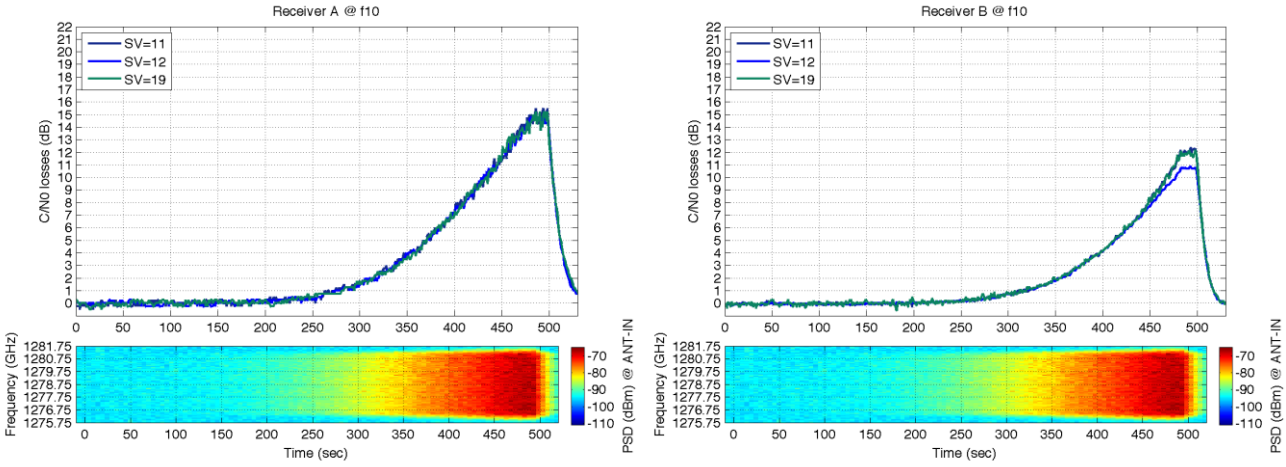

FIGURE 6-40 (DVBT-5M@CENTER) C/N0 DEGRADATION FOR THE DIFFERENT SATELLITES IN VIEW.

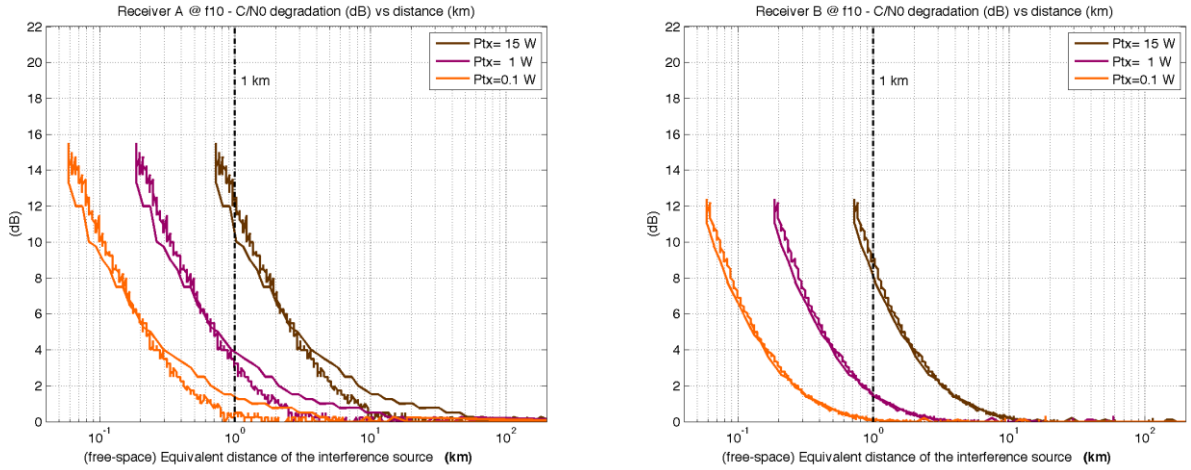

FIGURE 6-41 (DVBT-5M@CENTER) C/N0 DEGRADATION AS A FUNCTION OF DISTANCE BETWEEN ATV TRANSMITTER AND GNSS RECEIVER.

6.4.1.3 IMPACT AT THE FIRST NULL OF GALILEO E6B/C SPECTRUM

At the first null we now observe a smaller degradation than for the DVB-S signal at 5 Msps, with maximum values on the order of 6 dB for receiver A and nearly 8 dB for receiver B.

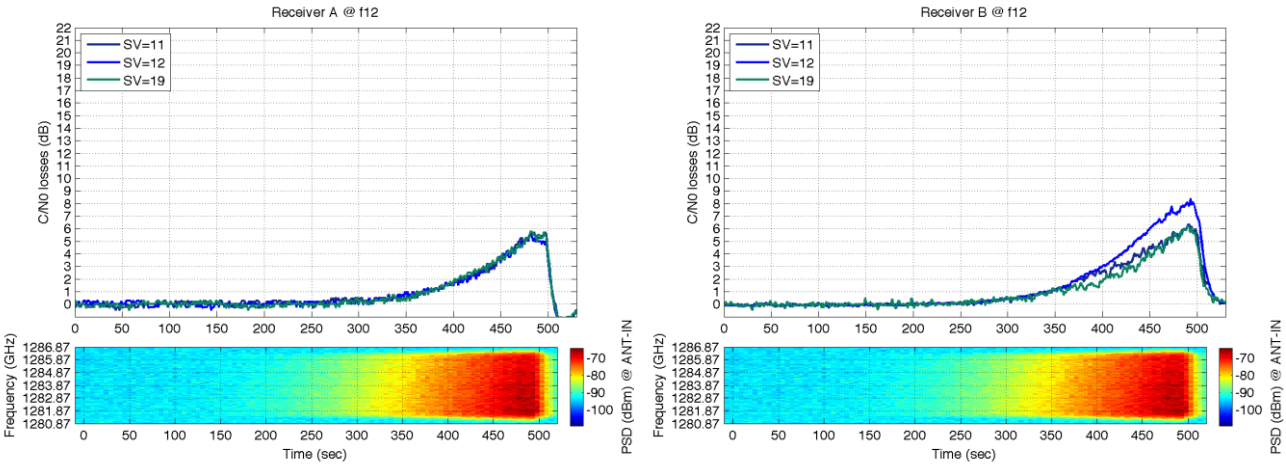

FIGURE 6-42 (DVBT-5M@NULL1) C/N0 DEGRADATION FOR THE DIFFERENT SATELLITES IN VIEW.

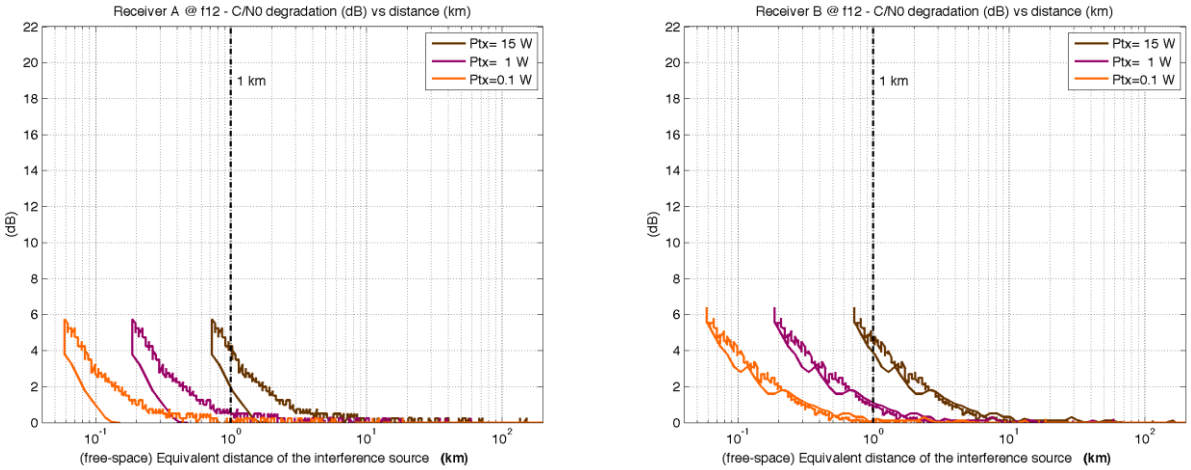

FIGURE 6-43 (DVBT-5M@NULL1) C/N0 DEGRADATION AS A FUNCTION OF THE DISTANCE BETWEEN ATV TRANSMITTER AND GNSS RECEIVER.

6.4.1.4 IMPACT AT THE EDGE OF THE E6 BAND

At the edge of the band we also observe a smaller C/N_0 degradation compared to the previous interference signals and bandwidths. For DVB-T we now have on the order of 2 dB degradation for receiver A and 5 dB for receiver B, as observed in Figure 6-44.

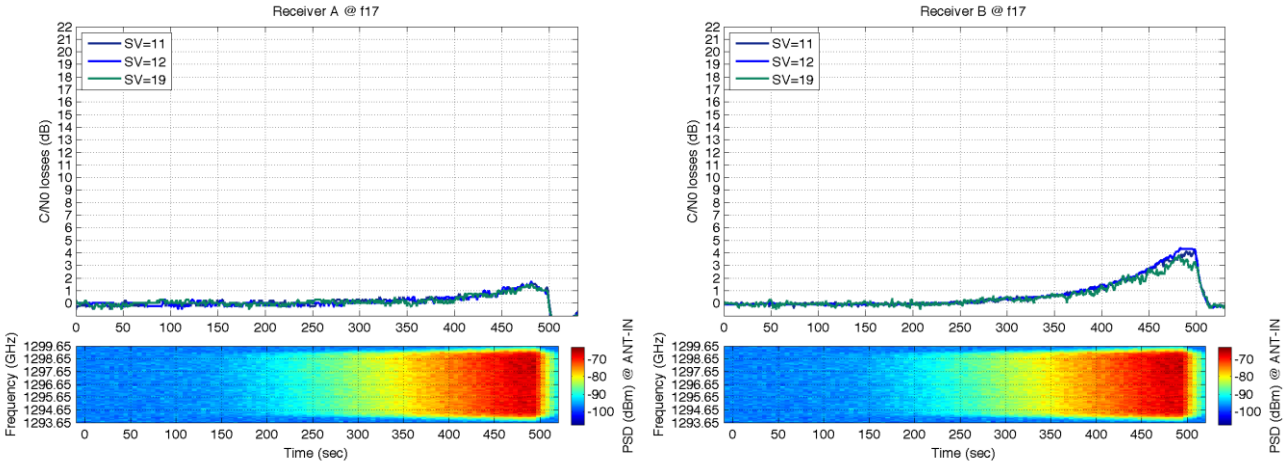

FIGURE 6-44 (DVBT-5M@EDGE) C/N0 DEGRADATION FOR THE DIFFERENT SATELLITES IN VIEW.

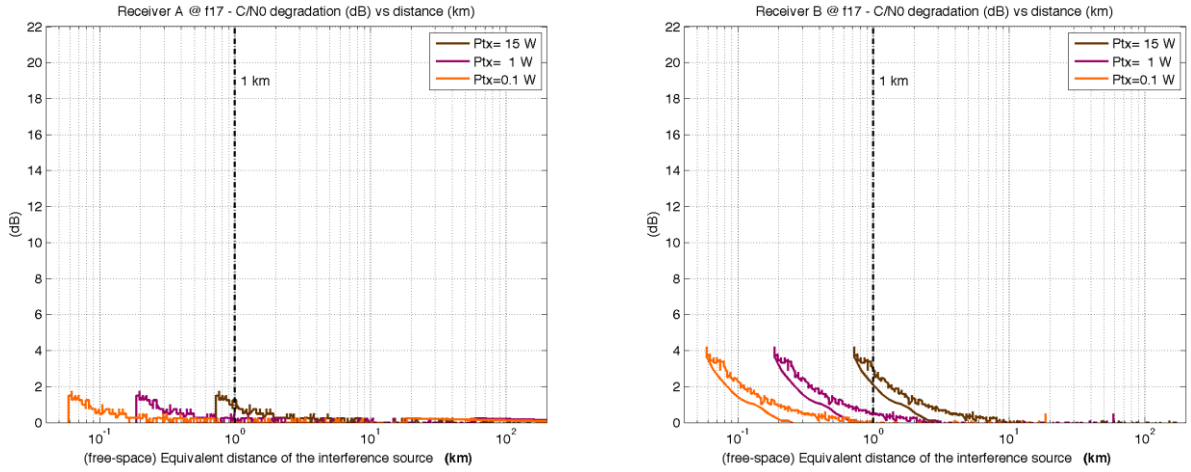

FIGURE 6-45 (DVBT-5M@EDGE) C/N0 DEGRADATION AS A FUNCTION OF THE DISTANCE BETWEEN ATV TRANSMITTER AND GNSS RECEIVER.

For the pseudorange performance of this test case, there does not seem to be a noticeable difference between the equivalent C/N_0 (based on the pseudorange variance) and the one actually reported by the receiver.

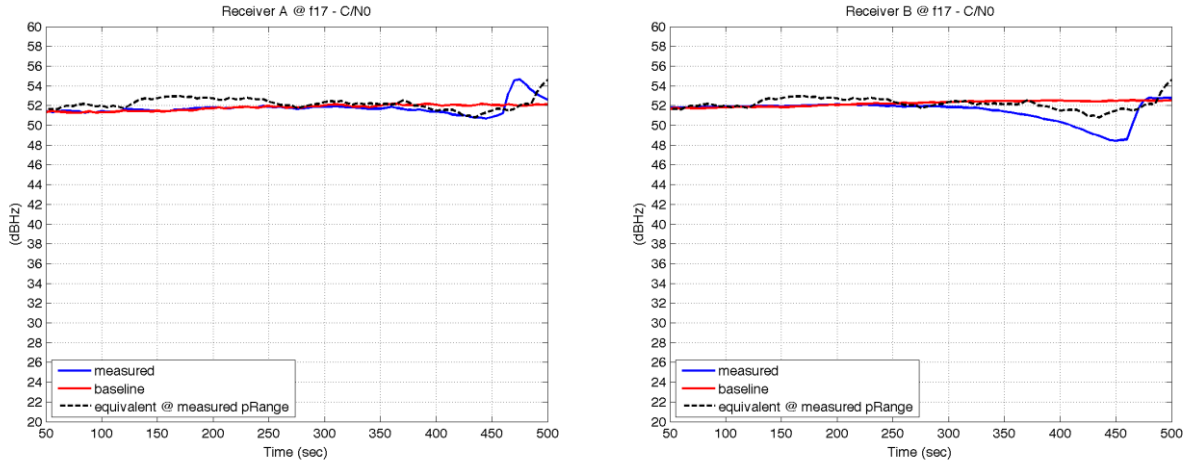

FIGURE 6-46 (DVBT-5M@EDGE) EQUIVALENT C/N0 CORRESPONDING TO THE BASELINE PSEUDORANGES AND TO THE MEASURED ONES IN THE PRESENCE OF INTERFERENCE.

6.4.1.5 C/N0 DEGRADATION ALONG THE E6 BAND

The lower C/N_0 degradation for DVB-T interference signals (as compared to CW and DVB-S ones) can be clearly observed in Figure 6-47. In spite of that, we still have a maximum degradation of about 12-14 dB, and an average degradation of about 4-6 dB within the band, for the interference levels being tested with $C_i/N_0 = 110$ dBHz.

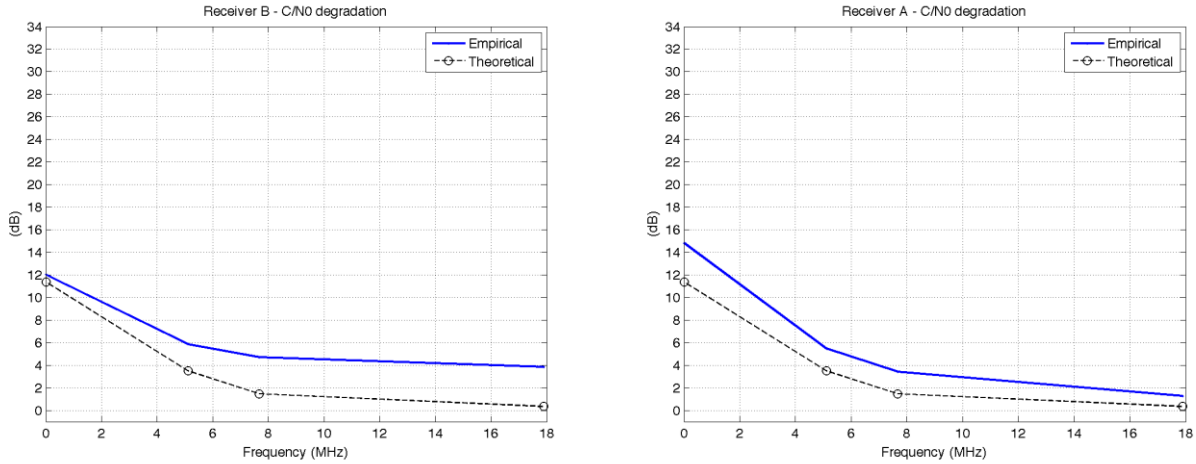

FIGURE 6-47 (DVBT-5M) C/N0 DEGRADATION AS A FUNCTION OF FREQUENCY FOR THE MAXIMUM INTERFERENCE LEVEL CONSIDERED IN THE TESTS (Ci/N0=110 dBHz).

7 CONCLUSIONS

In this report we have addressed the compatibility between amateur TV and Galileo E6B/C signals within the E6 band. A twofold approach has been followed by using both analytical and empirical results. On the one hand, we have formulated the problem of finding the performance degradation experienced by a GNSS receiver when subject to a generic interference. Analytical results have been provided to model the C/N_0 degradation, the pseudorange variance and the bit error rate. Later on, an extensive measurement campaign has been conducted at the EMSL of the JRC using high-end Galileo E6 receivers. A test plan was designed, also following discussions with IARU members in Fall 2014, involving a selective frequency scan of the E6 band and the use of an interference power ramp to assess the sensitivity of the receivers under test. The maximum interference power levels led to a C_i/N_0 on the order of 100 to 110 dBHz, which correspond to a representative scenario of an ATV station with 1W EIRP at 3 to 1 km distance from the Galileo receiver, respectively, or with 15W EIRP at 10 to 4 km distance, respectively. Both power and distance levels are similar (though optimistic) to the ones that would be found in practice.

In general terms, both analytical and empirical results show a significant performance degradation of Galileo E6 receivers when subject to the working conditions considered in this study:

For ***narrowband ATV interferences*** with a maximum $C_i/N_0 = 100$ dBHz, the C/N_0 degradation reached a peak of up to 30 dB when placed at the center of the band, and an average of about 8 to 10 dB for the rest of the band, even when the interference is placed far away from the central lobe of the Galileo spectrum. In this latter case, some of the receivers under test even showed a larger pseudorange variance than the one that would correspond to the working C/N_0 (i.e. 2 to 4 dB worse), thus confirming the sensitivity to interference sources even when they are placed at the edges of the band.

For ***wideband D-ATV interferences*** with a maximum of $C_i/N_0 = 110$ dBHz, the C/N_0 degradation reached a peak of about 20 dB when placed at the center of the band, and an average of about 8 to 10 dB (depending on the receiver) for the rest of the band, even when the interference is placed far away from the central lobe of the Galileo spectrum. When placing the interference at the first null of the Galileo E6B/C spectrum, the degradation was observed to increase as a function of the interference bandwidth. For instance, 8 dB, 9 dB and 11 dB of C/N_0 degradation were observed for DVB-S signals with 2, 4 and 5 Msps, respectively. In contrast, about 5 dB degradation were observed for DVB-T signals with 5 MHz bandwidth, when placed at the same first null of the spectrum. In that sense, DVB-T signals were found to incur in a smaller performance degradation than DVB-S signals, particularly when placed outside of the central part of the Galileo E6B/C spectrum.

Based on the C/N_0 degradation observed for both narrowband and wideband interference signals, the uncoded bit error rate was found to be contained within the range from 0.01 to 0.1, which implies a significant degradation with respect to the nominal (almost error free) performance. Therefore, either at C/N_0, pseudorange or bit error rate, the impact of ATV signals onto the performance of Galileo E6 receivers is noticeable. Furthermore, it is interesting to point out that the results of this study were obtained using high-end Galileo E6 receivers, so that presumably, similar or even larger performance degradations would be experienced in low-end/mass-market receivers.

8 REFERENCES

The following table contains all the referenced documents:

Ref.	Title
[1]	European Union, *Galileo Open Service (OS) Signal In Space (SIS) Interface Control Document (ICD)*, Issue 1, February 2010.
[2]	J. R. Sklar, "Interference mitigation approaches for the Global Positioning System", Lincoln Laboratory Journal, vol. 14, no. 2, pp. 167-180, 2003.
[3]	International Amateur Radio Union (IARU), *VHF Manager's handbook*, version 6.14, September 2014.
[4]	E. D. Kaplan, C. J. Hegarty, *Understanding GPS Principles and Applications*, Artech House, 2006.
[5]	D. Borio, *A statistical theory for GNSS signal acquisition*, Phd thesis, Politecnico di Torino, April 2008.
[6]	D. Borio, C. O'Driscoll and J. Fortuny-Gausch, "Impact of Pseudolite Signals on Non-participating GNSS Receivers", Proc. European Navigation Conference (ENC'11), Nov. 2011.
[7]	M. Abdizadeh, J. T. Curran, G. Lachapelle, "Quantization effects in GNSS receivers in the presence of interference", Proc. ION International Technical Meeting (ITM), pp. 742-753, Jan. 2012.
[8]	T. Shibata, H. Maeda, "Extended theory of spectral separation coefficient for GNSS signal interference", Proc. ION International Technical Meeting (ITM), pp. 930-940, Jan. 2010.
[9]	J. W. Betz, "Effect of partial-band interference on receiver estimation C/N0: theory", Proc. ION National Technical Meeting (NTM), pp. 817-828, Jan. 2001.
[10]	A. T. Balaei, A. G. Dempster, L. Lo Presti, "Characterization of the effects of CW and pulse CW interference on the GPS signal quality", IEEE Trans on Aerospace and Electronic Systems, vol. 45, no. 4, pp. 1418-1431, Oct. 2009.
[11]	J. Jang, M. Paonni, B. Eissfeller, "CW interference effects on tracking performance of GNSS receivers, "IEEE Trans. on Aerospace and Electronic Systems, vol. 48, no. 1, pp. 243-260, Jan. 2012.
[12]	J. W. Betz, "Effect of narrowband interference on GPS code tracking accuracy", Proc. ION National Technical Meeting (NTM), pp. 16-27, Jan. 2000.
[13]	J. W. Betz, K. R. Kolodziejski, "Generalized theory of code tracking with an early-late discriminator. Part I: lower bound on coherent processing", IEEE Trans. on Aerospace and Electronics Systems, vol. 45, no. 4, pp. 1538-1550, Oct. 2009.
[14]	J. W. Betz, K. R. Kolodziejski, "Generalized theory of code tracking with an early-late discriminator. Part II: noncoherent processing and numerical results", IEEE Trans. on Aerospace and Electronics Systems, vol. 45, no. 4, pp. 1551-1564, Oct. 2009.
[15]	B. W. Parkinson, J. J. Spilker, *Global positioning system: theory and applications*, American Institute of Aeronautics and Astronautics (AIAA), vol. I, 1996.
[16]	M. Anghileri, M. Paonni, D. Fontanella, B. Eissfeller, "Assessing GNSS data message performance", Inside GNSS, vol. March/April, pp. 60-70, 2013.
[17]	S. Kay, *Fundamentals of statistical signal processing. Volume I: Estimation theory*, Prentice-Hall, 1993.

[18]	International Telecommunication Union (ITU), “Recommendation ITU-R M.1787-1”, 2012.
[19]	International Telecommunication Union (ITU), “Radio regulations articles”, 2012.
[20]	Radio Society of Great Britation (RSGB), “RSGB 2014 Band plan”, January 2014.
[21]	ETSI EN 300 421 v1.1.2, “Digital Video Broadcasting (DVB); Framing structure, channel coding and modulation for 11/12 GHz satellite services (DVB-S)”, 08-1997.
[22]	ETSI EN 300 744 v1.6.1, “Digital Video Broadcasting (DVB); Framing structure, channel coding and modulation for digital terrestrial television”, 01-2009.
[23]	M. El-Hajjar, L.Hanzo, “A survey of digital television broadcast transmission techniques”, IEEE Communications Surveys and Tutorials, vol. 15, no. 4, pp. 1924-1949, Fourth Quarter 2013.

European Commission
Joint Research Centre – Institute for the Protection and Security of the Citizen

Title: Compatibility between Amateur Radio Services and Galileo in the 1260-1300 MHz Radio Frequency Band

Authors: José A. López-Salcedo, Matteo Paonni, Michele Bavaro, Joaquim Fortuny-Guasch

2015 – 74 pp. – 21.0 x 29.7 cm

Abstract
The focus of this study is to assess the potential impact that interference signals may cause onto Galileo E6 signals. Particularly, those related to secondary stations operating in the E6 band, which are mainly concerned with amateur radio transmissions.
The report is organized as follows: Section 2 presents some mathematical preliminaries regarding the signal model and the main tasks that are carried out within a GNSS receiver. Section 3 provides some analytical results to model the performance degradation of a GNSS receiver in terms of C/N0 degradation, pseudorange variance and bit error rate. Section 4 introduces the regulatory framework related to transmissions on the E6 band, and summarizes the main features of ATV signals considered in this study. Section 5 describes the experimental setup deployed at the JRC for the testing campaign, while Section 6 presents the experimental results for the different test cases. Finally, a summary of the main conclusions of this work is provided in Section 7.

JRC96769

As the Commission's in-house science service, the Joint Research Centre's mission is to provide EU policies with independent, evidence-based scientific and technical support throughout the whole policy cycle. Working in close cooperation with policy Directorates-General, the JRC addresses key societal challenges while stimulating innovation through developing new methods, tools and standards, and sharing its know-how with the Member States, the scientific community and international partners.